

**GAS PHASE KINETIC AND THERMODYNAMIC STUDIES OF
ORGANIC SPECIES USING MASS SPECTROMETRY**

by

YIJIE NIU

A dissertation submitted to the

School of Graduate Studies

Rutgers, The State University of New Jersey

In partial fulfillment of requirements

For the degree of

Doctor of Philosophy

Graduate Program in Chemistry and Chemical Biology

Written under the direction of

Professor Jeehiun K. Lee

And approved by

New Brunswick, New Jersey

January, 2018

ABSTRACT OF THE DISSERTATION

Gas Phase Kinetic and Thermodynamic Studies of Organic Species

Using Mass Spectrometry

By YIJIE NIU

Dissertation Director:

Professor Jeehiun K. Lee

This dissertation details our efforts in deploying both experimental (mass spectrometry) and computational (Gaussian) methods to study the kinetic and thermodynamic properties of organic species in the gas phase.

Most organic reactions can be broadly considered as a combination of an electrophile with a nucleophile. Therefore, the quantification of the nucleophilicity and electrophilicity of organic substances is of ongoing interest to organic chemists. The nucleophilicity-electrophilicity scale in solution has been well defined. However, gas-phase nucleophilicity-electrophilicity studies are scarce. One of our main focuses is to build a nucleophilicity-electrophilicity database with intrinsic reactivity parameters. More specifically, we have measured the rate constants (k) of the association reactions between

benzylhydrium electrophiles and amine nucleophiles in the gas phase. Kinetics isotope effect (KIE) studies have been carried out to establish the nature of the product. Potential pitfalls of using the association reactions to quantify gas-phase reactivities are discussed, and an improved reaction model has been proposed and studied. These results are discussed in Chapter 2.

In recent years, triazolylidene carbenes have been widely used in organocatalysis. Although the triazolylidenes have been studied in a wide range of catalytic transformations, the fundamental properties of these species remain largely unknown. In order to probe their intrinsic properties, we calculated and measured the gas phase acidities of a series triazolium precatalysts (the conjugate acids of triazolylidene carbenes). The relationship between the thermodynamic properties and the catalytic reactivities has also been investigated. We find that the gas phase acidities of the triazolium precatalysts are influenced by the subtle electronic properties of their substituents. Moreover, there are correlations between the gas phase acidities and the selectivities of two triazolylidene carbene-catalyzed *Umpolung* reactions. These correlations are the first of their kind and can be used to guide future catalyst design. These results are discussed in Chapter 3.

In Chapter 4, we explore the possibility of using a charge-tagged *N*-heterocyclic carbene (NHC) to catalyze *Umpolung* reactions, such as the benzoin condensation and Stetter reaction, in the gas phase. We designed and synthesized thiazolylidene catalysts

with charge tags, which allowed us to track NHC-catalyzed reactions *in vacuo* by mass spectrometry.

Last, in Chapter 5, a comprehensive fundamental study of two charge-tagged triazolylidene catalyst is described. These charge-tagged species are novel triazolylidene derivatives with a carboxylate tail. The relative stabilities of various isomers are probed by calculations in both gas-phase and condensed-phase environments; comparisons are made to known condensed phase structural data. Measurement of the proton affinities of the carboxylate-tagged carbenes is used, in combination with calculations, to establish the gas-phase structure of these species.

DEDICATION

To my grandfather for his love

ACKNOWLEDGEMENTS

Primarily, I would like to thank my advisor Professor Jeehiun K. Lee for giving me the opportunity to join her group. I thank her for guidance and mentorship, and the inspiration that she shared with me during my graduate career.

I would like to thank all my colleagues in the Lee research group, especially Dr. Mu Chen, Dr. Kai Wang, Dr. Anna Michelson, Dr. Landon Greene, Dr. Yuan Tian, Hao Zeng, Jiahui Xu, Ning Wang and Allison Krajewski for their generous help and friendship. I really enjoyed working in this friendly environment. Special thanks to Dr. Alexei Ermakov for all the knowledge he shared with me about mass spectrometry and the help he gave us in troubleshooting of the instruments.

I would like to thank our collaborators Prof. Tomislav Rovis from Columbia University and Prof. Christopher W. Bielawski from Ulsan National Institute of Science and Technology.

I also would like to acknowledge my previous publications and unpublished papers in Dr. Lee's group. My work in these publications are included in this dissertation with the permission from the publishers. I thank the contributions of all coauthors and collaborators.

Last but not least, I would like to thank my committee members, Professor Alan Goldman, Professor Laurence Romsted, and Professor Brian Buckley for their time, attention, and helpful discussions about my research.

TABLE OF CONTENTS

ABSTRACT OF THE DISSERTATION.....	ii
DEDICATION.....	v
ACKNOWLEDGEMENTS	vi
TABLE OF CONTENTS.....	vii
LIST OF FIGURES	xi
LIST OF TABLES.....	xvii
Chapter 1. Introduction.....	1
1.1 Overview	1
1.1.1 Nucleophilicity and Electrophilicity	1
1.1.2 <i>N</i> -Heterocyclic Carbenes (NHCs).....	5
1.1.3 Charge-Handled <i>N</i> -Heterocyclic Carbene Catalyst	7
1.2 Instrumentation	9
1.2.1 FT-ICR Mass Spectrometry	9
1.2.2 Electrospray Ion Source (ESI)	10
1.2.3 Quadrupole Ion Trap Mass Spectrometer	11
1.2.4 Modified Finnigan LCQ DUO Mass Spectrometer	13
1.3 Methodology	14

1.3.1 Reaction Kinetics Using FT-ICR Mass Spectrometer	14
1.3.2 Reaction Kinetics Using LCQ (ESI-Quadrupole Ion Trap)	15
1.3.3 Bracketing Method	16
1.3.4 Cooks Kinetic Method	17
1.3.5 Computational Method	17
1.4 References	19
Chapter 2. Gas Phase Studies of Nucleophilicity and Electrophilicity	22
2.1 Introduction	22
2.2 Experimental	24
2.3 Results and Discussion	26
2.3.1 Substrates Studied	26
2.3.2 Assessing Electrophilicity	27
2.3.3 Obtaining " k_2 "	29
2.3.4 Obtaining " N " and " S_N "	31
2.3.5 Nature of The Product	32
2.3.6 Potential Problem with Current Reaction Model	33
2.3.7 Alternative Models	38
2.4 Conclusions	40
2.5 References	42

Chapter 3. Proton Affinity of Triazolylidene Carbenes: Rationalizing Subtle

Electronic Effects	43
3.1 Introduction	43
3.2 Experimental	45
3.3 Results and Discussion.....	46
3.3.1 Achiral Pyrrolidine-based Triazoliums	46
3.3.2 Chiral Aminoindanol-based Triazoliums	56
3.3.3 Acidity and Diastereoselectivity	63
3.3.4 Acidity and Enantioselectivity	72
3.4 Conclusions	75
3.5 References	76
Chapter 4. Charge-Tagged Thiazolylidene Catalysts	79
4.1 Introduction	79
4.2 Experimental	82
4.2.1 Synthesis of Charge-handled Thiazolylidene Catalyst Precursors	82
4.3 Results and Discussion.....	86
4.4 Conclusions	92
4.5 References	93
Chapter 5. Charge-Tagged Triazolylidene Catalysts	94

5.1 Introduction	94
5.2 Experimental	102
5.2.1 LCQ Bracketing Method.....	102
5.2.2 Cooks Kinetic Method	103
5.2.3 Calculation	105
5.3 Results and Discussion.....	105
5.3.1 Computational Results in the Gas Phase	105
5.3.2 Experimental Results in the Gas Phase.....	111
5.3.3 Computational Results in the Solution Phase	114
5.3.4 Characterization of 11a(b) Precatalyst in the Solution Phase	115
5.3.5 Discussion	117
5.4 Conclusions	121
5.5 References	122

LIST OF FIGURES

Figure 1.1 Reference electrophile and nucleophile in Mayr Database	3
Figure 1.2 Linear relationship between natural log of reaction rate constants and E parameters of electrophiles	3
Figure 1.3 Singlet and triplet carbenes.....	5
Figure 1.4 An intramolecular benzoin condensation	6
Figure 1.5 N -Heterocyclic carbenes.....	7
Figure 1.6 Diagrammatic representation of ionization in an ESI ion source	11
Figure 1.7 Basic linear quadrupole ion trap structure	12
Figure 1.8 Paul Trap.....	13
Figure 1.9 Modified Finnigan LCQ DUO Mass Spectrometer.....	14
Figure 2.1 Nucleophiles and electrophiles studied	27
Figure 2.2 Plots of $\log(k_2)$ versus $E_{gas,app}$ in the gas phase.....	32
Figure 2.3 Experiments used to ascertain kinetic isotope effects	32
Figure 2.4 Plots of solutions-phase $\log k_2$ versus E in acetonitrile. ²²⁻²⁵ The data can be found on the website: http://www.cup.lmu.de/oc/mayr/reaktionsdatenbank/	34
Figure 2.5 Plot of N values from this work (N^a) versus that from reference 11 (N^a) ...	36
Figure 2.6 Energy surface depiction for benzhydryl cation reacting with amine in the gas phase	36

Figure 2.7 Solution phase E values versus gas phase $E_{gas,app}$ values	37
Figure 2.8 An improved model for gas phase nucleophilicity-electrophilicity studies: fragmentation after complexation	39
Figure 2.9 New nucleophilicity-electrophilicity system	39
Figure 3.1 Intramolecular Stetter reaction cycle as catalyzed by a triazolyldene NHC	44
Figure 3.2 NHCs studied by Mayr Group	45
Figure 3.3 Calculated acidities for a series of pyrrolidine-based achiral triazolium cations (kcal/mol). Calculations were conducted at B3LYP/6-31+G(d); reported values are ΔH at 298 K	48
Figure 3.4 Calculated acidities for a series of pyrrolidine-based achiral triazolium cations (kcal/mol), arranged in the order of acidity	49
Figure 3.5 Calculated (B3LYP/6-31+G(d)) geometries of the 3c and 3g achiral triazolium cations	50
Figure 3.6 Calculated acidities for a series of aminoindanol-based chiral triazolium cations, in kcal/mol. Calculations were conducted at B3LYP/6-31+G(d); reported values are ΔH at 298 K	58
Figure 3.7 Calculated acidities for a series of aminoindanol-based chiral triazolium cations (kcal/mol), arranged in the order of acidity	59
Figure 3.8 Calculated (B3LYP/6-31+G(d)) geometries of the 4a and 4m chiral	

triazolium cations.....	59
Figure 3.9 NHC-catalyzed homoenolate addition of enals to nitroalkenes, with proposed catalytic mechanism	64
Figure 3.10 Natural log plot of the <i>anti/syn</i> ratio for the reaction in Figure 3.9 (R=Et) versus calculated gas phase acidity of the precatalyst	65
Figure 3.11 Natural log plot of the <i>anti/syn</i> ratio for the reaction in Figure 3.9 (R=Et) versus calculated gas phase acidity of the precatalyst, for catalysts with diortho aryl substitution.....	67
Figure 3.12 Natural log plot of the <i>anti/syn</i> ratio for the reaction in Figure 3.9 (R=Et) versus calculated gas phase acidity of the precatalyst, for precatalysts lacking diortho aryl substitution.....	67
Figure 3.13 Various NHC enantioselective precatalysts	68
Figure 3.14 Transition states leading to the observed major isomers in asymmetric homoenolate reactions	68
Figure 3.15 Deprotonation to form either E or Z enol	69
Figure 3.16 Free energy profiles for E versus Z enol formation for 3c (A) and 3d (B).....	70
Figure 3.17 Calculated TSb structures for 3c and 3d.....	71
Figure 3.18 NHC-catalyzed intramolecular Stetter reaction with dienones	72
Figure 3.19 Natural log plot of the major/minor enantiomer ratio for the reaction in Figure 3.18 versus the calculated gas phase acidity of the precatalyst.....	73

Figure 4.1 Catalytic cycle of the benzoin condensation as proposed by Breslow	80
Figure 4.2 Designed and synthesized charge-tagged thiazolylidene catalysts 10c and 10d.....	82
Figure 4.3 Synthesis of charge-handled thiazolylidene catalyst precursors: Step 1	83
Figure 4.4 Synthesis of charge-handled thiazolylidene catalyst precursors: Step 2	83
Figure 4.5 Synthesis of charge-candled thiazolylidene catalyst precursors: Step 3	85
Figure 4.6 ^1H NMR spectrum of Step 1 product 10e.....	86
Figure 4.7 ^1H NMR spectrum of Step 2 product 10f	87
Figure 4.8 ^1H NMR spectrum of Step 3 methyl-substituted product 10a	88
Figure 4.9 ^1H NMR spectrum of Step 3 ethyl-substituted product 10b	89
Figure 4.10 MS/MS spectra of 10c (top) and 10d (bottom).....	90
Figure 4.11 Charged-tagged NHC catalysts (10c and 10d) and doubly charged NHC dimers (10c' and 10d').....	91
Figure 4.12 Fragmentation of 10c in positive ion mode	91
Figure 5.1 Second-generation Grubbs catalyst.....	94
Figure 5.2 Triazolium precatalysts used by Enders	95
Figure 5.3 Selected triazolium precatalysts	96
Figure 5.4 Chiral bicyclic triazolium frameworks	97
Figure 5.5 Two novel charge-tagged thiazolylidene catalysts	98
Figure 5.6 Charged tag-mediated formation of Breslow intermediate in the gas phase	

.....	98
Figure 5.7 Related species of charge-tagged triazolylidene catalysts.....	99
Figure 5.8 Relative stability of isomers of neutral 11a (kcal/mol). Calculations were conducted at B3LYP/6-31+G(d); reported values are ΔH at 298 K	106
Figure 5.9 Relative stability of isomers of neutral 11b (kcal/mol). Calculations were conducted at B3LYP/6-31+G(d); reported values are ΔH at 298 K	107
Figure 5.10 Relative stability of isomers of deprotonated 11a (kcal/mol). Calculations were conducted at B3LYP/6-31+G(d); reported values are ΔH at 298 K.....	107
Figure 5.11 Relative stability of isomers of deprotonated 11b (kcal/mol). Calculations were conducted at B3LYP/6-31+G(d); reported values are ΔH at 298 K.....	108
Figure 5.12 Relative stability of isomers of protonated 11a (kcal/mol). Calculations were conducted at B3LYP/6-31+G(d); reported values are ΔH at 298 K.....	108
Figure 5.13 Relative stability of isomers of protonated 11b (kcal/mol). Calculations were conducted at B3LYP/6-31+G(d); reported values are ΔH at 298 K.....	109
Figure 5.14 Calculated acidities for protonated 11a(b) cations (kcal/mol). Calculations were conducted at B3LYP/6-31+G(d); reported values are ΔH at 298 K.....	109
Figure 5.15 Calculated proton affinities of two different sites for 11a-anion and 11b-anion (kcal/mol). Calculations were conducted at B3LYP/6-31+G(d); reported values are ΔH at 298 K.....	110
Figure 5.16 Relative stabilities of isomers of neutral 11a and 11b in acetone	

(kcal/mol). Calculations were conducted at B3LYP/6-31+G(d) using PCM and SMD models; reported values are ΔH at 298 K	115
Figure 5.17 Crystal structure of 11b precatalyst	117
Figure 5.18 Measured (blue) and calculated (black, in parentheses) proton affinities of triazolylienes of 11a-neutral and 11b-neutral, kcal/mol. Calculations were conducted at B3LYP/6-31+G(d); reported values are ΔH at 298 K.....	120

LIST OF TABLES

Table 2.1 Rate constant and $E_{gas,app}$ data for the reaction of electrophiles with the reference nucleophile, piperidine.....	29
Table 2.2 Rate constants (k_2) and efficiencies (% , in parentheses) for the reactions of nucleophiles and electrophiles	30
Table 2.3 KIE data for the reaction of 1c versus 1c-D with nucleophiles.....	33
Table 3.1 Summary of results for gas phase acidity bracketing of achiral pyrrolidine-based triazoliums	53
Table 3.2 Calculated (B3LYP/6-31+G(d); 298 K) and experimental data for achiral triazolium cations.....	55
Table 3.3 Summary of results for acidity bracketing of chiral aminoindanol-based triazoliums.....	61
Table 3.4 Calculated (B3LYP/6-31+G(d); 298 K) and experimental data for chiral triazolium cations.....	63
Table 5.1 Summary of results for acidity bracketing of protonated 11a and 11b.....	111
Table 5.2 Calculated (B3LYP/6-31+G(d); 298 K) and experimental acidities for protonated 11a and protonated 11b	119

Chapter 1. Introduction

1.1 Overview

Mass spectrometry has long been used to study gas-phase ion chemistry reactions.¹⁻⁵

With both instrumental and computational research tools, we investigated the kinetic (nucleophilicity and electrophilicity) and thermodynamic (proton affinity and acidity) properties of organic and bioorganic molecules, especially *N*-heterocyclic carbene-related compounds.

1.1.1 Nucleophilicity and Electrophilicity

Ingold introduced the terms “nucleophile” and “electrophile” into the chemistry world with his ground-breaking work on the mechanism of organic reactions in the early 1930s.⁶ A chemical species that donates an electron pair to another molecule to form a covalent bond is called a nucleophile. Its counterpart, an electrophile, is a chemical compound that accepts the electron pair.

College students can quickly learn what “good” versus “bad” nucleophiles and electrophiles are, with some empirical relationships. For example, a more basic (basicity is a thermodynamic property) anion is often a better nucleophile (nucleophilicity is a kinetic property). However, such relationships between thermochemistry and kinetics are not always valid.

Since knowledge of the reactivities of nucleophiles and electrophiles are of interest for

both fundamental and applied purposes, for decades, people have been trying to quantitatively measure the extent to which a reagent is nucleophilic or electrophilic. Many nucleophilicity-electrophilicity scales have been developed in the condensed phase.

The first attempt to quantify relative nucleophilic strength was conducted by Swain and Scott.⁷ They used a free-energy relationship $\log(k/k_0)=s \cdot n$ to provide a given nucleophile with a nucleophilic constant n . In 1970s, Ritchie established another nucleophilicity-electrophilicity scale in the solution phase, where the reactions between carbocations and diazonium ions with various nucleophiles was studied. A parameter N_+ was defined as the nucleophilic reactivity for anions and alcohols.⁸

In recent years, Mayr and coworkers accomplished the most systematic and comprehensive nucleophilicity-electrophilicity scale.⁹⁻¹² They demonstrated that the kinetics of reactions between nucleophiles and electrophiles can be described by a linear-free energy relationship: $\log(k_2) = s_N \cdot (E + N)$, where two parameters, s_N and N , account for the reactivity of the nucleophile and the E parameter describes electrophile's reactivity.

Mayr research group examined a series of benzhydryl carbocations and aryl quinone methides to obtain the E parameters, which are further used to measure N values for the reaction counterparts, nucleophiles. The bis(*p*-methoxyphenyl)carbenium ion was chosen as the reference electrophile whose E parameter equals to 0.0. On the other hand, s_N value of the reference nucleophile 2-methyl-1-pentene was defined as 1.0 (Figure 1.1).

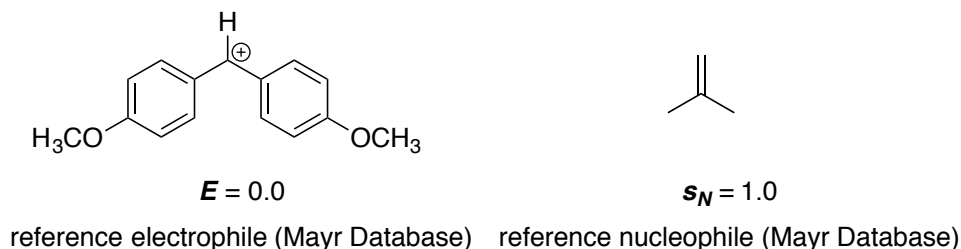


Figure 1.1 Reference electrophile and nucleophile in Mayr Database

It was found that the E parameter for electrophiles remains constant in varying reaction systems, no matter what nucleophiles and solvents are used. Once one has the E parameters, kinetics (reaction rate constant) between the nucleophiles and reference electrophiles can be used to generate a plot (Figure 1.2).

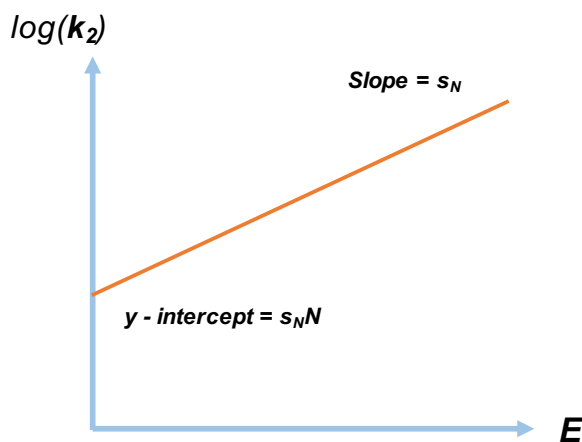


Figure 1.2 Linear relationship between natural log of reaction rate constants and E parameters of electrophiles

We can easily learn from Mayr's linear-free energy relationship equation that the slope of the plot is s_N value for a given nucleophile and the y-intercept is $s_N \cdot N$. As a result, E , N , and s_N values of a solution-phase reagent database can be obtained. The Mayr database currently has E , N , and s_N parameters for more than one thousand

chemical reactants and can be found at:

<http://www.cup.lmu.de/oc/mayr/reaktionsdatenbank/>.

Generally, higher N value means higher nucleophilic reactivity, and higher E value corresponds to higher electrophilic reactivity. It is worth noting that the s_N parameters are not fully understood.¹² Although it was found that s_N values display some structural information of nucleophiles; that is, nucleophiles with similar structures generally have similar s_N values, predictability can be difficult.

Much work has been established in the solution phase, while very little research of nucleophilicity and electrophilicity has been conducted to date in the gas phase, to probe intrinsic reactivity. More than a decade ago, Denekamp and coworkers reported the only attempt to experimentally apply Mayr's theory in the gas phase.¹³ A general linear relationship between gas- and solution-phase E values was found. However, no further investigations have been conducted to explore the differences of reactivities between media and to compare gas-phase data to that obtained in solution to ascertain solvent effects.

Chapter 2 describes my exploration of nucleophilicity and electrophilicity in the gas phase, with the goal of ultimately achieving an independent database of intrinsic reactivity parameters. The reactions between amine nucleophiles and benzhydryl cations are studied, and the limitations and challenges of using Mayr's solution-phase reaction model in the gas-phase study are discussed. An improved model is proposed.

1.1.2 *N*-Heterocyclic Carbenes (NHCs)

A carbene is a chemical species that contains a highly reactive neutral carbon center with a valence of two and a pair of unshared valence electrons. There exist two types of carbenes: the singlet and triplet carbenes.^{14,15} The singlet or triplet state of carbenes depends on the spins of the two unshared electrons. When the electrons are spin-paired, occupying the sp^2 orbital of the carbon center, the carbene displays the singlet state. Triplet carbenes have two unpaired electrons with the same spin direction (Figure 1.3).

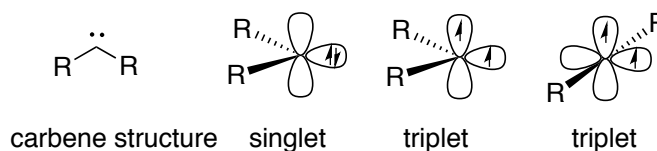


Figure 1.3 Singlet and triplet carbenes

Traditional carbenes, methylene ($\text{CH}_2:$), for example, tend to display the triplet ground state and are able to participate in reactions such as cyclopropanation, C-H insertion, H_2 activation, among other characteristic reactivities. However, these traditional carbenes are often very short lived and can be difficult to study directly. *N*-heterocyclic carbenes (NHC), on the other hand, are the largest subgroup of persistent carbenes, which demonstrate relatively higher stability than traditional carbenes.^{16,17} NHCs generally prefer the singlet ground state. In recent years, due to their utility and versatility, NHCs have become popular molecules at the frontier of chemistry research.¹⁸⁻²⁸ Protonated NHCs and their counterions together can form ionic liquids, which are reported as more environmentally friendly organic solvents.²⁹⁻³⁴

Neutral NHCs can function as ligands to transition metal catalysts. For example, the well-known Grubbs second generation ruthenium catalyst for olefin metathesis uses NHCs as ligands, as a substitute for the first generation ligand, PCy_3 .³⁵ In addition, NHCs themselves can serve as organic catalysts in synthetically usefully *Umpolung* reactions, such as the benzoin condensation (Figure 1.4).³⁶

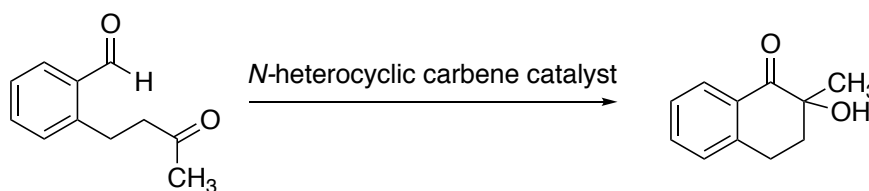


Figure 1.4 An intramolecular benzoin condensation

In such *Umpolung* reactions, the NHC catalyst first nucleophilically attacks an aldehyde and after a proton transfer step, the tetrahedral intermediate isomerizes to an enamine. During this process, the previously electrophilic carbon center of the carbonyl group is converted to a nucleophilic sp^2 carbon center. This polarity inversion is called *Umpolung*.³⁷⁻³⁹ Our group has entered into a collaboration with the Rovis group, who developed a series of triazolylidene carbenes as important organocatalysts for many *Umpolung* reactions.⁴⁰

Typical NHCs have various structures (Figure 1.5). They are often called “nucleophilic carbenes”. This is because NHCs are more nucleophilic than traditional carbenes but lack the characteristic carbene electrophilic reactivity such as C-H insertion, H_2 activation and ketene formation with CO.

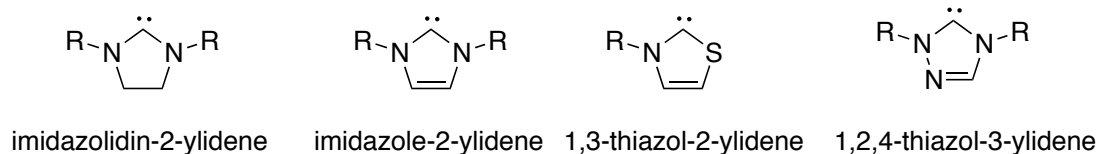


Figure 1.5 *N*-Heterocyclic carbenes

Most work focusing on NHCs has been conducted in the condensed phase, where factors such as solvent effect and diffusion control are at play. NHC research in a solvent-free environment to explore the intrinsic reactivity is rare. Our group is interested in using mass spectrometry and computational methods to quantitatively measure the intrinsic, thermodynamic and kinetic properties of organic species, including carbenes and their derivatives. With both solution-phase and gas-phase reactivities in hand, one can explore solvent effect in various reaction systems.

In Chapter 2, a gas-phase database was built attempting to ultimately measure the nucleophilicity of NHCs. In Chapter 3, a thermodynamic property (proton affinity) of a series of Rovis NHC catalysts is studied in the gas phase experimentally and computationally, and it is found that the proton affinity of NHC catalysts can be a powerful and convenient tool for predicting selectivity in NHC-catalyzed *Umpolung* reactions.

1.1.3 Charge-Handled N-Heterocyclic Carbene Catalyst

People have long been interested in NHC-catalyzed *Umpolung* reaction mechanisms.⁴¹⁻⁴⁴ In 1958, Breslow and coworkers proposed a catalytic mechanism with the thiazolyliidene as the catalytic species. His well-accepted mechanism involves a deprotonation of the thiazolium precatalyst to generate a thiazolyliidene, which attacks an

aryl aldehyde and yield a so-called Breslow intermediate after a proton transfer. The Breslow intermediate displays nucleophilic reactivity and is able to add to a second aldehyde to produce a benzoin, or nucleophilically attack a Michael acceptor, enone for example, through a Stetter reaction.^{45,46}

In the last several decades, much work has focused on developing NHC-catalyzed asymmetric Stetter reactions.⁴⁷⁻⁴⁹ However, limited work with detailed mechanistic studies for the Stetter reaction exists. Although the Breslow mechanism is commonly accepted, other mechanisms, proposed by Lemal and Castells involving a thiazolidine dimer, have also been postulated.^{50,51} There is evidence both in support of and against such mechanisms.

Gas phase studies in the absence of solvent are able to reveal intrinsic organic reactivity. Our lab is interested in exploring such NHC-catalyzed reactions in the solvent-free environment using mass spectrometry. Studying chemical reactions using mass spectrometry requires the chemical species to be charged, in order to be detectable.⁵² We designed and synthesized two series of thiazolidene and triazolidene catalysts with sulfonate and carboxylate charge tags, respectively. These charge-tagged NHCs are used to track the reagents and intermediates of the benzoin condensation and Stetter reaction *in vacuo* by mass spectrometry.^{53,54}

In Chapter 4, synthesis and characterization of two sulfonate tagged thiazolidene NHCs catalysts are described. Chapter 5 discusses the stability study and proton affinity measurement of two novel carboxylate tagged triazolidene NHCs.

1.2 Instrumentation

1.2.1 *FT-ICR Mass Spectrometry*

Mass spectrometry is a powerful analytical technique that enables scientists to study ionized chemical compounds. Fourier transform ion cyclotron resonance mass spectrometry (FTICR-MS, FT-ICR, or FTMS), is a unique type of mass spectrometry. It utilizes the cyclotron frequency of ions in a fixed magnetic field to determine the mass-to-charge ratio (m/z) information of the ions. Inspired by early technologies of ion cyclotron resonance (ICR) spectrometry and Fourier-transform nuclear magnetic resonance (FT-NMR) spectroscopy, Comisarow and Marshall developed the first FTICR-MS.^{55,56} After that, FTICR-MS soon became a powerful tool in ion chemistry research. With outstanding levels of both resolution and accuracy, FTMS outperforms most other mass spectrometry methods in terms of mass detection and analysis.⁵⁸

Ion cyclotron resonance is used to measure the mass of an ion in a magnetic field. The circular motion of an ion in a magnetic field is subject to Lorentz force. The Lorentz force that an ion feels in a magnetic field B can be depicted by Eq. 1.1, where v is the velocity of the ion and q is the charge on the ion.

$$F = qvB \quad \text{Eq. 1.1}$$

The circular trajectory of the ion can be stabilized when the Lorentz force F balances the centrifugal force F_c (Eq. 1.2).

$$F = F_c = \frac{mv^2}{r} \quad \text{Eq. 1.2}$$

$$\omega = 2\pi f = \frac{v}{r} = \frac{q}{m} B = \frac{1}{m/z} B \quad \text{Eq. 1.3}$$

Herein, m is the mass of the ion and r is the radius of the circular trajectory. As Eq. 1.3 shows, the angular frequency ω ($\omega = 2\pi f$) of the ion motion is proportionally related to the mass-to-charge ratio (m/z) of the ion.

After an ion is trapped in the ICR cell, it is excited by a radio electromagnetic wave that shares the same frequency as the circular motion, resulting in a larger motion trajectory radius. The excited ion can induce an alternating current, also called the image current, on the electrical conductive sensor. The information carried by the image current can be interpreted into frequency signals and further get translated into the mass-to charge ratio of the ion.

Our Finnigan 2001 FT-ICR mass spectrometer is equipped with two cubic ICR cells with a 3.3 Tesla superconducting magnetic field. We can introduce chemical compounds into the instrument via batch inlets, leak valves, pulsed valves, and a heatable solids probe inlet. Chemical samples can be ionized by electron ionization (EI), chemical ionization (CI), and electrospray ion (ESI) sources. The dual cell system allows ions to be selectively transferred between two cells. This enables users to prepare ions in one cell and study the properties of the ions in the other cell, which introduces flexibility to experimental designs.

1.2.2 Electrospray Ion Source (ESI)

Electrospray ionization (ESI) applies a high electronic voltage to a sample solution,

which turns into charged aerosol and generates ions in mass spectrometers.^{59,60} It is known as a “soft” ion source with little fragmentation during ionization. A diagram of ESI is illustrated in Figure 1.6.

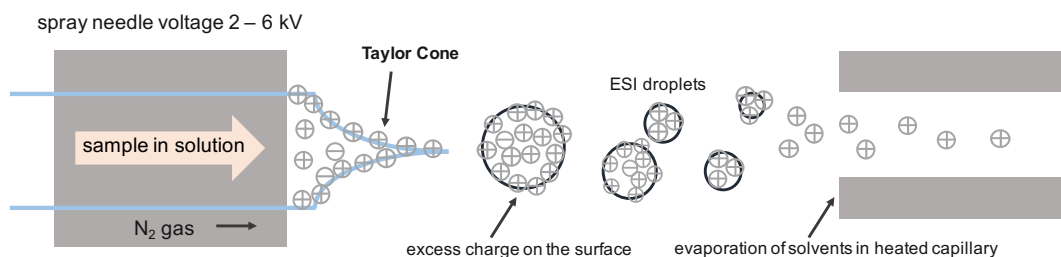


Figure 1.6 Diagrammatic representation of ionization in an ESI ion source

The analyte under study is dissolved in a volatile polar solvent (e.g. water, methanol, acetonitrile). Under atmospheric pressure, the sample solution passes through a heated capillary carrying a high electric potential difference of around 3kV. During this process, charge accumulates on the surface of the droplets. The size of charged droplets becomes smaller because of solvent evaporation. When the “Rayleigh limit point” is reached, the point where a droplet is not able to carry the amount of charge on its surface, it explodes and creates many smaller droplets.⁶¹ After this desolvation process, gas-phase ions form and are analyzed by mass spectrometer.

Our Thermo Finnigan LCQ DUO mass spectrometer is equipped with an ESI ion source that can be used to vaporize nonvolatile chemical compounds.

1.2.3 Quadrupole Ion Trap Mass Spectrometer

An ion trap can stabilize the motion trajectories of gas-phase ions by applying

electrical fields. Hans Dehmelt and Wolfgang Paul were awarded the Nobel Prize in 1989 for their invention of ion trap technique. A quadrupole consists of four rods, as shown in Figure 1.7.⁶²

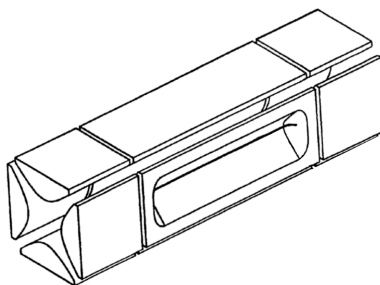


Figure 1.7 Basic linear quadrupole ion trap structure

The rods opposite to each other always carry the same polarity, while the rods next to each other carry opposite polarity. Ions traveling into the quadrupole space will be driven toward the rods with opposite charge. A constant polarity reversal is applied to the four rods, generating alternative electric fields within the quadrupole region. As a result, only ions with desired mass-to-charge ratio (m/z) will not hit any of the rods and can pass through the ion trap.

The original configuration of the quadrupole ion trap is the 3D ion trap, which is also known as the “Paul trap” (Figure 1.8).⁶³ Here, the 3D quadrupole ion trap is made up of three circular electrodes: one ring electrode and two cap electrodes. The fourth rod is reduced to a point.

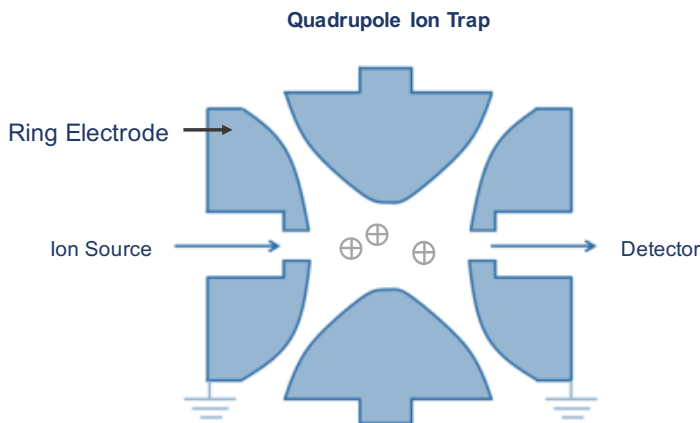


Figure 1.8 Paul Trap

Another embodiment of the quadrupole ion trap is the 2D ion trap, or the linear ion trap. The 2D ion trap was reported to be of improved trapping efficiency, simplicity of construction and increased ion capacity. Tandem mass analysis can be conducted on both 2D and 3D quadrupole ion traps.

Our group uses a modified Finnigan LCQ DUO (ESI-3D quadrupole ion trap) mass spectrometer for bracketing and gas-phase reaction kinetic study. We use both a Finnigan LCQ DUO (ESI-3D quadrupole ion trap) mass spectrometer and a Finnigan LTQ (ESI-linear quadrupole ion trap) mass spectrometer for Cooks kinetic experiments.

1.2.4 Modified Finnigan LCQ DUO Mass Spectrometer

As described in section 1.2.3, our Thermo Finnigan LCQ (ESI-3D quadrupole ion trap) mass spectrometer was utilized for bracketing experiments and gas-phase reaction kinetic studies. The 3D-quadrupole ion trap is used as a mass spectrometer as well as a gas-phase reaction container, wherein reactions of charged species with neutral gaseous molecules can be investigated. Ions are generated by ESI, and neutral compounds are introduced to

the ion trap with the flow of damping helium gas. Two leak valves are installed on the helium gas line to mix the vapor of neutral compounds with helium gas flow (Figure 1.9).

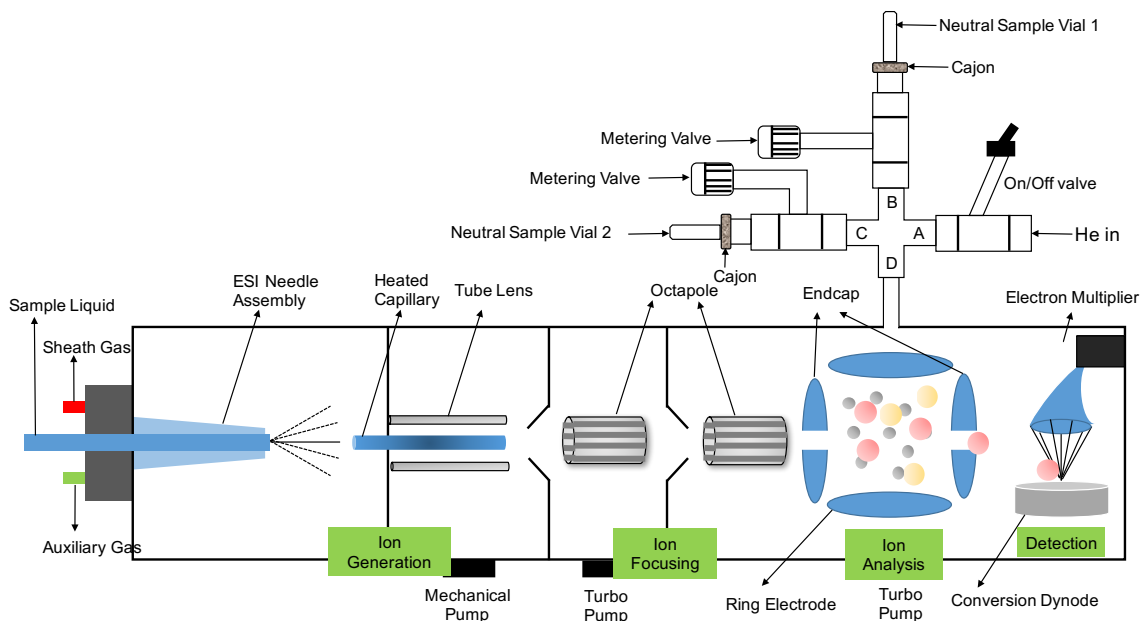


Figure 1.9 Modified Finnigan LCQ DUO Mass Spectrometer

1.3 Methodology

1.3.1 Reaction Kinetics Using FT-ICR Mass Spectrometer

Mass spectrometry is a powerful tool for studying kinetics of an ion reacting with a neutral molecule in the gas phase. The Finnigan 2001 FT-ICR mass spectrometer with the dual cell setup is used to conduct the experiments for kinetic research.

Rate constant k for the reaction of interest is measured by an FT-ICR mass spectrometer. The charged reagents are generated in one cell, called the source cell, via chemical ionization (CI) or electron ionization (EI) of vapor of a neutral precursor. The neutral reagents are introduced into a second cell, the analyzer cell via the batch inlet or leak valve.

The ions are then transferred from the source cell to the analyzer cell and trapped. A pulse of unreactive argon gas in the analyzer cell is used to cool down the ions. Then, the ions are allowed to react with the neutral molecules for varying reaction times, after which all the charged species are detected by mass spectrometry. The concentration of the neutral molecules in analyzer cell is kept constant and in excess. As a result, the reaction is under *pseudo*-first condition (Eq. 1.4).

$$\text{Pseudo-first order reaction rate: } r = k[\text{Neutral}][\text{ion}] = k_{obs}[\text{ion}] \quad \text{Eq. 1.4}$$

The reaction rate constant can be derived by plotting decrease in relative intensity of ion peaks against reaction time.

In order to increase the precision of kinetic measurements, a relative reaction rate constant measurement can be conducted, where two ions are allowed to react with the same neutral reagent. The relative reaction rate constant k_{rel} can be calculated without measuring the pressure of the neutral compound. For example, in the research project of quantifying gas-phase nucleophilicity of amines and electrophilicity of benzhydryl cations, two electrophilic carbocations were allowed to react with an amine nucleophile under the same conditions.

1.3.2 Reaction Kinetics Using LCQ (ESI-Quadrupole Ion Trap)

A similar reaction kinetic studies can be performed on the modified Finnigan LCQ DUO (ESI-quadrupole ion trap) mass spectrometer. As described in section 1.2.4, neutral molecules are introduced into the ion trap with the helium gas flow. Ions are generated and

introduced into the ion trap via ESI from a solution of the analytes. The ions are allowed to react with the neutral compounds for varying reaction times.

1.3.3 Bracketing Method

The bracketing method is used to measure the proton affinity (PA) and gas-phase acidity of organic bases and acids, respectively. Organic bases or acids with known proton affinities or acidities are used as references to “bracket” the corresponding thermodynamic property (PA or acidity) of the sample compounds into a narrow range (2-4 kcal/mol). Proton transfer reactions between a reference compounds and a sample compound are then studied. For example, if a reference base B_1 is unable to deprotonate the conjugated acid of the sample compound, but another reference base B_2 can; the resulting PA of the sample is *higher* than PA of B_1 and *lower* than that of B_2 . With the assumption of proton transfer reaction being barrier-free, reaction efficiency in the gas phase (Eq. 1.5) is used to determine whether a proton transfer reaction occurs or not, with a cutoff of 10%.

$$\text{efficiency (\%)} = \frac{k_{exp}}{k_{coll}} \times 100\% \quad \text{Eq. 1.5}$$

Herein, k_{exp} (experimental rate constant) is measured by the reaction kinetics study, as introduced in section 1.3.1; k_{coll} (collision rate constant) is defined as the theoretical ion-molecule collision rate constant and is calculated by an Average Dipole Orientation (ADO) program.^{64,65} An efficiency higher than 10% indicates the occurrence of proton transfer while an efficiency lower than 10% means there is no efficient proton transfer.

Bracketing experiments are performed using both our FT-ICR mass spectrometer and

the modified LCQ (ESI-quadrupole ion trap), described in sections 1.3.1 and 1.3.2, respectively.

1.3.4 Cooks Kinetic Method

First developed by Cooks in 1977, the Cooks kinetic method is another technique to measure proton affinity (PA) and gas phase acidity of organic compounds using mass spectrometers.⁶⁶ Thermodynamic properties, such as PA and acidity, can be obtained from the dissociation pattern of a proton-bound dimer. For example, after isolating the proton-bound dimer between a sample base B and a reference base B_{ref} (with known proton affinity), collision-induced dissociation (CID) energy is applied and the dimer can be dissociated by two different pathways: forming a protonated B and a neutral B_{ref}, or yielding a protonated B_{ref} and a neutral B. The relative intensity of two product ion peaks can be used to calculate the proton affinity of B.⁶⁷⁻⁶⁹

1.3.5 Computational Method

Computational methods are used to study the thermodynamic properties and structural information of molecules described in this dissertation. All ground state calculations were performed using density functional theory (B3LYP/6-31+G(d)) as implemented in Gaussian09.⁷⁰⁻⁷⁵ All the geometries were fully optimized and frequencies were calculated; no scaling factor was applied. The optimized structures had no negative frequencies. The temperature for the calculations was set to be 298 K. For the TS calculations for solution systems, the SMD model was used and M06/6-31+G(d,p) solution-phase single-point

energy calculations (on the B3LYP/6-31+G(d) geometry) were conducted. Reported energetics represent the sum of the Gibbs free energy correction at B3LYP/6-31+G(d) applied to the solution-phase single-point energy at M06/6-31+G(d,p).

1.4 References

- (1) Moon, J. H.; Yoon, S.; Bae, Y. J.; Kim, M. S. *Mass Spectrom. Rev.* **2015**, *34*, 94.
- (2) Palii, S. P.; *John Wiley & Sons Ltd.*, **2014**, p 65.
- (3) Nibbering, N. M. M. *Int. J. Mass Spectrom.* **2015**, *377*, 10.
- (4) Chen, C.-C.; Lin, P.-C., *Anal. Methods*, **2015**, *7*, 6947.
- (5) Richardson, D. E.; Plattner, D. A.; *Elsevier Ltd.*: **2007**; Vol. 1, p 801.
- (6) Ingold, C. K., *J. Chem. Soc.* **1933**, 1120.
- (7) Swain, C. G.; Scott, C. B. *J. Am. Chem. Soc.* **1953**, *75*, 141.
- (8) Ritchie, C. D. *Acc. Chem. Res.* **1972**, *5*, 348.
- (9) Mayr, H.; Patz, M. *Angew. Chem. Int. Ed.* **1994**, *33*, 938.
- (10) Mayr, H.; Ofial, A., *J. Phys. Org. Chem.* **2008**, *21*, 584.
- (11) Mayr, H.; Ofial, A., *Pure Appl. Chem.* **2005**, *77*, 1807.
- (12) Mayr, H.; Kempf, B.; Ofial, A., *Acc. Chem. Res.* **2003**, *36*, 66.
- (13) Denekamp, C.; Sandler, Y. *Angew. Chem. Int. Ed.* **2006**, *45*, 2093.
- (14) IUPAC, *Compendium of Chemical Terminology*, 2nd ed. (the "Gold Book"), **1997**.
- (15) Anslyn, E. V.; Dougherty, D. A. *Modern Physical Organic Chemistry* University Science Books, **2006**.
- (16) Igau, A.; Grutzmacher, H.; Baceiredo, A.; Bertrand, G. *J. Am. Chem. Soc.* **1988**, *110*, 6463.
- (17) Arduengo, A. J. I.; Harlow, R. L.; Kline, M. *J. Am. Chem. Soc.* **1991**, *113*, 361.
- (18) Sharma, S.; Lee, J. K. *J. Org. Chem.* **2002**, *67*, 8360.
- (19) Lee, J. K. *Int. J. Mass. Spectrom.* **2005**, 240.
- (20) Kurinovich, M. A.; Lee, J. K. *J. Am. Soc. Mass. Spectrom.* **2002**, *13*, 985.
- (21) NIST Chemistry WebBook, NIST Standard Reference Database Number 69; retrieved in 2011. Linstrom, P. J.; Mallard, W. G., Eds.; National Institute of Standards and Technology: Gaithersburg, MD 20899, <http://webbook.nist.gov>.
- (22) Huisgen, R.; Szeimies, G.; Mobius, L. *Chem. Ber.* **1967**, *100*, 2494.
- (23) Kolb, H. C.; Finn, M. G.; Sharpless, K. B. *Angew. Chem. Int. Ed.* **2001**, *40*, 2004.
- (24) Kolb, H. C.; Sharpless, K. B. *Drug Discovery Today* **2003**, *8*, 1128.
- (25) Bock, V. D.; Hiemstra, H.; van Maarseveen, J. H. *Eur. J. Org. Chem.* **2005**, *1*, 51.
- (26) Whiting, M.; Muldoon, J.; Lin, Y.-C.; Silverman, S. M.; Lindstrom, W.; Olson, A. J.; Kolb, H. C.; Finn, M. G.; Sharpless, K. B.; Elder, J. H.; Fokin, V. V. *Angew. Chem. Int. Ed.* **2006**, *45*, 1435.
- (27) Bock, V. D.; Speijer, D.; Hiemstra, H.; van Maarseveen, J. H. *Org. Biomol. Chem.* **2007**, *5*, 971.
- (28) Ye, C.; Gard, G. L.; Winter, R. W.; Syvret, R. G.; Twamley, B.; Shreeve, J. M. *Org. Lett.* **2007**, *9*, 3841.
- (29) Struble, J. R.; Kaeobamrung, J.; Bode, J. W. *Org. Lett.* **2008**, *10*, 957.

- (30) Welton, T. *Chem. Rev.* **1999**, *99*, 2071.
- (31) Formentin, P.; Garcia, H.; Leyva, A. *J. Mol. Catal. A: Chemical* **2004**, *214*, 137.
- (32) Wasserscheid, P.; Keim, W. *Angew. Chem. Int. Ed. Engl.* **2000**, *39*, 3772.
- (33) Dupont, J.; Spencer, J. *Angew. Chem. Int. Ed. Engl.* **2004**, *43*, 5296.
- (34) Debray, J.; Leveque, J.-M.; Philouze, C.; Draye, M.; Demeunynck, M. *J. Org. Chem.* **2010**, *75*, 2092.
- (35) Scholl, M.; Ding, S.; Lee, C. W.; Grubbs, R. H. *Org. Lett.* **1999**, *1*, 953.
- (36) Enders, D.; Niemeier, O.; Balensiefer, T., *Angew. Chem. Int. Ed.* **2006**, *45*, 1463.
- (37) Seebach, D., *Angew. Chem. Int. Ed. Engl.* **1979**, *18*, 239.
- (38) Gröbel, B. T.; Seebach, D., *Synthesis* **1977**, *5*, 357.
- (39) Seebach, D. *Angew. Chem. Int. Ed.* **1979**, *18*, 239.
- (40) Flanigan, D.; Romanov-Michailidis, F.; White, N. A.; Rovis, T., *Chem. Rev.* **2015**, *115*, 9307.
- (41) Ukai, T.; Tanaka, S.; Dokawa, S. *J. Pharm. Soc. Jpn.* **1943**, *63*, 296.
- (42) Lapworth, A. *J. Chem. Soc.* **1903**, *83*, 995.
- (43) Breslow, R. *J. Am. Chem. Soc.* **1958**, *80*, 3719.
- (44) Mizuhara, S.; Handler, P. *J. Am. Chem. Soc.* **1954**, *76*, 571.
- (45) Stetter, H.; Raemsch, R. Y.; Kuhlmann, H. *Synthesis* **1976**, *11*, 733.
- (46) Stetter, H.; Kuhlmann, H. *Organic Reactions* **1991**, *40*, 407.
- (47) Enders, D.; Breuer, K.; Runsink, J.; Teles, J. H., *Helvetica Chimica Acta* **1996**, *79*, 1899.
- (48) Kerr, M. S.; Read de Alaniz, J.; Rovis, T., *J. Am. Chem. Soc.* **2002**, *124*, 10298.
- (49) Kerr, M. S.; Rovis, T., *J. Am. Chem. Soc.* **2004**, *126*, 8876.
- (50) Arduengo, A. J. I.; Dias, H. V. R.; Harlow, R. L.; Kline, M. *J. Am. Chem. Soc.* **1992**, *114*, 5530.
- (51) Hopkinson, M. N.; Richter, C.; Schedler, M.; Glorius, F. *Nature* **2014**, *510*, 485.
- (52)
- (53) Tian, Y.; Lee, J. K. *J. Org. Chem.* **2015**, *80*, 6831.
- (54) Zeng, H.; Wang, K.; Tian, Y.; Niu, Y.; Greene, L.; Hu, Z.; Lee, J. K. *Int. J. Mass. Spec.* **2015**, *378*, 169.
- (55) Comisarow, M. B.; Marshall, A. G. *Chem. Phys. Lett.* **1974**, *25*, 282.
- (56) Amster, I. J. *J. Mass Spectrom.* **1996**, *31*, 1325.
- (57) Lawrence, E. O.; Edlefsen, N. E. *Science* **1930**, *72*, 376.
- (58) Marshall, A. G.; Grosshans, P. B. *Anal. Chem.* **1991**, *63A*, 215.
- (59) Yamashita, M.; Fenn, J. B. *Phys. Chem.* **1988**, *88*, 4451.
- (60) Yamashita, M.; Fenn, J. B. *Phys. Chem.* **1988**, *88*, 4671.
- (61) Kebarle, P.; Tang, L. *Anal. Chem.* **1993**, *65*, 972A.
- (62) Douglas, D. J.; Frank, A. J.; Mao, D. *Mass Spec. Rev.* **2005**, *24*, 1.
- (63) Paul, W. *Angew. Chem.* **1990**, *102*, 780.

- (64) Chesnavich, W. J.; Su, T.; Bowers, M. T. *J. Chem. Phys.* **1980**, *72*, 2641.
- (65) Su, T.; Chesnavich, W. J. *J. Chem. Phys.* **1982**, *76*, 5183.
- (66) Cooks, R. G.; Kruger, T. L. *J. Am. Chem. Soc.* **1977**, *99*, 1279.
- (67) MuLucky, S. A.; Cameron, D.; Cooks, R. G. *J. Am. Chem. Soc.* **1981**, *103*, 1313.
- (68) Brodbelt-Lustig, J. S.; Cooks, R. G. *Talanta* **1989**, *36*, 255.
- (69) Green-Church, K. B.; Limbach, P. A. *J. Am. Chem. Soc. Mass Spectrom.* **2000**, *11*, 24.
- (70) GAUSSIAN09, R. A.; Frisch, M. J.; Trucks, G. W.; Schlegel, H. B.; Scuseria, G. E.; Robb, M. A.; Cheeseman, J. R.; Scalmani, G.; Barone, V.; Mennucci, B.; Petersson, G. A.; Nakatsuji, H.; Caricato, M.; Li, X.; Hratchian, H. P.; Izmaylov, A. F.; Bloino, J.; Zheng, G.; Sonnenberg, J. L.; Hada, M.; Ehara, M.; Toyota, K.; Fukuda, R.; Hasegawa, J.; Ishida, M.; Nakajima, T.; Honda, Y.; Kitao, O.; Nakai, H.; Vreven, T.; Montgomery, J., J. A.; Peralta, J. E.; Ogliaro, F.; Bearpark, M.; Heyd, J. J.; Brothers, E.; Kudin, K. N.; Staroverov, V. N.; Kobayashi, R.; Normand, J.; Raghavachari, K.; Rendell, A.; Burant, J. C.; Iyengar, S. S.; Tomasi, J.; Cossi, M.; Rega, N.; Millam, J. M.; Klene, M.; Knox, J. E.; Cross, J. B.; Bakken, V.; Adamo, C.; Jaramillo, J.; Gomperts, R.; Stratmann, R. E.; Yazyev, O.; Austin, A. J.; Cammi, R.; Pomelli, C.; Ochterski, J. W.; Martin, R. L.; Morokuma, K.; Zakrzewski, V. G.; Voth, G. A.; Salvador, P.; Dannenberg, J. J.; Dapprich, S.; Daniels, A. D.; Farkas, Ö.; Foresman, J. B.; Ortiz, J. V.; Cioslowski, J.; Fox, D. J., Gaussian, Inc., Wallingford CT, 2009.
- (71) Lee, C.; Yang, W.; Parr, R. G. *Phys. Rev. B* **1988**, *37*, 785.
- (72) Kohn, W.; Becke, A. D.; Parr, R. G. *J. Phys. Chem.* **1996**, *100*, 12974.
- (73) Becke, A. D. *J. Chem. Phys.* **1993**, *98*, 5648.
- (74) Becke, A. D. *J. Chem. Phys.* **1993**, *98*, 1372.
- (75) Stephens, P. J.; Devlin, F. J.; Chabalowski, C. F.; Frisch, M. J. *J. Phys. Chem.* **1994**, *98*, 11623.

Note: Major parts of this chapter have been submitted to the *Journal of the American Chemical Society*: Niu, Y.; Chen, M.; Xu, J.; Lee, J. K. "Nucleophilicity and Electrophilicity in the Gas Phase: Challenges and Solutions", *J. Am. Chem. Soc.*, **2017**, submitted.

Chapter 2. Gas Phase Studies of Nucleophilicity and Electrophilicity

2.1 Introduction

Reactivity prediction is the cornerstone of rational organic chemical and synthetic design. The quantification of "nucleophilicity" and "electrophilicity" has a long and rich history. Swain and Scott were the first to attempt systematic quantification through the study of S_N2 rates.¹ Other contributions followed, along with frustration; in 1968 Pearson and coworkers declared "at present it is not possible to predict quantitatively the rates of nucleophilic displacement reactions when a number of substrates of widely varying properties are considered."²⁻⁵ This was followed four years later by the important discovery, by Ritchie, that for reactions of carbocations and diazonium ions with nucleophiles, a constant parameter for a given nucleophile can be defined. This parameter, which was called " N_+ ", is not dependent on the electrophile identity.⁶ Several years later, Kane-Maguire, Honig and Sweigart established an " N_{Fe} " scale for nucleophilic additions to metal-coordinated pi-electron systems.⁷

Since these early discoveries, the Mayr group has, without question, made the most important contributions toward a general nucleophilicity-electrophilicity scale.⁸ For correlation analysis, Mayr and coworkers use the following Eq. 2.1:

$$\log(k_2) = s_N \cdot (E + N) \quad \text{Eq. 2.1}$$

where k_2 is the rate constant for the reaction of an electrophile with a nucleophile; s_N is a "nucleophile-specific slope parameter"; E is an electrophilicity parameter and N is a nucleophilicity parameter. Application of this equation to a wide range of systems has yielded a database that currently contains reactivity parameters for over one thousand nucleophiles and nearly three hundred electrophiles.⁹

All values in the Mayr database were obtained in solution. Mayr has shown that for reactions of charged electrophiles with neutral π -nucleophiles and hydride donors, solvent effects are marginal.¹⁰ The argument is that solvent effects on the cationic reagents and the positively charged activated complexes are similar. Small differences of the solvation energies are covered by the noise of the correlations. However, other reactions of electrophiles with nucleophiles do show solvent dependence; diazonium ion electrophiles are influenced by solvent and certain nucleophiles such as alcohols, amines and several types of carbanions have " N " values that are greatly solvent dependent.

We explore nucleophilicity and electrophilicity in the gas phase, with the goal of ultimately building a database of intrinsic reactivity parameters, which would allow one to better understand both inherent reactivity and the influence of solvation on reactivity. One

prior study from more than a decade ago applied the Mayr equation to a series of reactions in the gas phase, but with a limited set of nucleophiles, and no further work has been done in this area.¹¹ We examined the reactions of fourteen amine nucleophiles with five benzhydryl cations. We are able to establish, through kinetic isotope effect studies, that the product of the reaction is the expected covalent complex. Comparison of our kinetic data with that in solution reveal limitations in this gas phase system; an improved model is then proposed.

2.2 Experimental

Amines and benzhydryl alcohols were purchased from Sigma-Aldrich and used as received. The deuterated benzhydryl alcohol precursor was synthesized following a literature procedure.¹² Gas phase experiments for the amines plus the benzhydryl cations were conducted using a Fourier Transform Ion Cyclotron Resonance Mass Spectrometer (FTMS) with a dual cell setup, which has been described previously.¹³

In our FTMS, two adjoining 1-inch. cubic cells are positioned collinearly with the magnetic field produced by a 3.3 T superconducting magnet. The pressure of the dual cell is pumped down to less than 1×10^{-9} Torr. Solid benzhydryl alcohols are introduced into the cell via a heatable solids probe (typical temperature is 50°C). The corresponding benzhydryl cations are generated via reaction with hydronium ions. Hydronium ions are produced by pulsing water into the cell, ionizing by an electron beam (typically 20 eV and 6 μ A, ionization time 0.5 s). Liquid amines are introduced via the batch inlet system.

For the reactions between the electrophiles and nucleophiles, benzhydryl cations are generated from alcohol via reaction with hydronium ion, selected, and transferred to another adjoining cell via a 2-mm hole in the center of the central trapping plate, cooled by a pulse of argon (that raises the cell pressure to 10^{-5} Torr), and then allowed to react with amine nucleophiles.

Gas phase experiments for the ethyl cation and tert-butyl cation with benzhydrol were also conducted using FTMS. Ethyl cation and tert-butyl cation are generated from iodoethane and 2-iodo-2-methylpropane, respectively, via electron ionization (EI). The reactant cation is then selected and transferred to the adjoining cell, cooled by a pulse of argon (that raises the cell pressure to 10^{-5} Torr) and allowed to react with benzhydrol.

We run all these reactions under pseudo-first order conditions, where the amount of the neutral is in excess relative to the reacting ions. Reading the pressure from an ion gauge is often unreliable, both because of the gauge's remote location as well as varying sensitivity for different substrates.^{14,15} We therefore "back out" the neutral pressure from a control reaction (described previously).^{16,17} As noted in the manuscript text, we also conducted "relative" rate constant measurements. For these experiments, a mixture of benzhydryl alcohols was vaporized using the solids probe, and ionized with hydronium. The resultant two benzhydryl cations were then allowed to react with a given amine in competing reactions, obviating the need to know the amine pressure. For all rate constants, we also calculate an efficiency, which is the ratio of the experimentally observed rate

constant divided by a theoretical collisional rate constant obtained from trajectory theory.

18-20

2.3 Results and Discussion

2.3.1 Substrates Studied

We examined the gas phase kinetics for the reaction of fourteen amine-based nucleophiles with five electrophiles. Propylamine, cyclohexylamine, aniline, benzylamine, piperidine, pyrrolidine, morpholine, diisopropylamine, diethylamine, N-methylpiperidine, N-methylpyrrolidine, pyridine, triethylamine and 1,4-diazabicyclo[2.2.2]octane (DABCO) were all allowed to react with para-substituted benzhydryls **1** ($X = \text{OCH}_3$, CH_3 , H , Cl , and CF_3) (Figure 2.1). The use of the Mayr equation 2.1 requires the definition of a reference electrophile and reference nucleophile; for us these are, respectively, the parent benzhydryl cation **1c** and piperidine.

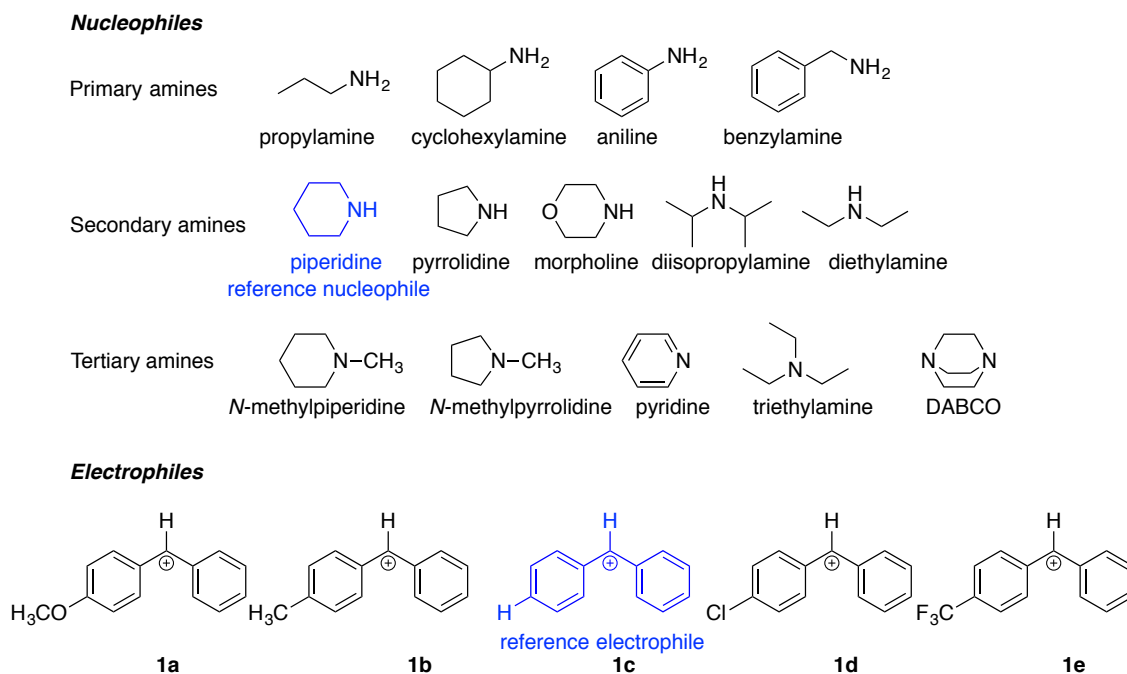


Figure 2.1 Nucleophiles and electrophiles studied

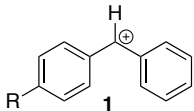
2.3.2 Assessing Electrophilicity

Following the Mayr equation 2.1, our first step is to assess electrophilicity. In solution, to obtain "*E*" values, one allows the reference nucleophile to react with varying electrophiles. In our case, this would be piperidine reacting with electrophiles **1a-1e**. We conducted these reactions, and measured the rate constants in the gas phase. To reduce error in the measurements, we conducted "relative" rate constant measurements. In a given experiment, we allowed two cations to react with piperidine, where one cation (the parent benzhydryl **1c**) is the reference cation. The reported rate constants (Table 2.1) are derived by multiplying the relative value with the absolute rate constant derived from the reaction of **1c** with piperidine. Typically rate constants in the gas phase are reported with the units $\text{cm}^3/\text{molecule}\cdot\text{s}$, but because the solution phase analysis uses the bimolecular rate constant

unit of L/mol·s, we do the same herein.

In order to obtain an "apparent gas phase electrophilicity" $E_{gas,app}$, each rate constant k is divided by k_{ref} , which is the rate constant for the reaction of the reference nucleophile piperidine with the reference electrophile **1c**. The $E_{gas,app}$ value for each electrophile is $\log (k/k_{ref})$. As can be seen from Table 2.1, as the substituent R becomes more electron withdrawing (moving down the table), the apparent electrophilicity parameter $E_{gas,app}$ increases, as would be expected since the electrophiles are becoming more electrophilic.

Table 2.1 Rate constant and $E_{gas,app}$ data for the reaction of electrophiles with the reference nucleophile, piperidine

Electrophile  1	k^a	$E_{gas,app}$
1a (R = OCH ₃)	4.81×10^{10}	-0.57
1b (R = CH ₃)	1.19×10^{11}	-0.18
1c (R = H)	1.79×10^{11}	0.00
1d (R = Cl)	2.11×10^{11}	+0.07
1e (R = CF ₃)	3.21×10^{11}	+0.25

^a Rate constant is for the reaction of each electrophile with the reference nucleophile, piperidine, in L/mol·s

2.3.3 Obtaining " k_2 "

The next step is to obtain the rate constants for the reactions of the fourteen nucleophiles with the five electrophiles; these data are compiled in Table 2.2. For each nucleophile, these are also derived from relative rate constant reactions, where the reference cation is **1c**. Table 2.2 also lists the efficiency for each reaction, which is the ratio of the experimental rate constant to the collisional rate constant.

Table 2.2 Rate constants (k_2) and efficiencies (% , in parentheses) for the reactions of nucleophiles and electrophiles^a

	1a	1b	1c	1d	1e
propylamine	3.17×10^9 (0.4)	1.64×10^{10} (2.1)	3.46×10^{10} (4.3)	4.24×10^{10} (5.4)	1.34×10^{11} (17.3)
cyclohexylamine	4.77×10^9 (0.6)	2.98×10^{10} (3.6)	8.67×10^{10} (10.6)	1.04×10^{11} (13.1)	2.04×10^{11} (26.4)
Aniline	N/A ^b	2.11×10^8 (0.03)	2.20×10^9 (0.3)	2.78×10^9 (0.4)	2.28×10^{10} (3.0)
benzylamine	5.09×10^9 (0.6)	3.77×10^{10} (4.6)	8.97×10^{10} (10.8)	1.25×10^{11} (15.5)	2.34×10^{11} (29.8)
piperidine	4.81×10^{10} (6.3)	1.19×10^{11} (15.4)	1.79×10^{11} (22.8)	2.11×10^{11} (27.7)	3.21×10^{11} (43.1)
pyrrolidine	1.46×10^{10} (2.0)	5.38×10^{10} (7.2)	7.71×10^{10} (10.2)	9.27×10^{10} (12.6)	1.51×10^{11} (21.0)
morpholine	1.69×10^9 (0.2)	1.20×10^{10} (1.4)	4.11×10^{10} (4.6)	5.29×10^{10} (6.1)	1.07×10^{11} (12.7)
diisopropylamine	1.13×10^9 (0.2)	1.36×10^{10} (1.7)	3.52×10^{10} (4.4)	6.86×10^{10} (9.0)	1.31×10^{11} (17.5)
diethylamine	5.42×10^9 (0.7)	2.62×10^{10} (3.5)	5.65×10^{10} (7.4)	7.71×10^{10} (10.3)	1.54×10^{11} (21.1)
<i>N</i> -methylpiperidine	3.38×10^9 (0.5)	2.37×10^{10} (3.3)	6.20×10^{10} (8.6)	1.01×10^{11} (14.6)	1.89×10^{11} (27.8)
<i>N</i> -methylpyrrolidine	8.73×10^9 (1.3)	3.93×10^{10} (5.9)	7.95×10^{10} (11.8)	1.02×10^{11} (15.7)	2.41×10^{11} (37.0)
pyridine	1.16×10^{10} (1.1)	5.66×10^{10} (5.4)	8.43×10^{10} (8.0)	1.25×10^{11} (12.2)	1.91×10^{11} (19.0)
triethylamine	N/A ^b	2.30×10^9 (0.3)	1.63×10^{10} (2.3)	2.44×10^{10} (3.6)	6.50×10^{10} (9.8)
DABCO	4.89×10^{10} (8.0)	1.19×10^{11} (19.2)	2.08×10^{11} (33.0)	2.56×10^{11} (42.1)	N/A ^c

^a Rate constant is for the reaction of each electrophile with the reference nucleophile,

piperidine, in L/mol·s. ^b The reactions of **1a** with aniline and trimethylamine were too

slow to measure under our conditions. ^c Weak signal precluded data collection.

2.3.4 Obtaining " N " and " s_N "

With the data in Tables 2.1 and 2.2 in hand, plots of the $\log k_2$ versus $E_{\text{gas},\text{app}}$ can be used to obtain the nucleophilicity parameter N and the nucleophile-specific slope parameter s_N , using Eq. 2.1 (Figure 2.2). For each line, the slope yields the s_N and the y-intercept is $s_N N$. These lines and their slopes, however, are most likely not reflective of nucleophilicity, which I will discuss further in 2.3.6.

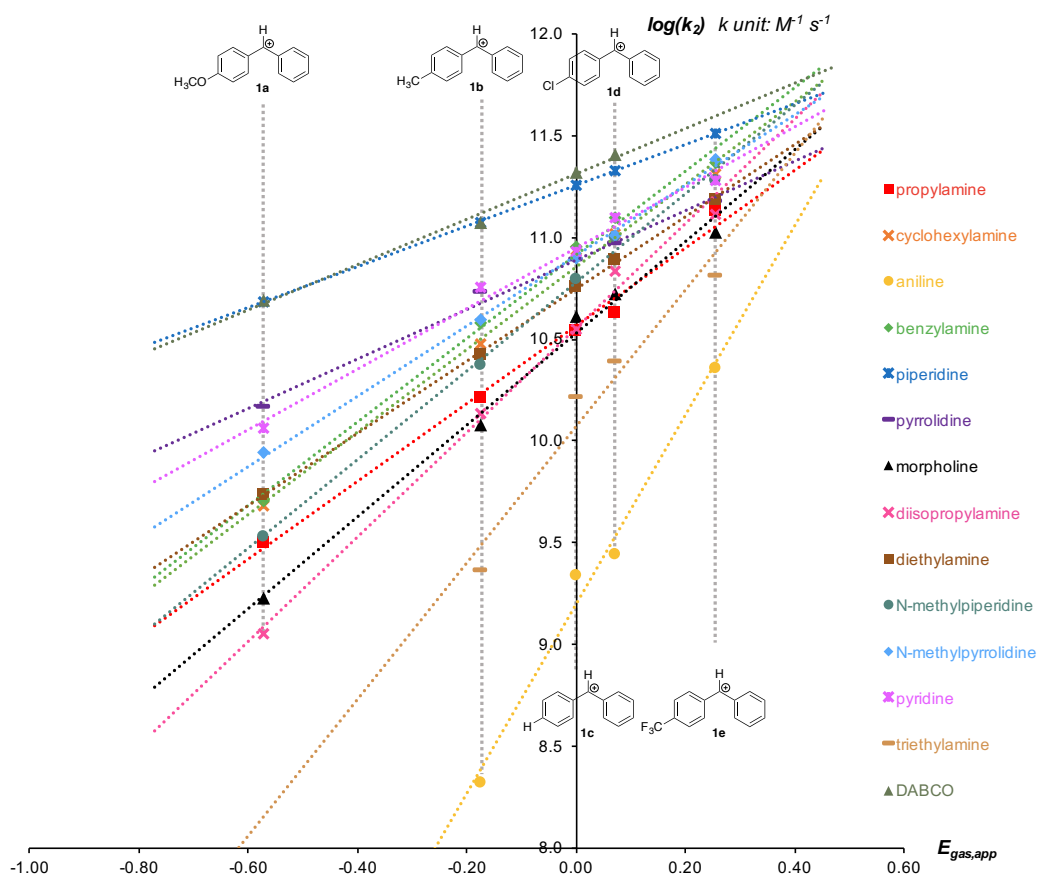


Figure 2.2 Plots of $\log(k_2)$ versus $E_{\text{gas},\text{app}}$ in the gas phase

2.3.5 Nature of The Product

One key concern is the nature of the products formed upon reactions of the amines with the electrophiles in the gas phase. The desired product from the reaction of the benzhydryl cations with the amine nucleophiles is the covalent complex shown in Figure 2.3.

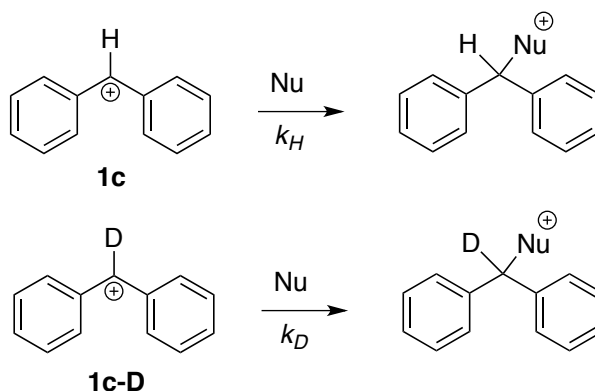


Figure 2.3 Experiments used to ascertain kinetic isotope effects

However, since our detection method is mass spectrometry, we simply track the mass-to-charge (m/z) ratio corresponding to the covalent complex, and do not know whether the structure is what we expect, or some other noncovalent or nonspecific complex. To gain insight into the structure of the product, we conducted kinetic isotope effect studies. Our expectation is that if nucleophilic attack occurs as shown in Figure 2.3, the k_H/k_D for the reaction of **1c** versus **1c-D** should be inverse (< 1.0), as the reactive center is changing hybridization from sp^2 to sp^3 . We synthesized **1c-D** and conducted KIE experiments by measuring the rate constants k_H and k_D for various nucleophiles. To reduce error, relative rate constant experiments were conducted, with the methyl-substituted benzhydryl cation

1b as the reference. It was found that the KIEs for benzhydryl cation **1c** with three of our amine nucleophiles (primary propylamine, secondary piperidine and tertiary *N*-methylpiperidine), are all inverse (less than 1, Table 2.3). This is consistent with nucleophilic attack at the central carbon, and not consistent with a noncovalent/nonspecific complex. Furthermore, the KIE values (around 0.8) are consistent with those found in solution for these types of reactions.²¹

Table 2.3 KIE data for the reaction of **1c** versus **1c-D** with nucleophiles.

Nucleophile	KIE
propylamine	0.76
piperidine	0.81
<i>N</i> -methylpiperidine	0.86

2.3.6 Potential Problem with Current Reaction Model

What, if anything, do our gas phase parameters indicate? Can any conclusions be drawn by comparison to solution phase data? In Figure 2.4, we plot data corresponding to the reactions of a series of amines with electrophiles in the solvent acetonitrile.²²⁻²⁵

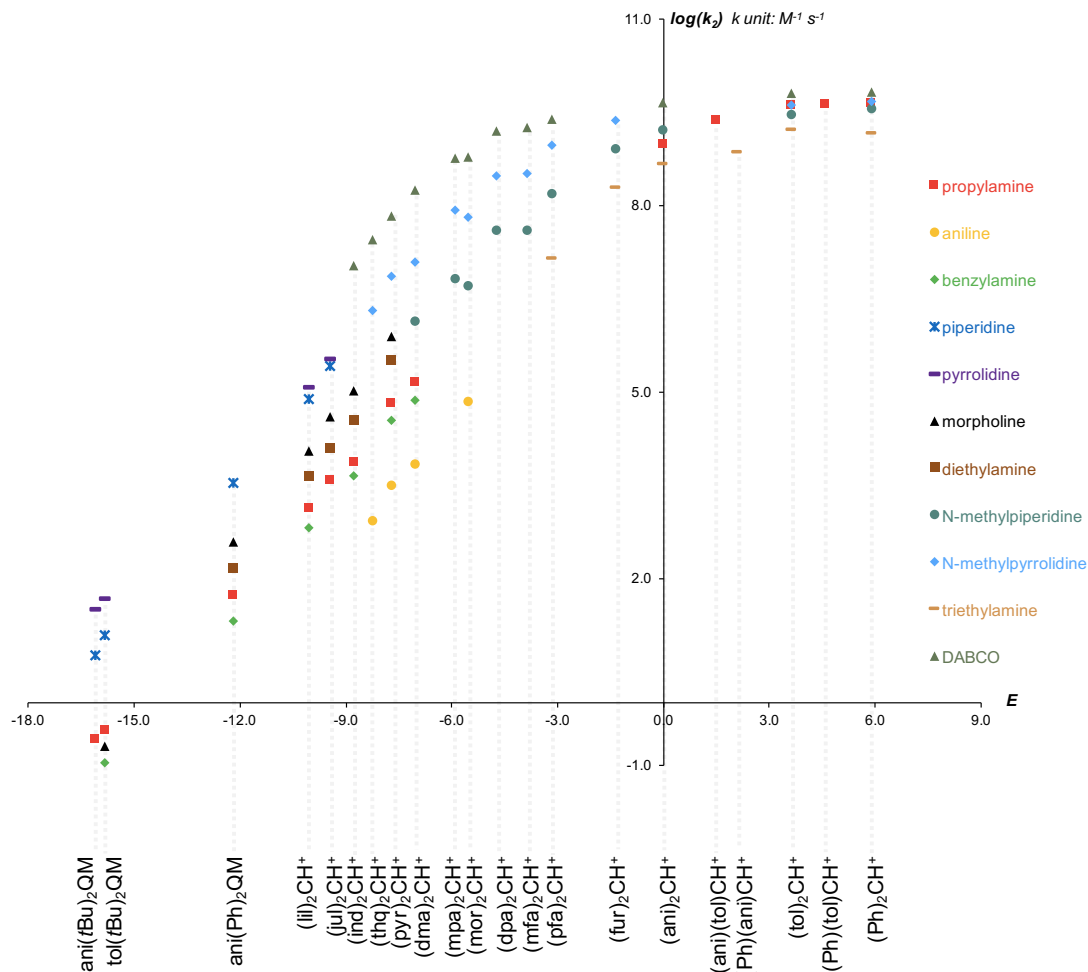


Figure 2.4 Plots of solutions-phase $\log k_2$ versus E in acetonitrile.²²⁻²⁵ The data can be found on the website: <http://www.cup.lmu.de/oc/mayr/reaktionsdatenbank/>

One intriguing feature of the gas phase versus the solution phase data is the measurable rate constant range. In the solution phase reaction of amines with electrophiles, reactions with the most electrophilic electrophiles will ultimately hit the diffusion limit. Thus in Figure 2.4, the plots all level off as electrophilicity increases (to the right, along the x-axis). Interestingly, all the data we obtained in the gas phase are for reactions that are in the diffusion limit region in acetonitrile. This observation immediately raised red flags for us:

an association reaction that is barrierless in solution would be expected to be barrierless in the gas phase. However, the rate constants we measured in the gas phase are not at the collision rate. If every collision resulted in reaction, the "efficiency" would be 100%; our reactions in the gas phase all have efficiencies of less than 50%.²⁶⁻²⁸

Another piece of evidence that our data are not reflective of electrophilicity and nucleophilicity in the gas phase is the lack of correlation between our data and that of the previous gas phase study (by Denekamp and Sandlers).¹¹ While that paper did not report absolute rate constants, we can plot their N values versus ours (obtained from Figure 2.2). We defined a different reference nucleophile and electrophile for our studies, but we would still expect our data and theirs to have a linear correlation, which clearly does not exist (Figure 2.5).

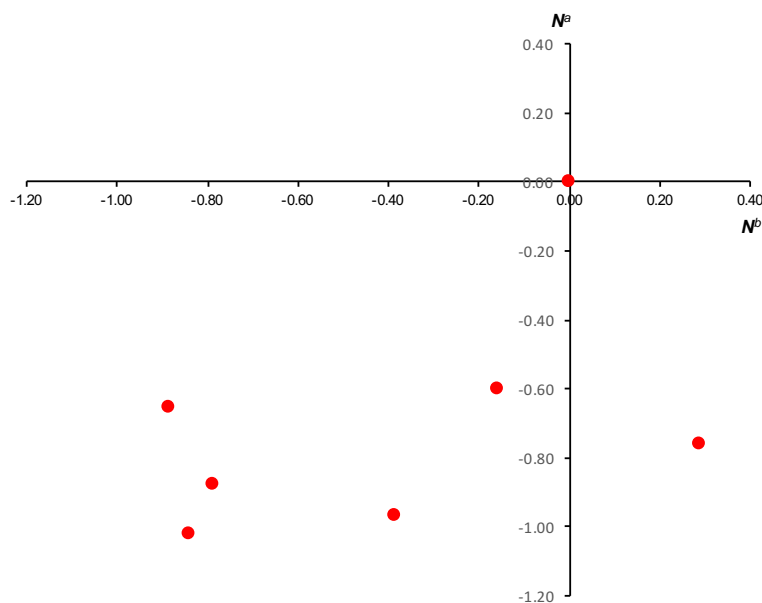


Figure 2.5 Plot of N values from this work (N^a) versus that from reference 11 (N^b)

One concern of both ours and that of the prior study is that the association of the electrophile and nucleophile is exothermic, and that dissipation of the excess energy thus rendered may be the slowest step in the reaction. That is, we may well have the situation shown in Figure 2.6, where the association step (Step 1) is barrierless, but the slow step - and the overall rate constant that we measure - reflects the energy dissipation (Step 2).

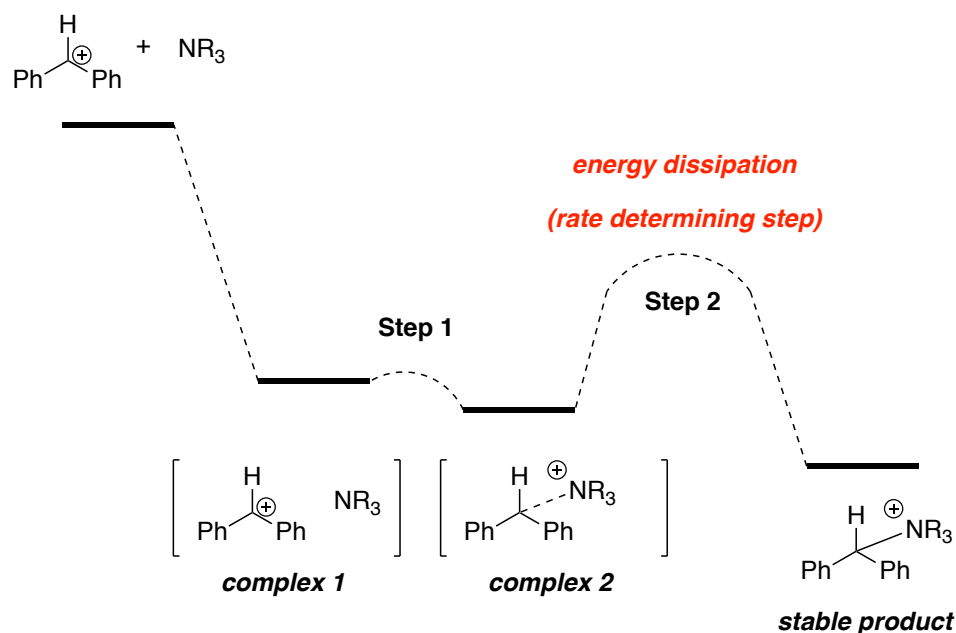


Figure 2.6 Energy surface depiction for benzhydryl cation reacting with amine in the gas phase

Our isotope effect studies do indicate that reaction occurs, and that we likely obtain the expected product. However, the low rate efficiencies and the lack of reproducibility of the N values provide evidence that any parameters obtained via this type of study are suspect, as they may not reflect the actual nucleophile-electrophile reactivity.

As an interesting aside, in terms of the electrophilicity parameter $E_{\text{gas,app}}$, a plot of the

electrophiles for which we have both gas phase and solution phase data shows a linear correlation (Figure 2.7). This linearity between respective E values was also observed in the prior gas phase studies.¹¹ The slope of this plot is not particularly meaningful; the $E_{gas,app}$ is by necessity defined by the reference nucleophile, and the slope will change with a different reference nucleophile. It is difficult to know whether this correlation implies electrophilicity is *relatively* the same in solution and in the gas phase, or the correlation simply somehow coincidentally reflects a similar dependence for electrophilicity in solution, but energy dissipation in the gas phase.

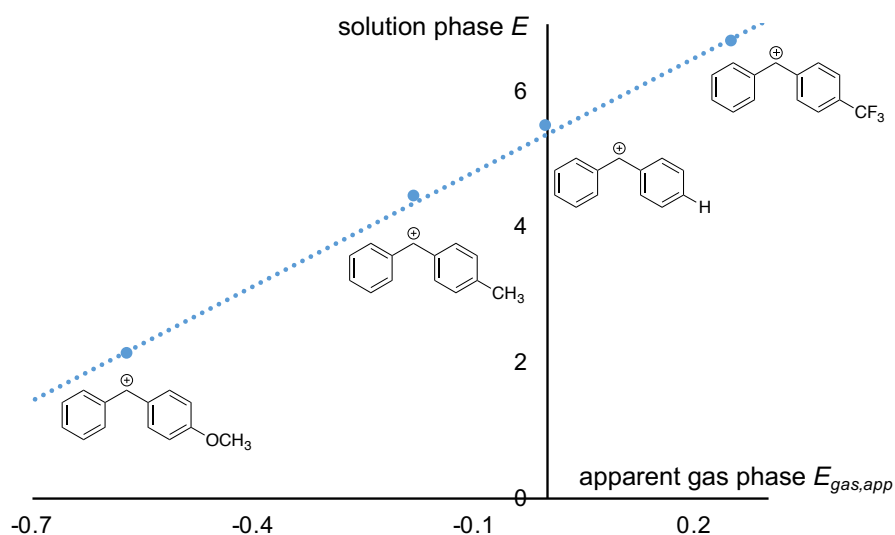


Figure 2.7 Solution phase E values versus gas phase $E_{gas,app}$ values

Also, we note that our KIE experiments are still valid and of interest; because we use mass spectrometry, we cannot be certain that our product m/z ratio corresponds to the

expected structure. We were able to show that the gas phase reaction between benzhydryl cation and amines does involve covalent attachment of the amine to the benzhydryl cation, not the formation of some other noncovalent complex. Our KIEs of roughly 0.8 are also consistent with those found in solution by Mayr and coworkers.²¹

2.3.7 *Alternative Models*

Having established that the gas phase study of association reactions between a nucleophile and electrophile may not reflect the respective nucleophilicity and electrophilicity, we sought to design appropriate systems for such studies. The main goal is to find a system where energy dissipation is not an issue. One way to do this is to build a system that would fragment after addition, to release excess energy. Pictorially this is shown in Figure 2.8. A nucleophile containing a moiety that will quickly fragment after association would solve the excess energy issue. The key is that the second step - fragmentation - is fast, such that the measured rate constant reflects the initial association reaction.

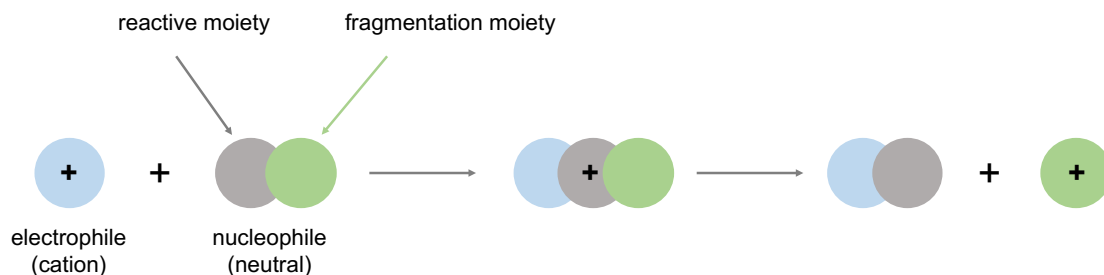


Figure 2.8 An improved model for gas phase nucleophilicity-electrophilicity studies:

fragmentation after complexation

Because the benzhydryl cation is so stable, we envisioned it as the fragmentation moiety (green sphere in Figure 2.8). This is more or less "converse" of the initial system we studied, where the benzhydryl cation is the electrophile. Now it is just a convenient fragmentation moiety. To establish the viability of this proposal, we examined the system shown in Figure 2.9.

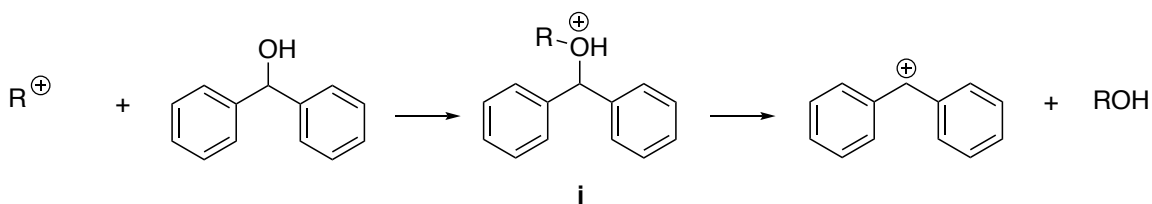


Figure 2.9 New nucleophilicity-electrophilicity system

Here an alkyl cation would be the electrophile and the benzhydryl alcohol is the nucleophile. We do not expect to observe intermediate **i**; this intermediate should quickly release the benzhydryl cation fragment, which we would then detect via mass spectrometry. Because the fragmentation is fast, the rate constant measured will reflect the reaction of nucleophile with electrophile.

To our delight, we have found, experimentally, that we can measure the rate constants for reactions of benzhydrol with both the ethyl cation and the *tert*-butyl cation; the respective efficiencies of these reactions are 100% and 86% -- fast, efficient reactions that provide support for the theory that previous gas phase studies suffered from the inability to dissipate complexation energy. This current system is a valuable complement to

condensed phase data as we can examine cations that are too reactive to be studied in solution. Having established this proof of concept, our lab is now working on further studies, both with this system, as well as newly designed models that will be comparable to existing solution phase data.

2.4 Conclusions

Our study of fourteen amine nucleophiles with five benzhydrylium electrophiles reveals new insights into nucleophilicity and electrophilicity. Kinetic isotope effect studies establish that a specific covalent complex between the amine nitrogen and benzhydrylium is formed, as is desired. Analysis of the data indicates that electrophilicity trends appear to be constant between the gas phase and solution, while nucleophilicity is much more complex. However, such conclusions must be taken with caution, since we believe that any measurement of nucleophilicity and electrophilicity parameters wherein two species form an association complex under vacuum do not accurately reflect the rate of reaction. Instead, the rate determining step is the dissipation of excess complexation energy. We were able to provide evidence supporting this theory by designing an alternate system in which excess energy can be released via fragmentation. We also studied the fast reactions involving alkyl cations and benzhydryl alcohols. Such systems can be used to begin to build a new gas-phase nucleophilicity-electrophilicity scale; cations (different alkyl groups) and nucleophiles (benzhydryl ethers, benzhydryl thiols) can be varied to achieve this. We are also contemplating alternate models that will better mimic reactions in solution for which

parameters are known. Ultimately, direct comparison of rate constants and parameters between the gas phase and solution will allow us to better understand the factors at play in the solution phase reactions.

2.5 References

- (1) Swain, C. G.; Scott, C. B. *J. Am. Chem. Soc.* **1953**, 75, 141.
- (2) Edwards, J. O. *J. Am. Chem. Soc.* **1954**, 76, 1540.
- (3) Parker, A. J. *Chem. Rev.* **1969**, 69, 1.
- (4) Bunnett, J. F. *Annu. Rev. Phys. Chem.* **1963**, 14, 271.
- (5) Pearson, R. G.; Sobel, H. R.; Songstad, J. *J. Am. Chem. Soc.* **1968**, 90, 319.
- (6) Ritchie, C. D. *Acc. Chem. Res.* **1972**, 5, 348.
- (7) Kane-Maguire, L. A. P.; Honig, E. D.; Sweigart, D. A. *Chem. Rev.* **1984**, 84, 525.
- (8) Mayr, H.; Patz, M. *Angew. Chem. Int. Ed.* **1994**, 33, 938.
- (9) Mayr, H. **2017**, Mayr's Database of Reactivity Parameters; <http://www.cup.lmu.de/oc/mayr/reaktionsdatenbank/>.
- (10) Mayr, H.; Kempf, B.; Ofial, A. R. *Acc. Chem. Res.* **2003**, 36, 66.
- (11) Denekamp, C.; Sandler, Y. *Angew. Chem. Int. Ed.* **2006**, 45, 2093.
- (12) Srivastava, P.; Ali, R.; Razi, S. S.; Shahid, M.; Patnaik, S.; Misra, A. *Tetrahedron Lett.* **2013**, 54, 3688.
- (13) Kurinovich, M. A.; Lee, J. K. *J. Am. Chem. Soc.* **2000**, 122, 6258.
- (14) Bartmess, J. E.; Georgiadis, R. M. *Vacuum* **1983**, 33, 149.
- (15) Sharma, S.; Lee, J. K. *J. Org. Chem.* **2004**, 69, 7018.
- (16) Liu, M.; Xu, M.; Lee, J. K. *J. Org. Chem.* **2008**, 73, 5907.
- (17) Sun, X.; Lee, J. K. *J. Org. Chem.* **2007**, 72, 6548.
- (18) Chesnavich, W. J.; Su, T.; Bowers, M. T. *J. Chem. Phys.* **1980**, 72, 2641.
- (19) Su, T.; Chesnavich, W. J. *J. Chem. Phys.* **1982**, 76, 5183.
- (20) Miller, K. J.; Savchik, J. A. *J. Am. Chem. Soc.* **1979**, 101, 7206.
- (21) Mayr, H.; Schneider, R.; Schade, C.; Bartl, J.; Bederkes, R. *J. Am. Chem. Soc.*, **1990**, 112, 4446.
- (22) Baidya, M.; Kobayashi, S.; Brotzel, F.; Schmidhammer, U.; Riedle, E.; Mayr, H. *Angew. Chem. Int. Ed.* **2007**, 46, 6176.
- (23) Brotzel, F.; Chu, Y. C.; Mayr, H. *J. Org. Chem.* **2007**, 72, 3679.
- (24) Kanzian, T.; Nigst, T. A.; Maier, A.; Pichl, S.; Mayr, H. *Eur. J. Org. Chem.* **2009**, 6739.
- (25) Ammer, J.; Baidya, M.; Kobayashi, S.; Mayr, H. *J. Phys. Org. Chem.* **2010**, 23, 1029.
- (26) Chesnavich, W. J.; Su, T.; Bowers, M. T. *J. Chem. Phys.* **1980**, 72, 2641.
- (27) Su, T.; Chesnavich, W. J. *J. Chem. Phys.* **1982**, 76, 5183.
- (28) Miller, K. J.; Savchik, J. A. *J. Am. Chem. Soc.* **1979**, 101, 7206.

Note: Major parts of this chapter have been published: [Niu, Y.](#); Wang, N.; Munoz, A.; Xu, J.; Zeng, H.; Rovis, T.; Lee, J. K. “Experimental and Computational Gas Phase Acidities of Conjugate Acids of Triazolylidene Carbenes: Rationalizing Subtle Electronic Effects”, *J. Am. Chem. Soc.* **2017**, Article ASAP.

Chapter 3. Proton Affinity of Triazolylidene Carbenes: Rationalizing Subtle Electronic Effects

3.1 Introduction

Since the discovery of stable carbenes, first reported independently by Bertrand and Arduengo, these species have become key players in organic and organometallic chemistry.^{1,2} *N*-Heterocyclic carbenes (NHCs), particularly imidazolylienes, have come to the forefront as effective ligands for transition-metal catalysts, with perhaps the best-known example being the Grubbs second-generation ruthenium catalysts for olefin metathesis.³ In addition to their role as key ligands for organometallic catalysts, NHCs themselves can also function as organocatalysts, and in recent years, triazolylidene carbenes have emerged as the most prominent structure.^{4,5} Work in this field has encompassed both *Umpolung* and non-*Umpolung* reactions, with an eye to stereoselectivity.⁴⁻⁶

For reactions catalyzed by triazolylidene carbenes, the carbene is often generated *in situ* by deprotonation of the corresponding triazolium precatalyst. The resultant carbene

behaves as a nucleophile; for most reactions catalyzed by NHCs, the first step in the catalytic cycle is NHC attack of an electrophile. An example of an NHC-catalyzed reaction from our lab, the intramolecular Stetter reaction, is shown in Figure 3.1. Because of the requisite deprotonation of the precatalyst and the nucleophilic nature of the carbene, the acidity of the triazolium precatalyst (which is equivalent to the basicity of the free carbene) and the nucleophilicity of the triazolylidene carbene catalyst are of great interest.

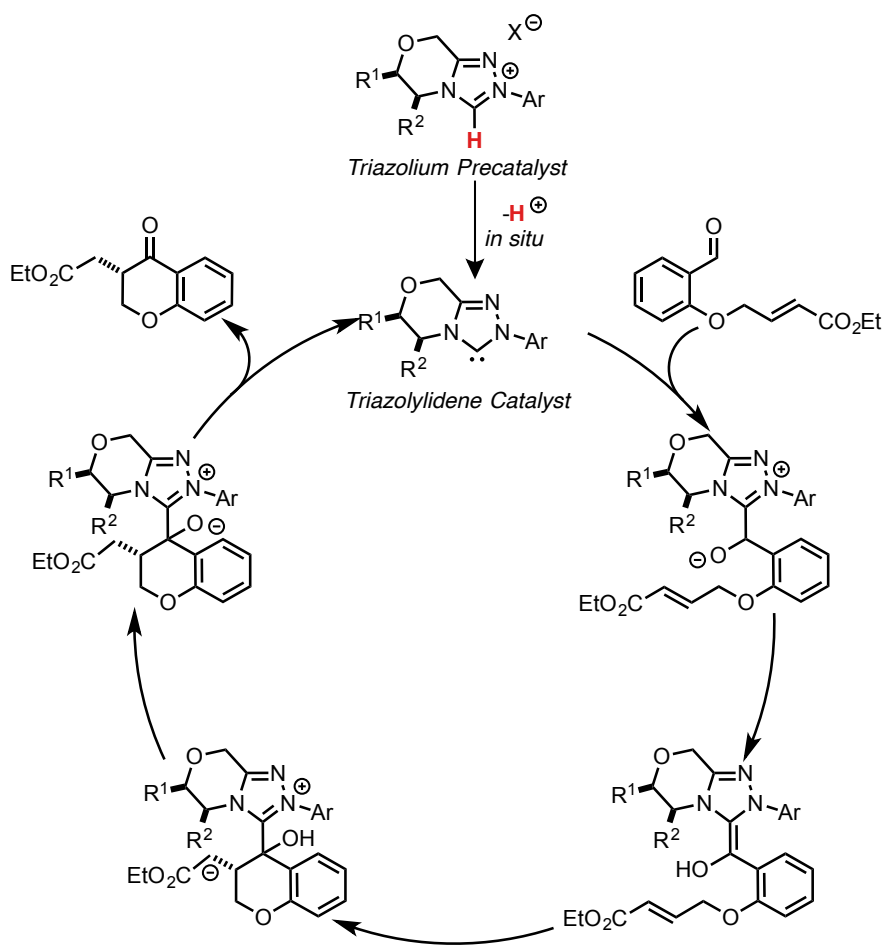


Figure 3.1 Intramolecular Stetter reaction cycle as catalyzed by a triazolylidene NHC

Despite great progress in the development and optimization of triazolylidene carbenes as catalysts for enantioselective reactions, fundamental studies of these species are

relatively limited. With respect to the evaluation of the acidity of these triazoliums, Smith, O'Donoghue and coworkers conducted a seminal study that yielded the acidity of twenty triazolium salts in aqueous solution.^{7,8} Mayr and coworkers examined a series of NHCs to evaluate nucleophilicity and Lewis basicity.⁹ They found that triazolylidene **2c** is less nucleophilic than imidazolylidene **2a** and imidazolinylidene **2b**; all three had moderate nucleophilicity relative to a high Lewis basicity (Figure 3.2).

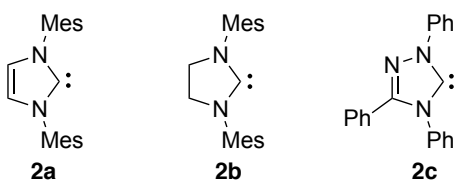


Figure 3.2 NHCs studied by Mayr Group

In this chapter, we describe our studies of two series of triazolium cations that, upon deprotonation, deliver catalysts that are active in a variety of transformations.⁴ We use experiment and theory to characterize the intrinsic basicity of triazolyliidenes by measuring and computing the acidity of the corresponding triazolium cations in the gas phase, for a wide range of achiral and chiral species not heretofore examined *in vacuo*.

3.2 Experimental

The synthesis of the protonated carbenes studied herein have been previously described.⁴ The reference bases were purchased from Sigma-Aldrich and used as received.

Bracketing experiments were conducted using a house-modified quadrupole ion trap mass spectrometer as previously described (1.3.3).¹⁰ To generate the protonated carbene

ions via electrospray ionization (ESI), the triazolium cations were dissolved in 1:10 water/methanol. About 2 μL formic acid was added into every 10ml water/methanol solution to facilitate ionization. Final concentrations of these solutions were $\sim 10^{-4}$ M.

The flow rates of ESI injection were 15-25 $\mu\text{L}/\text{min}$. The capillary temperature was 190°C . Neutral reference bases were added with helium gas flow. The protonated carbene ions were allowed to react with neutral reference bases for 0.03-10000 ms. A total of 10 scans were averaged. The typical electrospray needle voltage was ~ 1.80 kV.

All calculations were performed using density functional theory (B3LYP/6-31+G(d)) as implemented in Gaussian 09.¹¹⁻¹⁶ All the geometries were fully optimized and frequencies were calculated; no scaling factor was applied. The optimized structures had no negative frequencies. The temperature for the calculations was set to be 298 K. For the enol TS calculations, the SMD model was used with ethanol as the solvent. M06/6-31+G(d,p) solution-phase single-point energy calculations (on the B3LYP/6-31+G(d) geometry) were conducted.¹⁷⁻²¹ Reported energetics are the sum of the Gibbs free energy correction at B3LYP/6-31+G(d) applied to the solution-phase single-point energy at M06/6-31+G(d,p).

3.3 Results and Discussion

3.3.1 Achiral Pyrrolidine-based Triazoliums

i. Calculations: Achiral Pyrrolidine-based Triazolium Cations

We first studied a series of achiral pyrrolidine-based triazolium cations as shown in

Figure 3.3. These compounds were chosen to assess the electronic effect of the various substituted phenyl moieties; also, the aqueous pK_a has been measured for some of these, which would allow us to compare gas and solution phase values. The calculated acidities of the triazolium cations, which correspond to the proton affinity of their respective triazolylidene carbenes, are listed in Figure 3.3 and Figure 3.4. In our experience, density functional theory (DFT) methods generally yield accurate values for thermochemical properties of heterocyclic rings, so we utilized B3LYP/6-31+G(d) to calculate the acidities (ΔH_{acid}).²²⁻²⁷ The overall trend in terms of acidity for these substrates is as follows (from most acidic to least acidic; note that as with pK_a values, more acidic species have lower ΔH_{acid} values): **3c** > **3b** = **3e** > **3g** > **3f** > **3i** > **3h** > **3a** > **3l** > **3d** > **3j** > **3k**. Overall, this trend makes sense: **3c** is most acidic, with a 3,5-di- CF_3 substitution on the phenyl, followed by perfluorophenyl and 4-cyanophenyl. Ultimately the least acidic is **3k**, with a largely electron donating N-aryl group substituent.

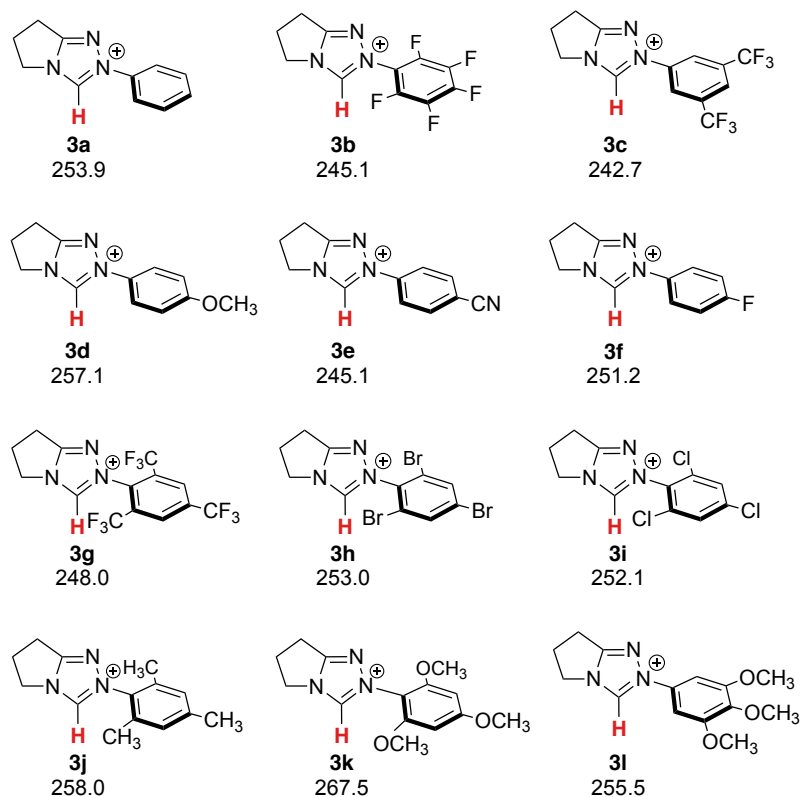


Figure 3.3 Calculated acidities for a series of pyrrolidine-based achiral triazolium cations (kcal/mol). Calculations were conducted at B3LYP/6-31+G(d); reported values are ΔH at

298 K

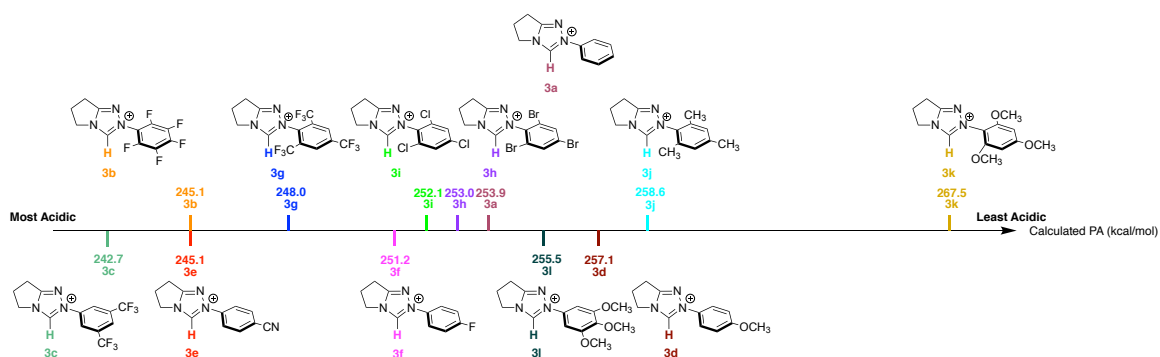


Figure 3.4 Calculated acidities for a series of pyrrolidine-based achiral triazolium cations (kcal/mol), arranged in the order of acidity

There is one surprise in this trend, however, which is the higher acidity of **3c** (242.7 kcal/mol) versus **3g** (248.0 kcal/mol). **3c** has a phenyl ring with 3,5-di- CF_3 substitution while **3g** has a phenyl ring with an additional trifluoromethyl group, as well as diortho substitution (2,4,6-tri- CF_3). One might initially expect **3g** to be more acidic than **3c**, due to the additional electron withdrawing trifluoromethyl group. However, we suspected that the additional trifluoromethyl group (as well as the diortho substitution pattern) alters the phenyl ring geometry unfavorably, which calculations confirmed (Figure 3.5). For **3c**, the phenyl ring is relatively planar relative to the triazolium ring; the dihedral angle for the calculated structure (for the atoms labeled 1-2-3-4) is 34.7° . For **3g**, however, the relatively bulky trifluoromethyl groups, placed at the ortho positions of the phenyl ring, cause the ring to become nearly perpendicular to the triazolium ring (dihedral 90.4°). A perpendicular disposition of the aryl ring leads to reduced orbital overlap with the azolium and a minimization of its impact on the electronic character of the carbene center. Therefore, although the additional trifluoromethyl would be expected to increase the acidity, the lack of planarity of the phenyl ring relative to the triazolium core mitigates the effect of the third CF_3 . This is reminiscent of the surprisingly similar acidities of diphenylmethane and triphenylmethane; the third phenyl ring is less effective than might be expected due to the inability of all three phenyl rings to be in the same plane.

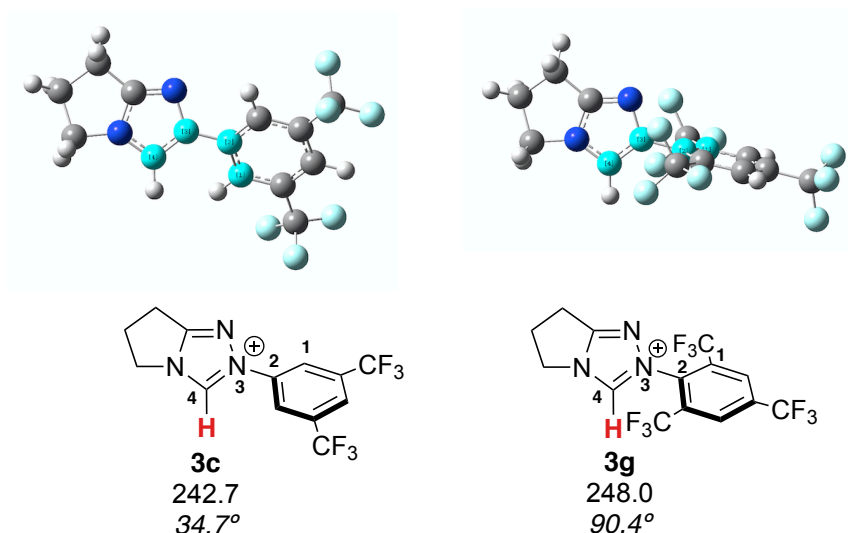


Figure 3.5 Calculated (B3LYP/6-31+G(d)) geometries of the **3c** and **3g** achiral triazolium cations

To avoid this type of complication when looking at trends, a more reasonable comparison is to focus on structures that have the same substitution pattern. For example, among the 2,4,6-substituted phenyl compounds, the order from most to least acidic is: **3g** (2,4,6-tri- CF_3) > **3i** (2,4,6-tri-Cl) > **3h** (2,4,6-tri-Br) > **3j** (2,4,6-tri- CH_3 (mesityl)) > **3k** (2,4,6-tri- OCH_3). In terms of electron withdrawing capability, this trend is reasonable: the most acidic is the compound with the 2,4,6-tri- CF_3 -phenyl moiety and the least acidic has a 2,4,6-tri- OCH_3 -phenyl group. For the 4-substituted phenyls, the acidity order is (from most to least acidic): **3e** (4-CN) > **3f** (4-F) > **3d** (4-OMe), which also makes sense.

ii. Experiments: Achiral Pyrrolidine-based Triazolium Cations

To experimentally measure the gas phase acidity of the achiral triazolium cations, we utilized mass spectrometry and proton transfer reactions between the protonated carbene

precursors and various bases in the gas phase whose proton affinities are known. Electrospray ionization of the protonated carbene successfully yields the triazolium cation as the major signal. Reference bases are then added and the presence or absence of proton transfer is assessed.

DBU (PA = 250.5 kcal/mol) is unable to deprotonate **3a**, but MTBD (PA = 254.0 kcal/mol) can. We therefore bracket the acidity of **3a** to be between DBU and MTBD (252 ± 4 kcal/mol). For **3b**, as well as **3e**, *N,N,N',N'*-tetramethyl-1,3-propanediamine (PA = 247.4 kcal/mol) is unable to effect deprotonation, but DBN (PA = 248.2 kcal/mol) can, placing the acidity of **3b** and **3e** at 248 ± 3 kcal/mol. 1-(Cyclopent-1-en-1-yl)pyrrolidine (PA = 243.6 kcal/mol) cannot deprotonate **3c**, but *N,N,N',N'*-tetramethyl-1,3-propanediamine (PA = 247.4 kcal/mol) can; we therefore bracket the acidity of **3c** to be 246 ± 4 kcal/mol. For **3d**, no reaction is observed with MTBD (PA = 254.0 kcal/mol), but proton transfer occurs with HP₁(dma) (PA = 257.4 kcal/mol), placing the acidity of **3d** at 256 ± 4 kcal/mol. For **3f**, **3h** and **3i**, no proton transfer is observed with DBU (PA = 250.5 kcal/mol) but MTBD (PA = 254.0 kcal/mol) deprotonates all three, allowing us to bracket the acidity of **3f**, **3h** and **3i** to be the same, 252 ± 4 kcal/mol. **3j** is least acidic; HP₁(dma) (PA = 257.4) cannot deprotonate it, but *t*buP₁(dma) (PA = 260.6) can, bracketing the acidity of **3j** to 259 ± 4 kcal/mol. MTBD (PA = 254.0 kcal/mol) does not deprotonate **3l**, but HP₁(dma) (PA = 257.4 kcal/mol) does, placing the acidity of **3l** at 256 ± 4 kcal/mol.

The overall trend for the experimental acidity values tracks reasonably well with

calculation (from most acidic to least acidic): **3c** > **3b** = **3e** > **3a** = **3f** = **3h** = **3i** > **3d** = **3l** > **3j** (Table 3.1). Reference bases are limited in this region, which is at the high basicity range for compounds in the gas phase. Therefore, although calculations indicate that **3a**, **3f**, **3h**, and **3i** have different acidities (ranging from about 251-254 kcal/mol), all four substrates have a measured acidity of 252 ± 4 kcal/mol. There are simply not enough reference bases to differentiate within this region. However, the calculations and experiments are in agreement, within the experimental uncertainty.

Table 3.1 Summary of results for gas phase acidity bracketing of achiral pyrrolidine-based triazoliums

Reference base ^{a,b}	PA (kcal/mol) ^c	Proton transfer to reference base ^d									
		3c	3b	3e	3f	3i	3h	3a	3l	3d	3j
N,N,N',N'-tetramethylethylenediamine	242.1	–									
1-(cyclopent-1-en-1-yl)pyrrolidine	243.6	–	–	–		–					
N,N,N',N'-tetramethyl-1,3-propanediamine	247.4	+	–	–		–	–	–			
DBN	248.2	+	+	+	–	–	–	–			
DBU	250.5	+	+	+	–	–	–	–	–	–	
MTBD	254.0				+	+	+	+	–	–	–
HP ₁ (dma)	257.4				+	+	+	+	+	+	–
tBuP ₁ (dma)	260.6								+	+	+
tOctP ₁ (dma)	262.0										+

^a Reference²⁸ ; ^bDBN = 1,5-Diazabicyclo[4.3.0]non-5-ene; DBU = 1,8-diazabicyclo[5.4.0]undec-7-ene; MTBD = 7-Methyl-1,5,7-triazabicyclo[4.4.0]dec-5-ene; HP₁(dma) = Imino-tris(dimethylamino)phosphorane; tBuP₁(dma) = *tert*-Butylimino-tris(dimethylamino)phosphorane; tOctP₁(dma) = *tert*-Octylimino-tris(dimethylamino)phosphorane; BEMP = 2-*tert*-Butylimino-2-diethylamino-1,3-dimethylperhydro-1,3,2-diazaphosphorine. ^c Reference base PAs typically have an error of ± 2 kcal/mol. ^d The “+” symbol indicates the occurrence and the “–” symbol indicates the absence of proton transfer.

The aqueous pK_a values for some of these achiral triazoliums have been determined.⁷

In Table 3.2, we list our calculated and experimental gas phase acidity values as well as

known pK_a values. The data in Table 3.2 is arranged in order of decreasing calculated gas phase acidity. The aqueous acidity trend more or less reflects the gas phase trend, meaning, as one moves down the table, the acidity generally decreases for both the gas phase and solution. There are two exceptions: the first is for **3b** ($-\text{F}_5$ substituted phenyl) versus **3e** (4-CN). The gas phase calculations predict the same gas phase acidity but in water **3e** is less acidic than **3b** by 0.4 pK_a units. The second exception is for **3d** (4-OMe) versus **3j** (1,3,5-trimethyl (Mes)). Calculations predict that **3d** is more acidic than **3j**, by 1.5 kcal/mol. In water, **3d** is less acidic than **3j** by 0.1 pK_a units.

Table 3.2 Calculated (B3LYP/6-31+G(d); 298 K) and experimental data for achiral triazolium cations.^a

Substrate	Calculated ΔH_{acid}	Experimental ΔH_{acid} ^b	pK _a ^c
3c	242.7	246	
3b	245.1	248	16.5
3e	245.1	248	16.9
3g	248.0		
3f	251.2	252	17.4
3i	252.1	252	
3h	253.0	252	
3a	253.9	252	17.5
3l	255.5	256	
3d	257.1	256	17.8
3j	258.6	259	17.7
3k	267.5		

^a ΔH_{acid} values are in kcal/mol; ^b Error is ± 3 -4 kcal/mol; ^c Reference⁷

It is well known that acidity trends will sometimes differ in the gas versus solution phases; the classic case is that *tert*-butanol is more acidic than methanol in the gas phase, while the opposite is true in water.²⁹ In the gas phase, the polarizable methyl groups in *tert*-butoxide stabilize the anion; this is less keenly felt in solution, and also, water molecules may more poorly solvate the bulkier *tert*-butyl group. For our substrates, the gas phase results indicate that perfluoro and 4-CN phenyl moieties in **3b** and **3e**, respectively, have similar intrinsic anion stabilizing ability. In solution, however, the polarizability of the

cyano group may have less of an influence, causing **3e** to be slightly less acidic than **3b**.

The other feature that is true for relative gas phase versus solution phase acidities is that the range is generally wider in the gas phase than solution. Thus, in Table 3.2, the range of gas phase acidities for those cations for which we have solution phase data is 13.5 kcal/mol (245.1 kcal/mol for **3b** to 258.6 kcal/mol for **3j**). The pK_a range is 16.5 to 17.7, which is 1.2 pK_a units, or roughly 1.6 kcal/mol at room temperature. This tighter range for the solution phase acidities makes it less surprising that **3d** and **3j**, which only differ by 1.5 kcal/mol in the gas phase, have a mere 0.1 pK_a unit difference in solution (0.14 kcal/mol).

The wider range of acidity for the catalysts in the gas phase also implies that differences in reactivity of catalysts will be more pronounced in nonpolar environments. Thus, for example, using a less polar solvent will allow for nuances among catalyst reactivity to stand out. Also, less solvent interference can increase catalyst efficacy; recent work by Kimura and coworkers using NHCs in solvent-free benzoin and Stetter reactions indicated efficient reactions with low catalyst loading.³⁰

3.3.2 Chiral Aminoindanol-based Triazoliums

i. Calculations: Chiral Triazolium Cations

We also studied a series of chiral aminoindanol-based triazoliums that over the years have been used as precatalysts for a wide range of reactions.⁴⁻⁶ The calculated acidities of the triazolium cations are shown in Figure 3.6 and Figure 3.7. The overall trend from most to least acidic, in the gas phase, is: **4f** > **4d** > **4j** = **4c** > **4g** > **4i** = **4h** ≥ **4l** > **4k** = **4a** > **4m** >

4b > **4e**. As with the achiral triazoliums, the overall trend in acidity seems reasonable, with the most acidic species being the 3,5-bis(trifluoromethylphenyl) and the least being the mesityl-substituted catalyst. One perhaps surprising ordering is **4a** versus **4m**; the aminoindanol triazolium with an unsubstituted phenyl is more acidic than that with a 2,6-dibromo substituted phenyl. As with the achiral series, however, we find that the dihedral angle for **4a** indicates a nearly flat phenyl ring (36.6°) whereas for **4m**, the dibromophenyl substituent is perpendicular (95.0°) to the triazolium ring. Presumably that perpendicularity will mean less of an electronic influence on the carbene center basicity (triazolium acidity) (Figure 3.8).

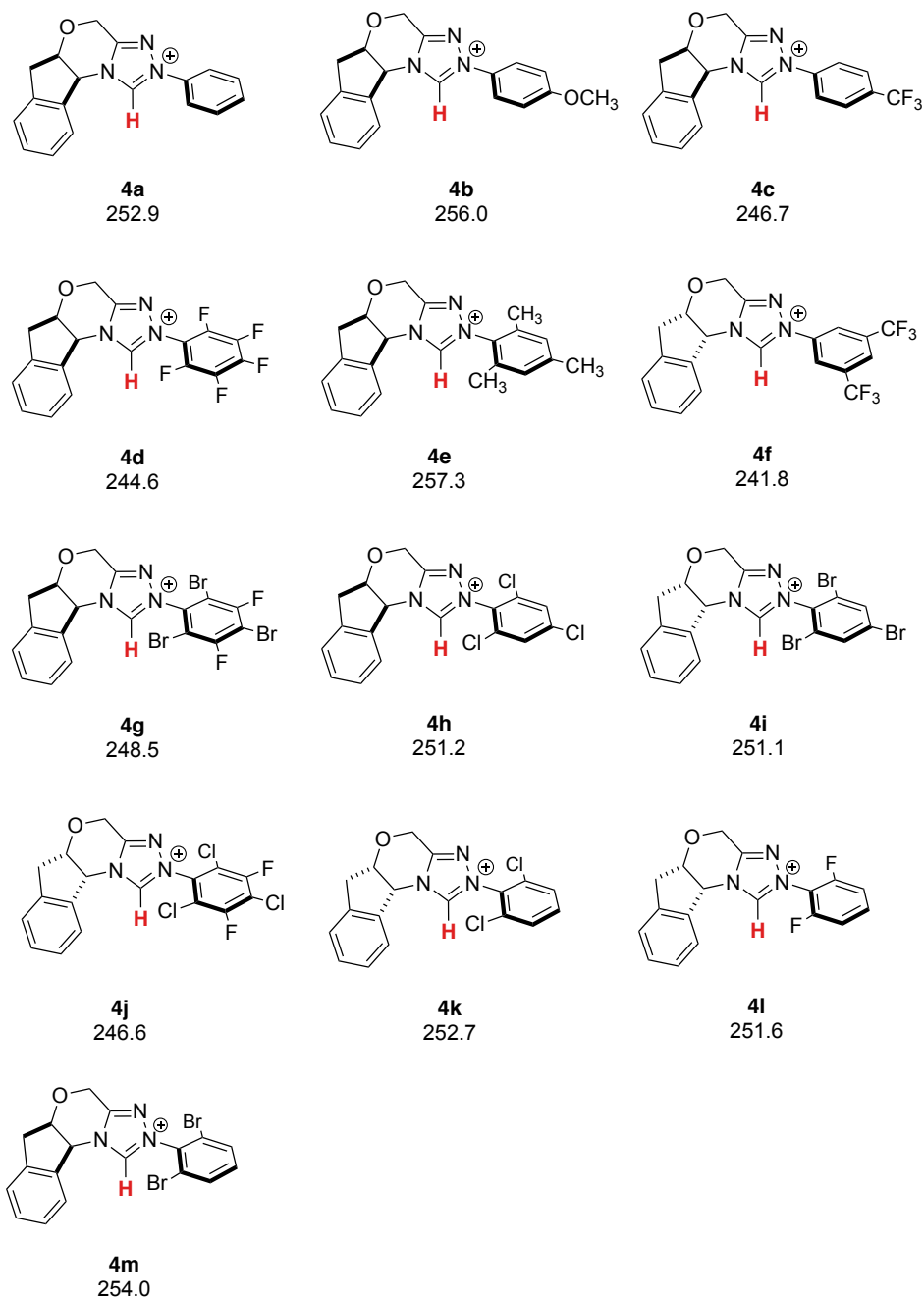


Figure 3.6 Calculated acidities for a series of aminoindanol-based chiral triazolium cations, in kcal/mol. Calculations were conducted at B3LYP/6-31+G(d); reported values are ΔH at 298 K

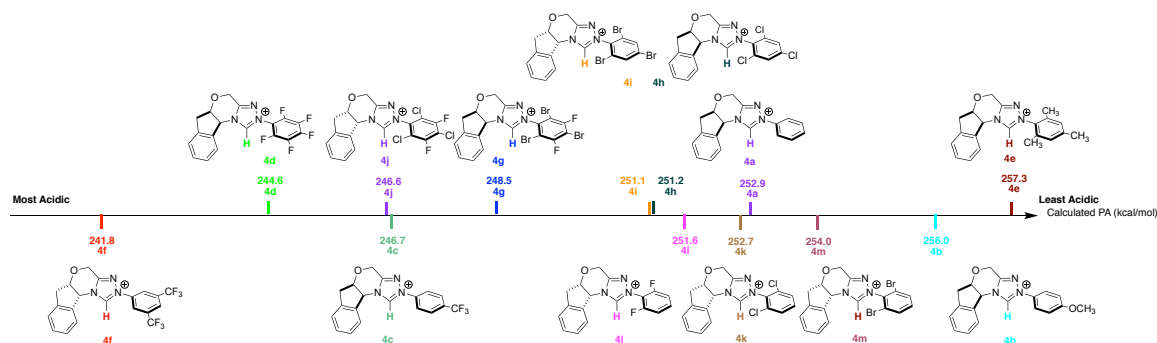


Figure 3.7 Calculated acidities for a series of aminoindanol-based chiral triazolium cations (kcal/mol), arranged in the order of acidity

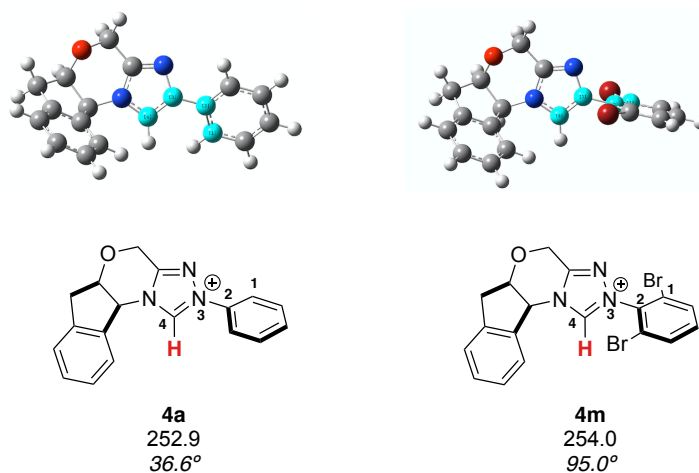


Figure 3.8 Calculated (B3LYP/6-31+G(d)) geometries of the **4a** and **4m** chiral triazolium cations.

A comparison between achiral and chiral triazoliums and phenyl substitution also shows consistency in terms of the influence of the phenyl ring substitution on the triazolium carbene center acidity. Both series have a 3,5-bis(trifluoromethylphenyl) substituent that renders the triazolium to be the most acidic of their respective groups (**3c** and **4f**). This is followed by the perfluorophenyl substituted triazoliums and the 1,3,5-trihalophenyl

substituted species, for both the **3** and **4** series. The acidity trend then continues for both series with an unsubstituted phenyl followed by 4-OMe then mesityl.

ii. Experiments: Chiral Triazolium Cations

The experimental bracketing for the **4** series are shown in Tables 3.3. DBU (PA = 250.5 kcal/mol) cannot deprotonate **4a** but MTBD (PA = 254.0 kcal/mol) can, placing the acidity of **4a** at 252 ± 4 kcal/mol. Triazoliums **4k** and **4m** bracket to the same acidity. For **4b**, MTBD (PA = 254.0 kcal/mol) cannot deprotonate the triazolium but HP₁(dma) (PA = 257.4 kcal/mol) can, which allows us to bracket the acidity of **4b** to be 256 ± 4 kcal/mol. We find that *N,N,N',N'*-tetramethyl-1,3-propanediamine (PA = 247.4 kcal/mol) is unable to effect deprotonation of **4c**, but DBN (PA = 248.2 kcal/mol) can, placing the acidity of **4c** at 248 ± 3 kcal/mol. Triazoliums **4d** and **4j** bracket to 248 kcal/mol as well. For **4e**, HP₁(dma) (PA = 257 kcal/mol) cannot effect deprotonation but tBuP₁(dma) (PA = 260.6 kcal/mol) does, placing the acidity of **4e** at 259 ± 4 kcal/mol. 1-(Cyclopent-1-en-1-yl)pyrrolidine (PA = 243.6 kcal/mol) cannot deprotonate **4f** but *N,N,N',N'*-tetramethyl-1,3-propanediamine (PA = 247.4 kcal/mol) can, which gives an acidity of 246 ± 4 kcal/mol. Last, DBN (PA = 248.2 kcal/mol) cannot deprotonate **4g**, but DBU (PA = 250.5 kcal/mol) can. We thus bracket **4g** to be 249 ± 3 kcal/mol; substrates **4h**, **4i**, and **4l** have the same acidity.

Table 3.3 Summary of results for acidity bracketing of chiral aminoindanol-based triazolium **4a-4m**

Reference base ^{a,b}	PA (kcal/mol) ^c	Proton transfer to reference base ^d												
		4f	4d	4j	4c	4g	4i	4h	4l	4k	4a	4m	4b	4e
TMEDA	242.1	–	–											
1-CP	243.6	–	–	–	–	–		–				–	–	
TMPDA	247.4	+	–	–	–	–	–	–	–			–	–	
DBN	248.2	+	+	+	+	–	–	–	–	–	–	–	–	
DBU	250.5	+	+	+	+	+	+	+	+	–	–	–	–	–
MTBD	254.0		+	+	+	+	+	+	+	+	+	+	–	–
HP ₁ (dma)	257.4			+		+	+		+	+	+	+	+	–
tBuP ₁ (dma)	260.6										+		+	+
tOctP ₁ (dma)	262.0										+			+
BEMP	263.8										+			+

^aReference²⁸; ^b TMEDA = *N,N,N',N'*-tetramethylethylenediamine; 1-CP = 1-(cyclopent-1-en-1-yl)pyrrolidine; TMPDA = *N,N,N',N'*-tetramethyl-1,3-propanediamine; DBN = 1,5-Diazabicyclo[4.3.0]non-5-ene; DBU = 1,8-diazabicyclo[5.4.0]undec-7-ene; MTBD = 7-Methyl-1,5,7-triazabicyclo[4.4.0]dec-5-ene; HP₁(dma) = Imino-tris(dimethylamino)phosphorane; tBuP₁(dma) = *tert*-Butylimino-tris(dimethylamino)phosphorane; tOctP₁(dma) = *tert*-Octylimino-tris(dimethylamino)phosphorane; BEMP = 2-*tert*-Butylimino-2-diethylamino-1,3-dimethylperhydro-1,3,2-diazaphosphorine. ^cReference base PAs typically have an error of ± 2 kcal/mol. ^dThe “+” symbol indicates the occurrence and the “–” symbol indicates the absence of proton transfer.

The computed and experimental gas phase acidity values for the chiral triazoliums are compiled in Table 3.4; the catalysts are listed in order of decreasing calculated gas phase acidity. The experiment gas phase acidities roughly track with the calculated values. Given the small number of available reference bases in this superbasic range, it is not surprising that some of the experimental values are not exactly the same as the calculated values, though all are within error. Taken together, the achiral and chiral experimental data benchmark B3LYP/6-31+G(d) as a reasonable method and level to calculate the triazolium acidities.

Table 3.4 Calculated (B3LYP/6-31+G(d); 298 K) and experimental data for chiral triazolium cations.^a

Substrate	Calculated ΔH_{acid}	Experimental ΔH_{acid} ^b
4f	241.8	246
4d	244.6	248
4j	246.6	248
4c	246.7	248
4g	248.5	249
4i	251.1	249
4h	251.2	249
4l	251.6	249
4k	252.7	252
4a	252.9	252
4m	254.0	252
4b	256.0	256
4e	257.3	259

^a ΔH_{acid} values are in kcal/mol; ^b Error is ± 3 -4 kcal/mol.

3.3.3 Acidity and Diastereoselectivity

To further explore the relationship between the acidity of triazolylidenes **3** and reactivity, we explored the NHC-catalyzed homoenolate addition of cinnamaldehyde to nitroalkenes, shown in Figure 3.9.³¹⁻³³

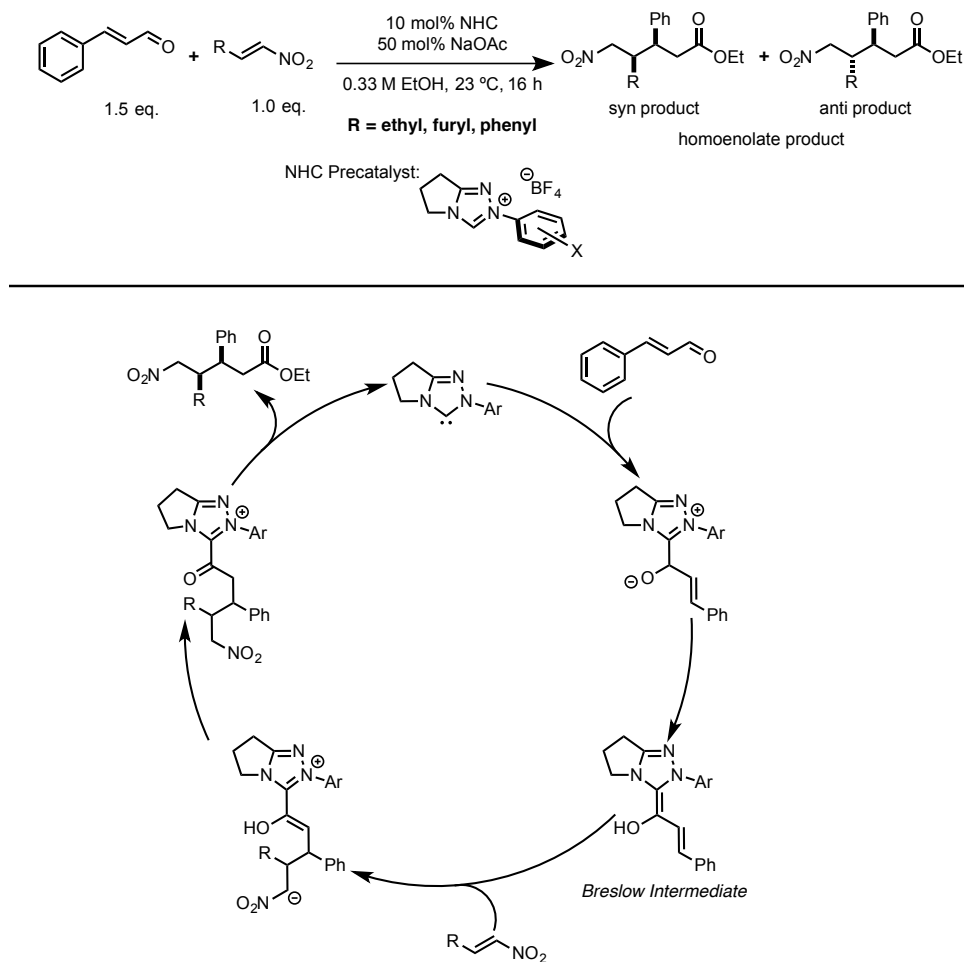


Figure 3.9 NHC-catalyzed homoenolate addition of enals to nitroalkenes, with proposed catalytic mechanism

This reaction has two potential products, *anti* and *syn* (one enantiomer of each is shown in Figure 3.9, but this racemic reaction yields both enantiomers for *anti* and for *syn*). An examination of the *anti* versus *syn* preference reveals a correlation to gas phase acidity. Figure 3.10 shows a plot of the natural log of the ratio of the *anti* to *syn* products versus the calculated acidity, for the reaction with (E)-1-nitrobut-1-ene. A correlation is observable, wherein a more acidic triazolium precatalyst corresponds to more *syn* product,

and conversely, decreasing acidity correlates to increasing *anti* selectivity.³⁴

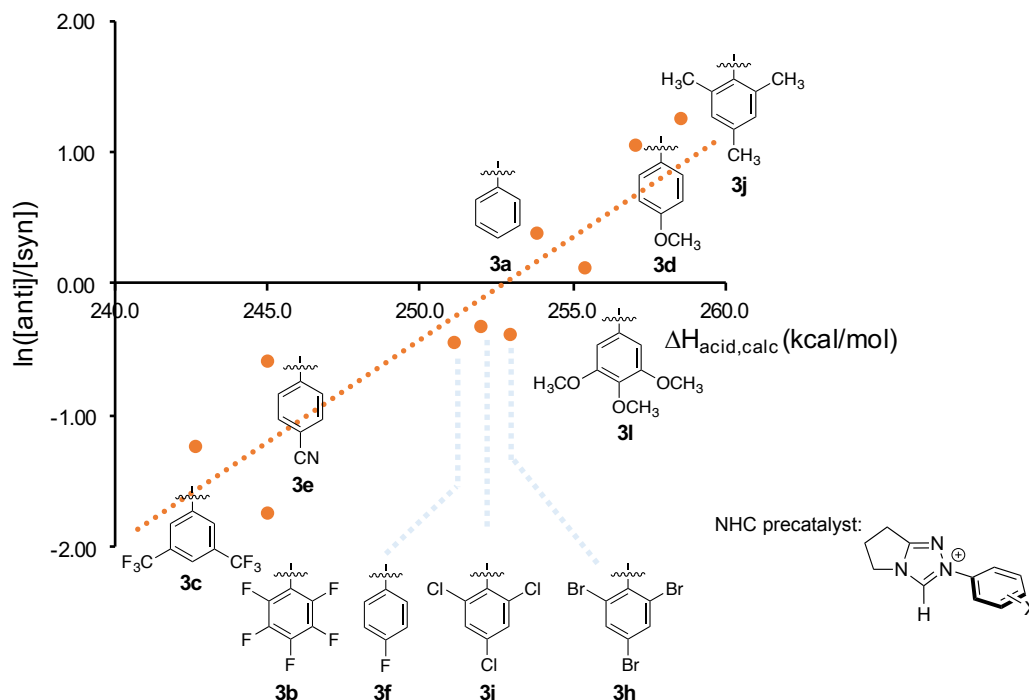


Figure 3.10 Natural log plot of the *anti*/*syn* ratio for the reaction in Figure 3.9 (R=Et) versus calculated gas phase acidity of the precatalyst

While there is a clear overall trend, one pair of data points stands out: **3b** and **3e**. Both of these precatalysts have the same acidity (245.1 kcal/mol); however, they have different *anti*/*syn* selectivity, with 4-CN precatalyst **3e** showing more *anti* selectivity than the perfluorinated precatalyst **3b**. We suspect this difference is related to the substitution pattern for the two precatalysts. The N-aryl group on **3b** has diortho substitution, while **3e** does not.³⁵ Therefore, we also composed separate analyses, one with precatalysts that have diortho substituents and one with precatalysts that do not (Figures 3.11 and 3.12); these plots show the same trend (more acidic, more *syn* selectivity), but with slightly better

correlations. In a study with this same class of catalysts, for the benzoin and Stetter reactions, O'Donoghue, Smith and coworkers proposed that perpendicularity of the N-aryl group, which should be greater with diortho substitution, influences reactivity.³⁶ Our calculations do indicate that the catalysts with diortho substitution examined herein adopt geometries with a more perpendicular *N*-aryl group, which we assume influences the selectivity slightly differently than those catalysts without diortho substituents, which are less nonplanar.

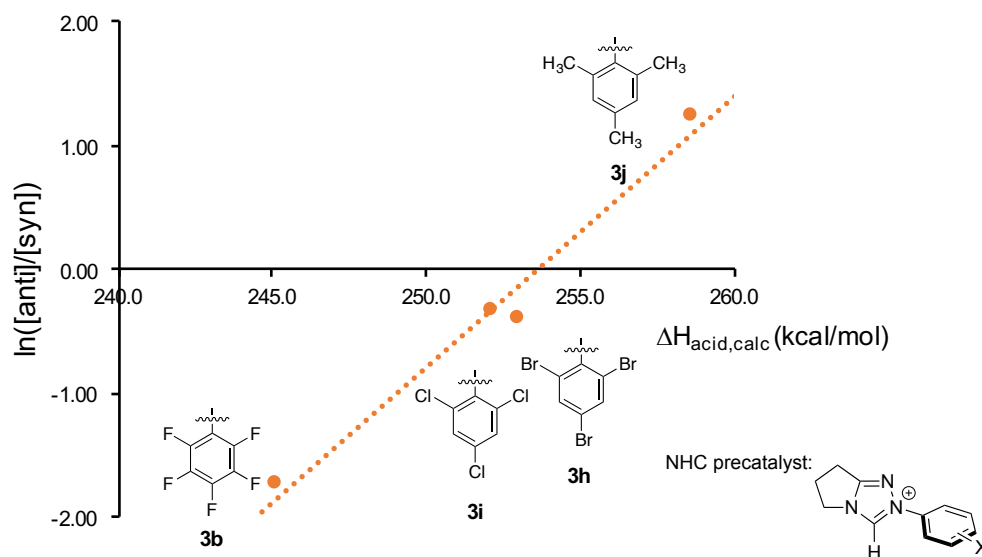


Figure 3.11 Natural log plot of the *anti*/*syn* ratio for the reaction in Figure 3.9 (R=Et) versus calculated gas phase acidity of the precatalyst, for catalysts with diortho aryl substitution

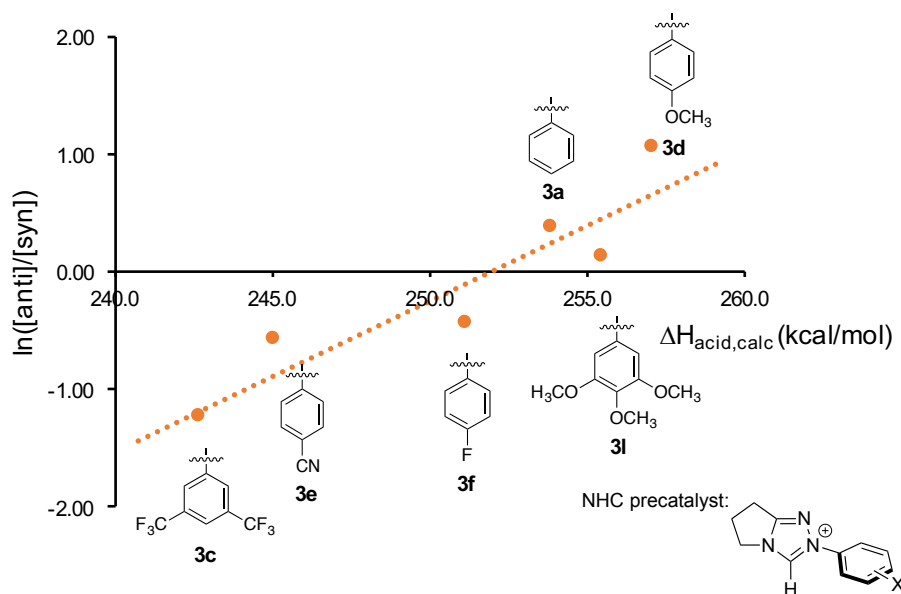


Figure 3.12 Natural log plot of the anti/syn ratio for the reaction in Figure 3.9 (R=Et) versus calculated gas phase acidity of the precatalyst, for precatalysts lacking diortho aryl substitution.

What is the Provenance of this Selectivity?

This type of reaction was first reported by Nair, using imidazolium precatalyst **5** (Figure 3.13), which yielded the *anti* product as the major diastereomer.³¹ Enantioselective variations, using chiral triazolium precatalysts, were reported by the Rovis and Liu groups, respectively, in 2013 and 2012.^{32,33} Liu's precatalyst, **6**, favors the *anti* isomer, while Rovis' precatalyst **7** favors the *syn* isomer. The difference in diastereoselectivity is proposed to arise from a difference in the Breslow intermediate geometry. Because the two chiral precatalysts **6** and **7** only allow approach from one face, the observed stereochemistry can be explained by E versus Z Breslow enol geometry (Figure 3.14).

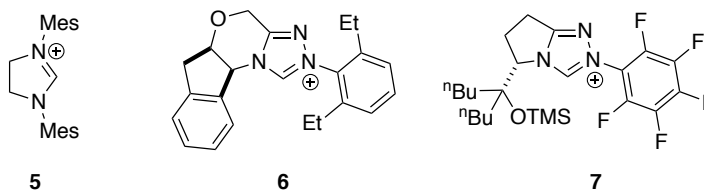


Figure 3.13 Various NHC enantioselective precatalysts

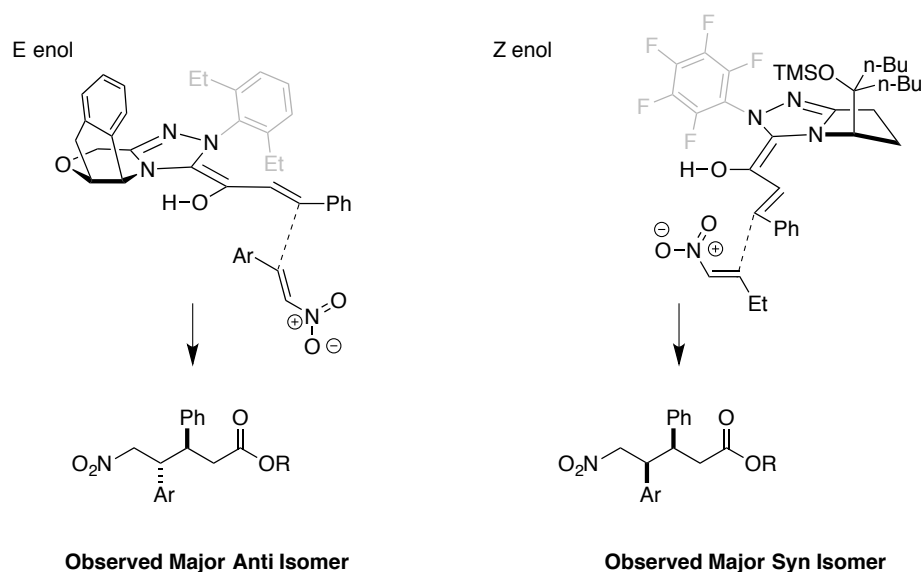


Figure 3.14 Transition states leading to the observed major isomers in asymmetric homoenolate reactions

Applying what we learned from these chiral catalysts to our achiral system, we postulate that *anti* selectivity corresponds to a preference for the E enol, while *syn* selectivity arises from a preference for the Z enol. To further probe this hypothesis, we calculated the transition states for the formation of the E and Z enols via deprotonation by acetate (Figure 3.15). Intermediate **8a** is deprotonated by acetate, via **TSa**, to form the E enol **9a**; intermediate **8b** reacts via **TSb** to form Z enol **9b**. For **3c** (Ar = 3,5-di-CF₃), experimentally, we see *syn* selectivity (Figure 3.10). Our calculations show that the

transition state to form the Z enol (**TSb**) is *lower* than that to form the E enol (**TSa**) by 3.3 kcal/mol (Figure 3.16A). This is consistent with our hypothesis that *syn* selectivity arises from the Z enol. For **3d** (Ar = 4-OMe), we find that the transition state for Z enol formation is *higher* than that for E enol formation, by 1.5 kcal/mol (Figure 16B). This reversal, as compared to **3c**, is consistent with the *anti* selectivity we experimentally observe for catalyst **3d**.

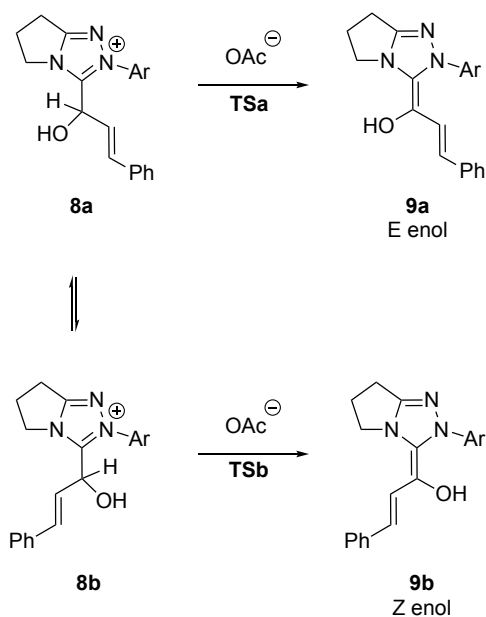


Figure 3.15 Deprotonation to form either E or Z enol

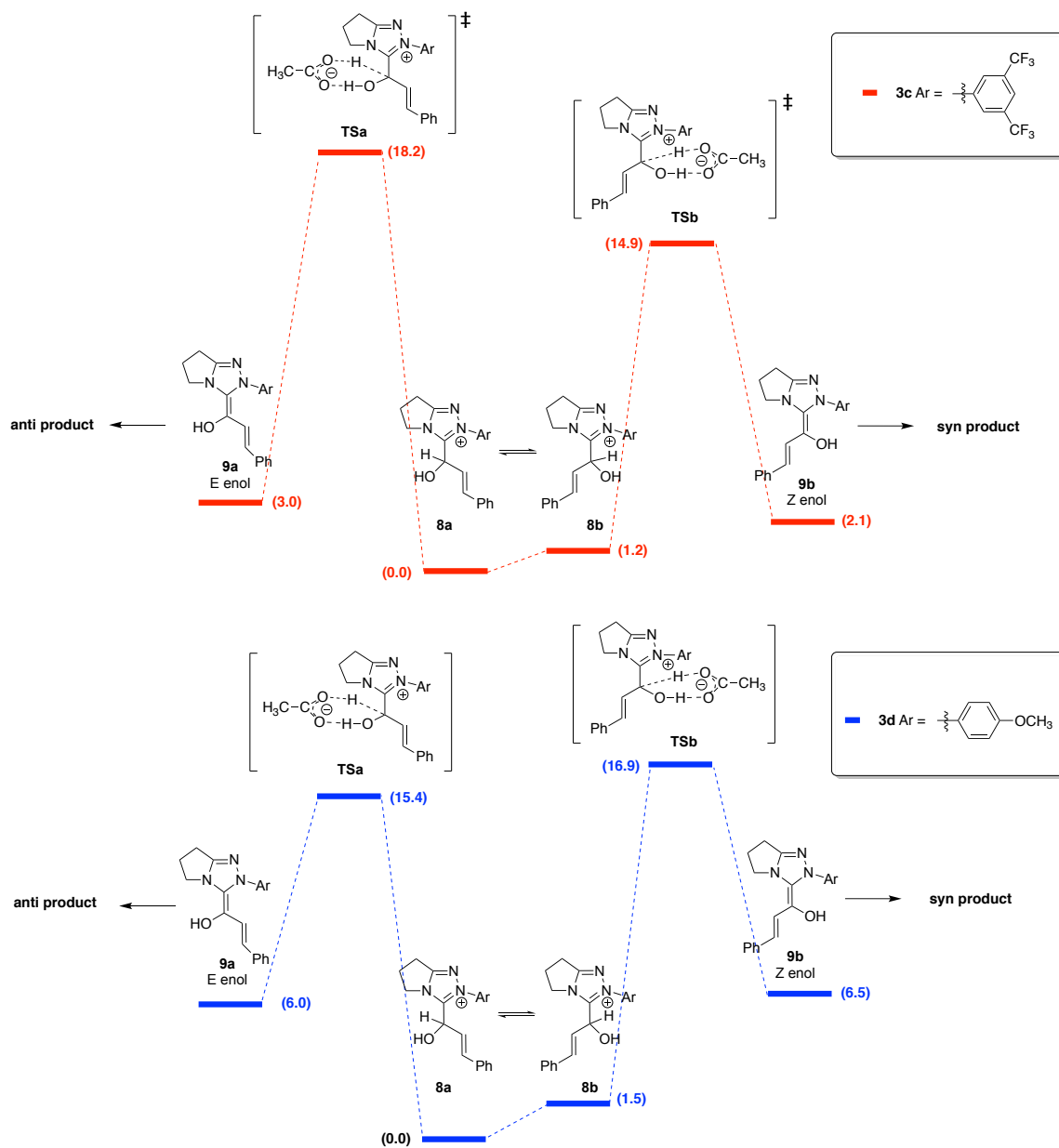


Figure 3.16 Free energy profiles for E versus Z enol formation for **3c** (A) and **3d** (B)

We are not certain why electron withdrawing groups would favor Z-enol formation. An examination of the calculated geometries for the transition state leading to the Z-enol (TSb) indicates that TSb might be stabilized by an interaction between the enol oxygen and the *N*-aryl substituent (Figure 3.17). This interaction would be more favorable for an

electron deficient ring; we find that the distance between the enol oxygen and the N-aryl ring plane is indeed less for **3c** (2.23 Å) than for **3d** (2.39 Å), indicating a possibly stronger interaction.

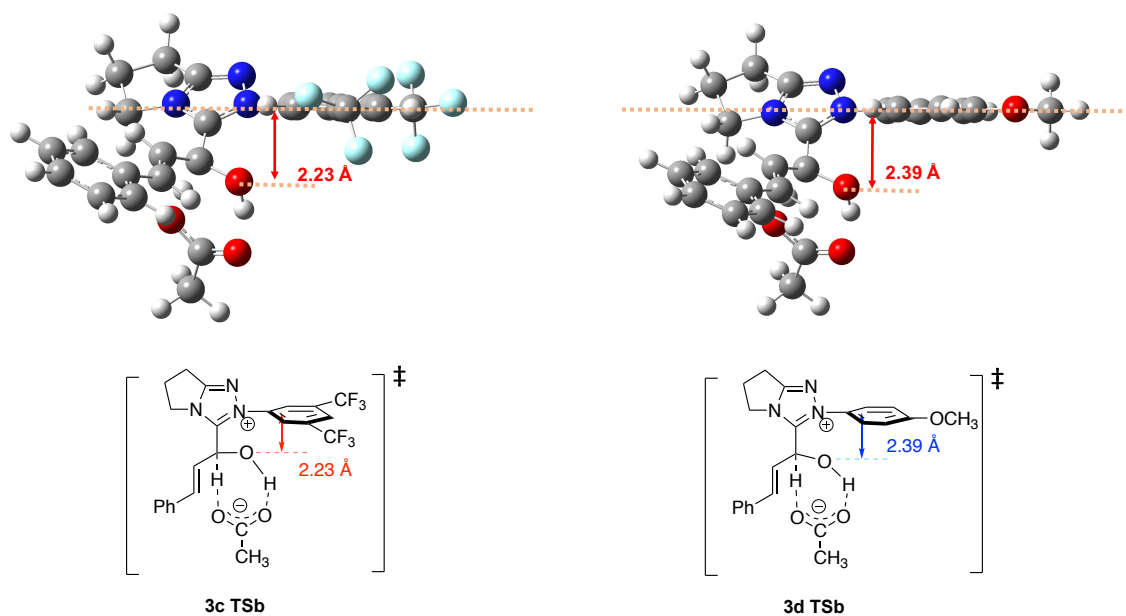


Figure 3.17 Calculated TSb structures for **3c** and **3d**

The postulate that the E enol leads to *anti* selectivity and the Z enol to *syn* selectivity is also consistent with calculations conducted by Fu and coworkers on precatalyst **7**, which shows *syn* selectivity.³⁷ Their computations indicate that for **7**, the Z enol is afforded via a lower energy transition state relative to the E enol, consistent with the *syn* selectivity that **7** presents.

Thus, subtle electronic changes appear to exert their effect on these relative transition states, favoring formation of the Z enol for electron withdrawing groups, and the E enol for electron donating groups. These electronic changes are reflected nicely in the gas phase

acidities.

3.3.4 Acidity and Enantioselectivity

To explore whether a correlation between acidity and enantioselectivity exists for reactions catalyzed by chiral triazolyldenes **4**, we examined an NHC-catalyzed asymmetric intramolecular Stetter reaction (Figure 3.18).³⁸

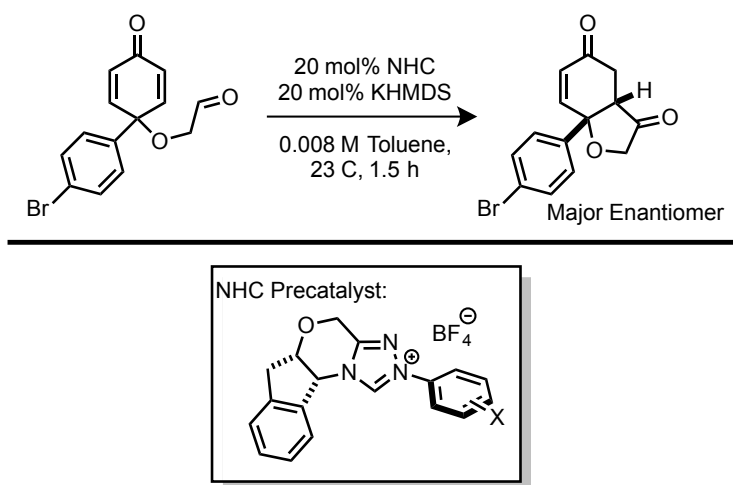


Figure 3.18 NHC-catalyzed intramolecular Stetter reaction with dienones

An examination of the stereochemical outcome of this reaction reveals a linear correlation for the natural log of the ratio of major to minor enantiomer products versus the gas phase acidity of triazolium precatalysts **4** (Figure 3.19).³⁹ For this reaction, a more acidic triazolium corresponds to reduced enantioselectivities and a less acidic triazolium results in higher enantiomeric excesses.

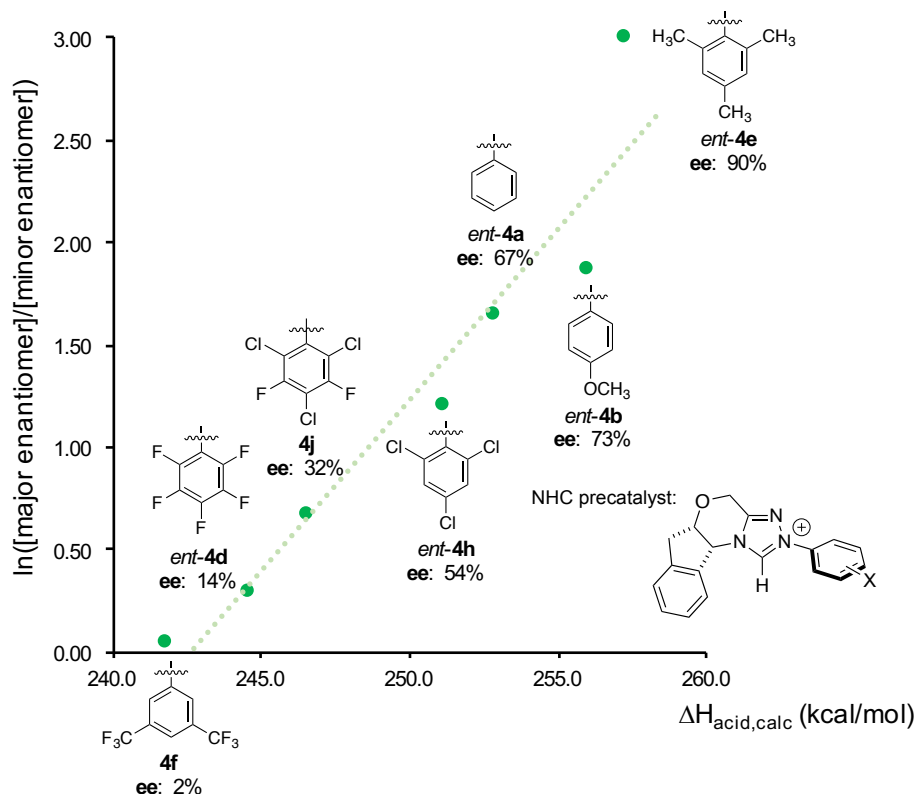


Figure 3.19 Natural log plot of the major/minor enantiomer ratio for the reaction in Figure 3.18 versus the calculated gas phase acidity of the precatalyst

This correlation with acidity also allowed us to improve the ee of this reaction. The previous ee benchmark for this particular substrate and for the antipode of precatalyst **4b** was an acceptable 73%. Realizing that a precatalyst with a lower gas phase acidity should improve enantioselectivity, we tried precatalyst *ent-4e*, resulting in 90% ee, exceeding our previous benchmark for this substrate by 17% (~0.6 kcal/mol at ambient temperature). Thus, calculated and experimental acidities may aid in a more rational catalyst optimization for *Umpolung*-themed reactions.

We postulate that the correlation between acidity and enantioselectivity for this

reaction may be related to a bimolecular event in the mechanism. In a previous study of this reaction, we found that when using a solvent mixture of toluene and isopropanol, increasing the concentration of the alcohol decreased the ee.⁴⁰

We proposed that the alcohol was involved in the transition state structure via hydrogen bonding, either to the Breslow enol oxygen or the dienone carbonyl, or both. In the absence of alcohol, another species could provide the hydrogen bonding. Since more hydrogen bonding decreases the ee, then it should follow that a more acidic Breslow enol would favor hydrogen bonding, and decrease the ee. More electron withdrawing aryl substituents should increase the acidity of the precatalyst as well as the acidity of the Breslow intermediate. Thus, we see the correlation in Figure 3.19, between higher acidity and lower ee.

Our achiral and chiral selectivity studies, taken together, indicate that using gas phase acidity is a powerful and simple method to assess intrinsic properties of carbenes that can thus provide the backbone for predictive models for *Umpolung*-themed reactions. The nonpolar environment of the gas phase enhances the differences among acidities, making acidity trends clear. These acidity trends correlate with selectivity. Solution phase acidities should also correlate to selectivity, but are generally more difficult to obtain;^{7,8,41-47} furthermore, it is potentially more difficult to ascertain acidity trends among pK_a values since the overall acidity range, as we show herein, is much tighter in solvent than in the gas phase. Gas phase acidity calculations are easily obtained, and the experimental measurements of acidity validate the calculations.

3.4 Conclusions

In this chapter, we calculate and measure the gas phase acidity of a series of achiral and chiral triazolium precatalysts whose acidities were heretofore unknown. The measurements benchmark the calculations, indicating that the DFT method (B3LYP/6-31+G(d)) is reasonably accurate. Calculations aid in the explanation of surprising trends in gas phase acidity, which are attributable to geometry and the planarity of the N-aryl substituent, relative to the triazolium ring. For the achiral catalysts, the few pK_a values that are known track reasonably well with the gas phase acidity values, though the acidity range is much tighter in solution than in the gas phase. This wider range of acidities in the gas phase allows for a clear correlation to be tracked between intrinsic acidity values and selectivity in both a homoenolate addition reaction, as catalyzed by achiral triazolylidene catalysts, and a Stetter reaction, as catalyzed by chiral triazolylidene catalysts. Acidity is shown to be a useful and powerful predictive tool for these types of reactions, and may well extend to other *Umpolung* reactions as well. We believe that different substituents affect the stereoelectronics of the system in such a way that is reflected in the acidity, allowing the gas phase acidity to track with selectivity.

3.5 References

- (1) Igau, A.; Baceiredo, A.; Trinquier, G.; Bertrand, G. *Angew. Chem. Int. Ed.* **1989**, *101*, 617.
- (2) Arduengo, A. J. I.; Harlow, R. L.; Kline, M. *J. Am. Chem. Soc.* **1991**, *113*, 361.
- (3) Samojłowicz, C.; Bieniek, M.; Grela, K. *Chem. Rev.* **2009**, *109*, 3708.
- (4) Flanigan, D. M.; Romanav-Michailidis, F.; White, N. A.; Rovis, T. *Chem. Rev.* **2015**, *115*, 9307.
- (5) Enders, D.; Niemeier, O.; Henseler, A. *Chem. Rev.* **2007**, *107*, 5606.
- (6) Bugaut, X.; Glorius, F. *Chem. Soc. Rev.* **2012**, *41*, 3511.
- (7) Massey, R. S.; Collett, C. J.; Lindsay, A. G.; Smith, A. D.; O'Donoghue, A. C. *J. Am. Chem. Soc.* **2012**, *134*, 20421.
- (8) O'Donoghue, A. C.; Massey, R. S. In *Contemporary Carbene Chemistry*; Moss, R. A., Doyle, M. P., Eds.; Wiley: Hoboken, New Jersey, 2013; Vol. 7, p 75.
- (9) Maji, B.; Breugst, M.; Mayr, H. *Angew. Chem. Int. Ed.* **2011**, *50*, 6915.
- (10) Liu, M.; Chen, M.; Zhang, S.; Yang, I.; Buckley, B.; Lee, J. K. *J. Phys. Org. Chem.* **2011**, *24*, 929.
- (11) Lee, C.; Yang, W.; Parr, R. G. *Phys. Rev. B* **1988**, *37*, 785.
- (12) Becke, A. D. *J. Chem. Phys.* **1993**, *98*, 5648.
- (13) Becke, A. D. *J. Chem. Phys.* **1993**, *98*, 1372.
- (14) Stephens, P. J.; Devlin, F. J.; Chabalowski, C. F.; Frisch, M. J. *J. Phys. Chem.* **1994**, *98*, 11623.
- (15) Kohn, W.; Becke, A. D.; Parr, R. G. *J. Phys. Chem.* **1996**, *100*, 12974.
- (16) GAUSSIAN09, R. A.; Frisch, M. J.; Trucks, G. W.; Schlegel, H. B.; Scuseria, G. E.; Robb, M. A.; Cheeseman, J. R.; Scalmani, G.; Barone, V.; Mennucci, B.; Petersson, G. A.; Nakatsuji, H.; Caricato, M.; Li, X.; Hratchian, H. P.; Izmaylov, A. F.; Bloino, J.; Zheng, G.; Sonnenberg, J. L.; Hada, M.; Ehara, M.; Toyota, K.; Fukuda, R.; Hasegawa, J.; Ishida, M.; Nakajima, T.; Honda, Y.; Kitao, O.; Nakai, H.; Vreven, T.; Montgomery, J., J. A.; Peralta, J. E.; Ogliaro, F.; Bearpark, M.; Heyd, J. J.; Brothers, E.; Kudin, K. N.; Staroverov, V. N.; Kobayashi, R.; Normand, J.; Raghavachari, K.; Rendell, A.; Burant, J. C.; Iyengar, S. S.; Tomasi, J.; Cossi, M.; Rega, N.; Millam, J. M.; Klene, M.; Knox, J. E.; Cross, J. B.; Bakken, V.; Adamo, C.; Jaramillo, J.; Gomperts, R.; Stratmann, R. E.; Yazyev, O.; Austin, A. J.; Cammi, R.; Pomelli, C.; Ochterski, J. W.; Martin, R. L.; Morokuma, K.; Zakrzewski, V. G.; Voth, G. A.; Salvador, P.; Dannenberg, J. J.; Dapprich, S.; Daniels, A. D.; Farkas, Ö.; Foresman, J. B.; Ortiz, J. V.; Cioslowski, J.; Fox, D. J., Gaussian, Inc., Wallingford CT, 2009.
- (17) Marenich, A. V.; Cramer, C. J.; Truhlar, D. G. *J. Phys. Chem. B* **2009**, *113*, 6378.
- (18) Miertuš, S.; Scrocco, E.; Tomasi, J. *Chem. Phys.* **1981**, *55*, 117.
- (19) Pascual-Ahuir, J. L.; Silla, E.; Tuñón, I. *J. Comput. Chem.* **1994**, *15*, 1127.

- (20) Zhao, Y.; Truhlar, D. G. *Theor. Chem. Acc.* **2008**, *120*, 215.
- (21) Zhao, Y.; Truhlar, D. G. *Acc. Chem. Res.* **2008**, *41*, 157.
- (22) Kurinovich, M. A.; Lee, J. K. *J. Am. Soc. Mass. Spectrom.* **2002**, *13*, 985.
- (23) Xuejun, S.; Lee, J. K. *J. Org. Chem.* **2007**, *72*, 6548.
- (24) Liu, M.; Li, T.; Amegayibor, F. S.; Cardoso, D. S.; Fu, Y.; Lee, J. K. *J. Org. Chem.* **2008**, *73*, 9283.
- (25) Michelson, A. Z.; Chen, M.; Wang, K.; Lee, J. K. *J. Am. Chem. Soc.* **2012**, *134*, 9622.
- (26) Liu, M.; Yang, I.; Buckley, B.; Lee, J. K. *Org. Lett.* **2010**, *12*, 4764.
- (27) Liu, M.; Chen, M.; Zhang, S.; Yang, I.; Buckley, B.; Lee, J. K. *J. Phys. Org. Chem.* **2011**, *24*, 929.
- (28) Kaljurand, I.; Koppel, I. A.; Kutt, A.; Room, E.-I.; Rodima, R.; Koppel, I.; Mishima, M.; Leito, I. *J. Phys. Chem. A* **2007**, *111*, 1245.
- (29) Brauman, J. I.; Blair, L. K. *J. Am. Chem. Soc.* **1970**, *92*, 5986.
- (30) Ema, T.; Nanjo, Y.; Shiratori, S.; Terao, Y.; Kimura, R. *Org. Lett.* **2016**, *18*, 5764.
- (31) Nair, V.; Sinu, C. R.; Babu, B. P.; Varghese, V.; Jose, A.; Suresh, E. *Org. Lett.* **2009**, *11*, 5570.
- (32) Maji, B.; Ji, L.; Wang, S.; Vedachalam, S.; Ganguly, R.; Liu, X.-W. *Angew. Chem. Int. Ed.* **2012**, *51*, 8276.
- (33) White, N. A.; DiRocco, D. A.; Rovis, T. *J. Am. Chem. Soc.* **2013**, *135*, 8504.
- (34) Plots of selectivity versus calculated acidity for the furyl and phenyl nitroalkenes, as well as a plot of selectivity versus experimental acidity for the ethyl nitroalkene are in the Supporting Information.
- (35) H and F are not isosteric. F has an A-value of 0.25, and a van der Waals radius of 1.47 (compared to 1.22 for H).
- (36) Collett, C. J.; Massey, R. S.; Maguire, O. R.; Batsanov, A. S.; O'Donoghue, A. C.; Smith, A. D. *Chem. Sci.* **2013**, *4*, 1514.
- (37) Zhang, Q.; Yu, H.-Z.; Fu, Y. *Org. Chem. Front.* **2014**, *1*, 614.
- (38) Liu, Q.; Rovis, T. *J. Am. Chem. Soc.* **2006**, *128*, 2552.
- (39) For precatalysts **6a**, **6b**, **6d**, **6e** and **6h**, the enantiomers were utilized for the ee experiments; however, the gas phase acidity is still relevant since this value remains the same regardless of enantiomer.
- (40) Liu, Q.; Rovis, T. *Org. Process Res. Dev.* **2007**, *11*, 598.
- (41) Kim, Y.-J.; Streitwieser, A. *J. Am. Chem. Soc.* **2002**, *124*, 5757.
- (42) Sievers, A.; Wolfenden, R. *J. Am. Chem. Soc.* **2002**, *124*, 13986.
- (43) Washabaugh, M. W.; Jencks, W. P. *J. Am. Chem. Soc.* **1989**, *111*, 674.
- (44) Alder, R. W.; Allen, P. R.; Williams, S. J. *J.C.S. Chem. Commun.* **1995**, 1267.
- (45) Chu, Y.; Deng, H.; Cheng, J.-P. *J. Org. Chem.* **2007**, *72*, 7790.
- (46) Amyes, T. L.; Diver, S. T.; Richard, J. P.; Rivas, F. M.; Toth, K. *J. Am. Chem. Soc.* **2004**, *126*, 4366.

- (47) Higgins, E. M.; Sherwood, J. A.; Lindsay, A. G.; Armstrong, J.; Massey, R. S.; Alder, R. W.; O'Donoghue, A. C. *Chem. Comm.* **2011**, 47, 1559.

Note: Major parts of this chapter have been published: Zeng, H.; Wang, K.; Tian, Y.; Niu, Y.; Greene, L.; Hu, Z.; Lee, J. K. “The benzoin condensation: charge tagging of the catalyst allows for tracking by mass spectrometry” *Int. J. Mass Spectrom.* **2014**, 369, 92.

Reprinted (adapted) with permission from Zeng, H.; Wang, K.; Tian, Y.; Niu, Y.; Greene, L.; Hu, Z.; Lee, J. K. “The benzoin condensation: charge tagging of the catalyst allows for tracking by mass spectrometry” *Int. J. Mass Spectrom.* **2014**, 369, 92. Copyright 2015 ScienceDirect (see the end of this dissertation for the permission)

Chapter 4. Charge-Tagged Thiazolylidene Catalysts

4.1 Introduction

Polarity inversion of a functional group is called *Umpolung*.¹ It is a particularly intriguing class of organic reactions. A classic example of *Umpolung* is the benzoin condensation, a coupling reaction between two aromatic aldehydes to form α -hydroxyketones. The benzoin condensation can be catalyzed by a cyanide anion or an *N*-heterocyclic carbene (NHC).²⁻⁶ In 1903, Lapworth proposed the reaction mechanism of a cyanide-catalyzed benzoin condensation.⁶ Half a century later, the mechanism of NHC-catalyzed benzoin condensation was proposed by Breslow, who postulated that the deprotonated thiazolium - thiazolylidene, is the catalytic species (Figure 4.1).⁷

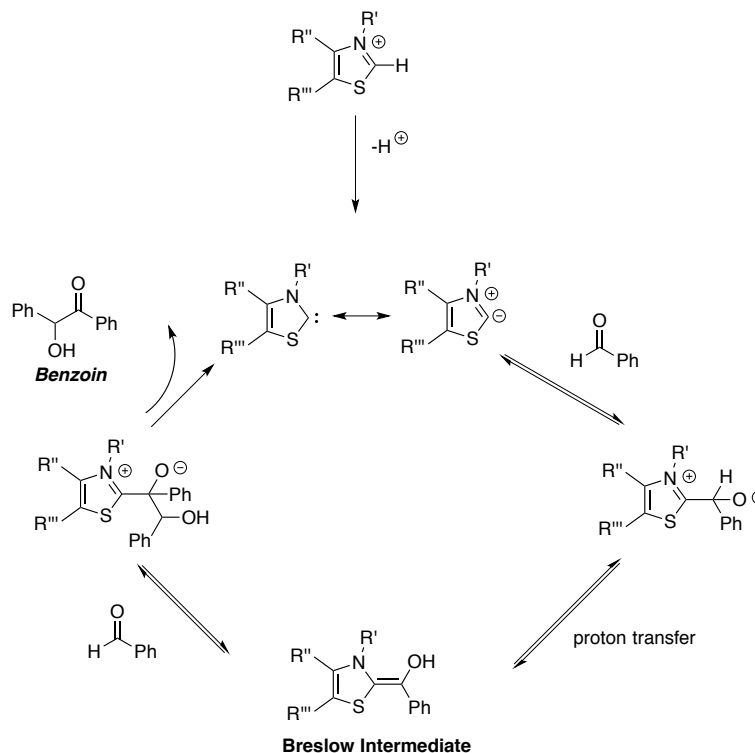


Figure 4.1 Catalytic cycle of the benzoin condensation as proposed by Breslow

The enaminol-like structure generated from the addition of the thiazolylidene to a benzaldehyde, followed by a proton transfer is called the Breslow intermediate, which displays *Umpolung* reactivity (the aldehyde carbon center becomes nucleophilic rather electrophilic, adding to a second aldehyde). Similarly, the Stetter reaction involves an addition of Breslow intermediate to an α,β -unsaturated ketone, rather than benzaldehyde.⁸

The Breslow mechanism is commonly accepted for the NHC-catalyzed benzoin condensation. Much evidence has been found in support of this mechanism. In 2012, Berkessel and coworkers successfully isolated and spectroscopically characterized Breslow intermediates formed by imidazolinylienes and aromatic aldehydes.⁹ However, other mechanisms suggested by Lemal and Castells *et al.* also exist. In their alternative

mechanisms, the NHC dimer can act as a nucleophilic catalyst in its own right.^{10,11} For Stetter reactions catalyzed by NHCs, the mechanisms are assumed to be similar to the benzoin condensations, via the Breslow intermediate; however, reports of detailed mechanistic studies are limited.

Understanding the mechanism of organocatalytic reactions is significant for the development of synthetic methods and transformations. Because the NHC-catalyzed *Umpolung* reactions have great synthetic utility, we aim to use electrospray ionization mass spectrometry (ESI-MS) to investigate the mechanisms of such reactions in a solvent-free environment. Reactions in the gas phase can display intrinsic reactivity without the influence of solvent effects. ESI is a well-established method for transferring ions from solution sample directly to analytes in gas phase with little fragmentation. In recent years, ESI-MS opens the door to tracking the progress of organic reactions.^{12,13}

Using ESI-MS to study the reaction mechanisms requires relevant species to be charged. We designed and synthesized two thiazolylidene catalysts with sulfonate charge tags (**10c** and **10d**, Figure 4.2).¹⁴ The synthesized compounds were detected by ESI-MS under negative ion mode and were used to explore the potential of investigating gas-phase NHC-catalyzed reactions in the absence of solvent.^{15,16}

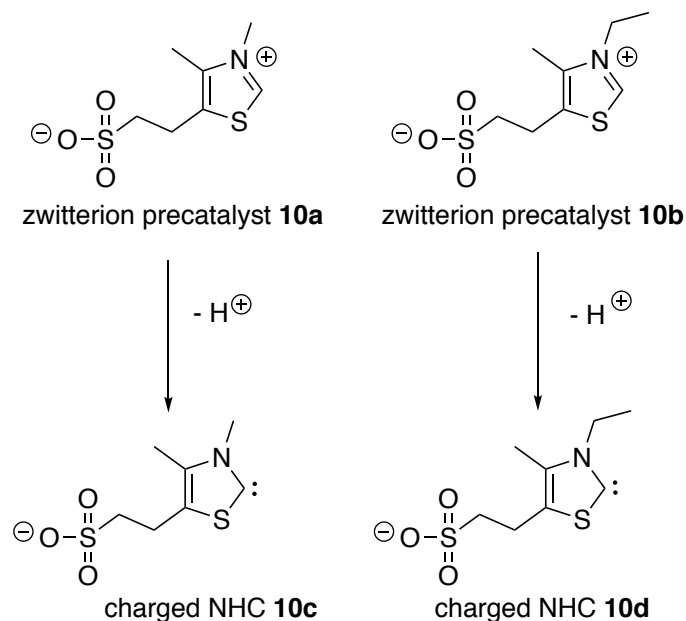


Figure 4.2 Designed and synthesized charge-tagged thiazolylidene catalysts **10c** and **10d**

4.2 Experimental

4.2.1 Synthesis of Charge-handled Thiazolylidene Catalyst Precursors

As Figure 4.3 shows, a mixture of 4-methyl-5-thiazoleethanol (1 mmol, 143mg) and triethylamine (5 mmol, 0.5g) was dissolved in acetonitrile (5 mL) at 0 °C in a round-bottomed flask under protection of N₂. Methanesulfonyl chloride (1.2 mmol, 137 mg) was added dropwise while keeping the reaction stirring at 0 °C. After 0.5 hour, the flask was cooled to room temperature, and the reaction was run to completion (2 hours). Column chromatography with silica gel as the stationary phase and ethyl acetate as the mobile phase, was used to purify the crude product **10e** (4-methyl-5-(2-(methanesulfonyl)ethyl)thiazole). A light yellow oily liquid was obtained after rotary evaporation.

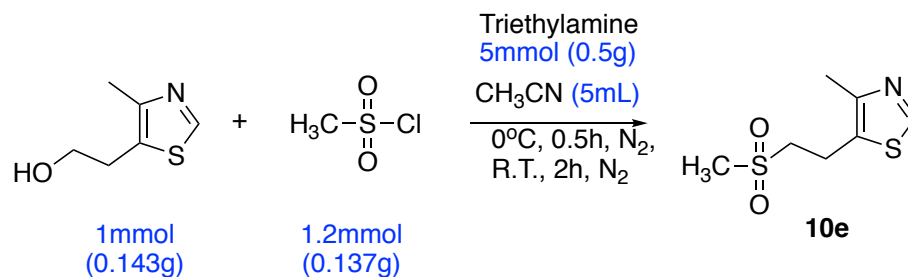


Figure 4.3 Synthesis of charge-handled thiazolylidene catalyst precursors: Step 1

The product **10e** from Step 1 (1 mmol, 200 mg) was dissolved in water (5mL). Then sodium sulfite (10 mmol, 1.26g) was added into the reaction system (Figure 4.4). After refluxing under 140°C for 4 hours, the reaction was neutralized using dilute hydrochloric acid solution (~1 mol/L) to pH = 7.0. After rotary evaporation of reaction solvent (water) and purification of column chromatography (1:1 ethyl acetate: methanol as the mobile phase and aluminum oxide as the stationary phase), 2-(4-methylthiazol-5-yl)ethane-1-sulfonic acid (Step 2 product, **10f**) was yielded as a white solid after evaporating the solvent.

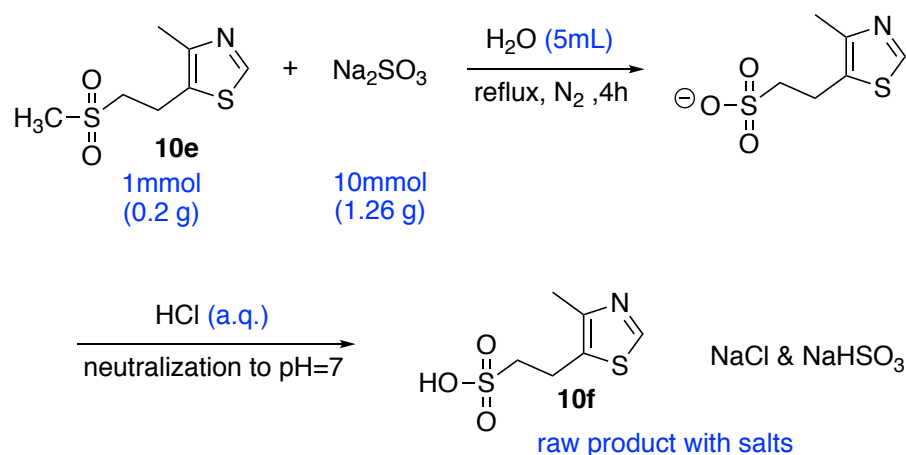


Figure 4.4 Synthesis of charge-handled thiazolylidene catalyst precursors: Step 2

The zwitterion precatalysts **10a** and **10b** were produced by Step 3. Dimethylformamide was used as solvent for both preparation reactions (Figure 4.5).

For the synthesis of the methyl-substituted precatalyst **10a**, methyl iodide (4 mmol, 700 mg) was added dropwise into a round-bottomed flask, which contains a solution of dimethylformamide (5 mL) and 2-(4-methylthiazol-5-yl)ethane-1-sulfonic acid (**10f**, 1 mmol). The reaction mixture was stirred for 12 hours at 70 °C in an open system, and then quenched with 5 mL of methanol. For the synthesis of the ethyl-substituted precatalyst **10b**, ethyl iodide (5 mmol, 760 mg) was used to react with 2-(4-methylthiazol-5-yl)ethane-1-sulfonic acid (**10f**, 1 mmol) under the same condition.

After column chromatography purification (1:1 dichloromethane: methanol as the mobile phase and aluminum oxide as the stationary phase), the zwitterion precatalysts **10a** and **10b** were collected as light yellow solids after evaporating the solvent. Final crude products were further purified by HPLC, using an HILIC column (Atlantis HILIC Silica, I.D. 4.6 mm, length 100 mm, particle size 3 microns) and acetonitrile as the mobile phase.

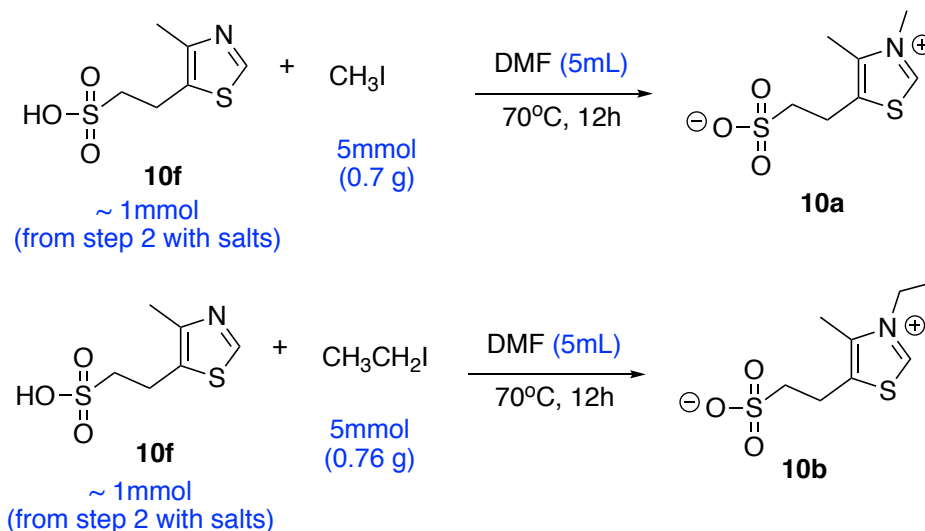


Figure 4.5 Synthesis of charge-canded thiazolylidene catalyst precursors: Step 3

Proton nuclear magnetic resonance spectra (^1H -NMR) were recorded on a Varian VNMR-300 MHz instrument and were reported in ppm using solvents as internal standards (CDCl_3 at 7.26 ppm, $(\text{CD}_3)_2\text{SO}$ at 2.50 ppm, CD_3OD at 3.31 ppm). Data were reported as app = apparent, s = singlet, d = doublet, t = triplet, dd = doublet of doublets, ddd = doublet of doublet of doublets, dddd = doublet of doublet of doublet of doublets, m = multiplet, comp = complex; integration; coupling constant(s) in Hz.

Structures of product **10a** and **10b** were also confirmed using a Finnigan LCQ DUO mass spectrometer. A 0.1 mM solution of the synthesized thiazolium in methanol with 0.1% ammonium hydroxide was injected using ESI. An electrospray needle voltage of 2.7 kV and a flow rate of 20 $\mu\text{L}/\text{min}$ were used, with a capillary temperature of 190 $^\circ\text{C}$. The ions were detected in negative ion mode. The charged species were isolated by MS/MS and analyzed by collision-induced dissociation (CID) experiments. Spectra were an average of

ten scans.

4.3 Results and Discussion

The synthesis of the pre-catalysts, the zwitterions **10a** and **10b**, is described in 4.2.1.

^1H NMR was used to confirm the structures of product in each step (Figure 4.6 - 4.9).

i. Step 1 Product 10e: 4-Methyl-5-(2-(methylsulfonyl)ethyl)thiazole

^1H NMR (300 MHz, Chloroform- d) δ 8.65 (s, 1H), 4.39 (t, J = 6.6 Hz, 2H), 3.25 (t, J = 6.6 Hz, 2H), 2.98 (s, 3H), 2.45 (s, 3H).

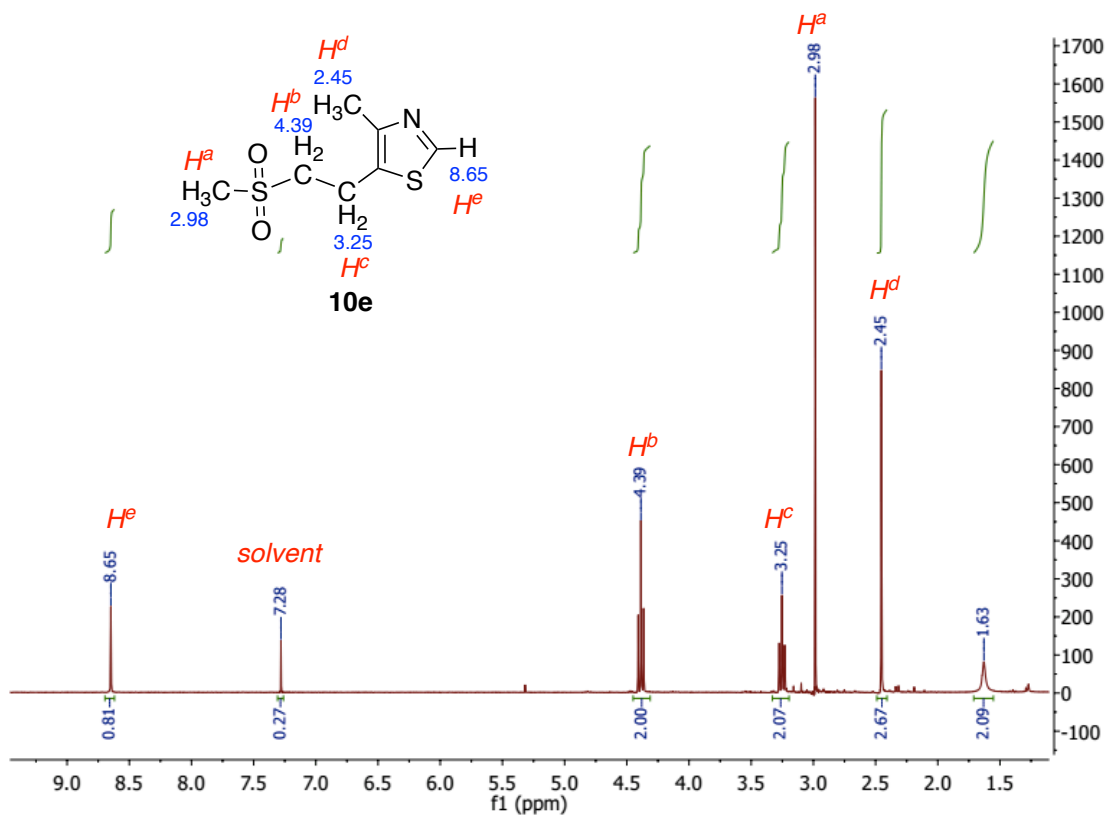


Figure 4.6 ^1H NMR spectrum of Step 1 product **10e**

ii. Step 2 Product **10f**: 2-(4-Methylthiazol-5-yl)ethane-1-sulfonic Acid

^1H NMR (300 MHz, DMSO- d_6) δ 8.78 (s, 1H), 3.11 – 2.92 (m, 2H), 2.74 – 2.56 (m, 2H), 2.29 (s, 3H).

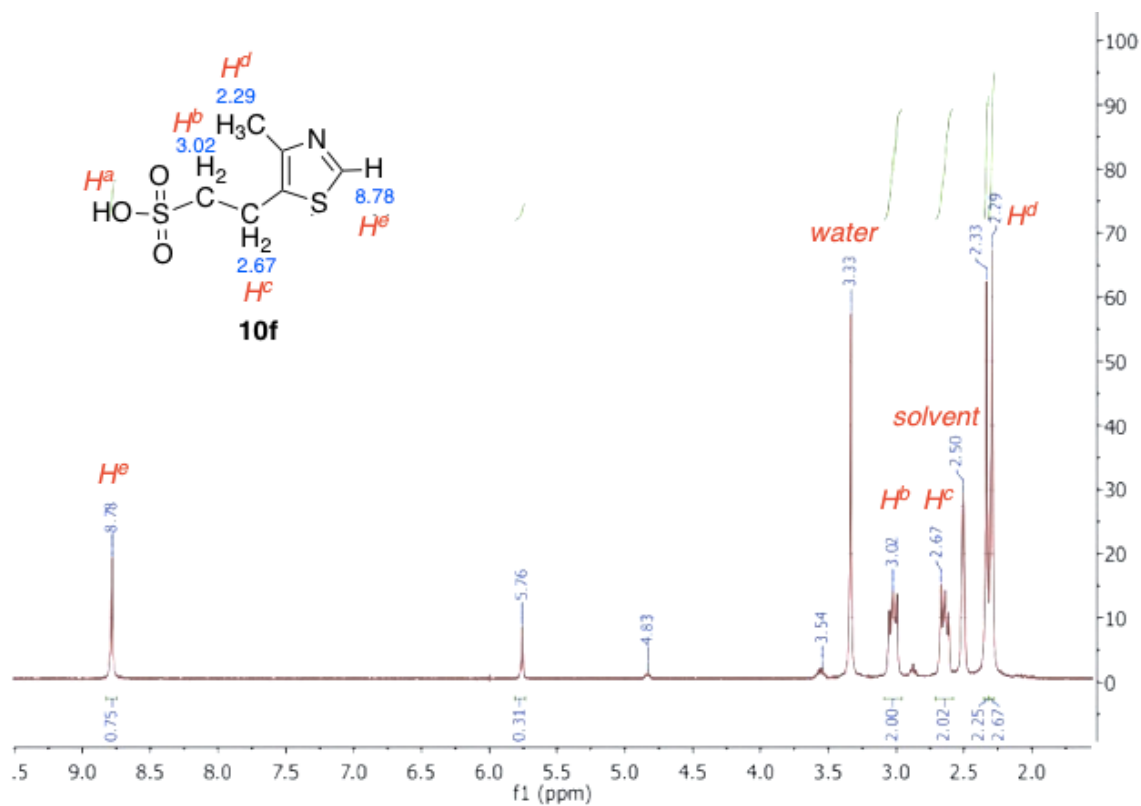


Figure 4.7 ^1H NMR spectrum of Step 2 product **10f**

iii. Methyl-substituted Step 3 Product 10a: 2-(3,4-dimethylthiazol-3-ium-5-yl)ethane-1-sulfonate

^1H NMR (300 MHz, Methanol- d_4) δ 4.18 (s, 3H), 3.44 – 3.37 (m, 2H), 3.21 – 3.09 (m, 2H), 2.56 (s, 3H).

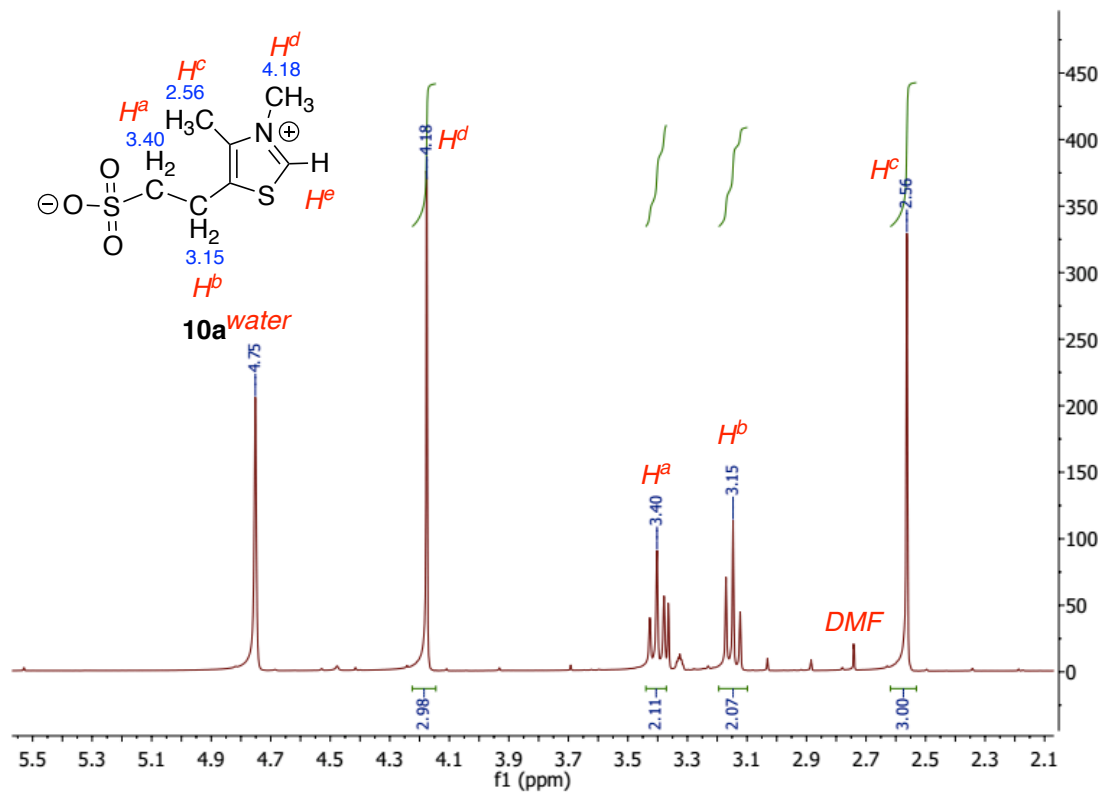


Figure 4.8 ^1H NMR spectrum of Step 3 methyl-substituted product 10a

iii. Ethyl-substituted Step 3 Product **10b**: 2-(3-ethyl-4-methylthiazol-3-ium-5-yl)ethane-1-sulfonate

^1H NMR (300 MHz, Methanol- d_4) δ 4.54 (qd, $J = 7.3, 0.8$ Hz, 2H), 3.42 (m, $J = 7.1$ Hz, 2H), 3.16 (m, $J = 7.1, 0.8$ Hz, 2H), 2.59 (s, 3H), 1.62 (td, $J = 7.3, 0.8$ Hz, 3H).

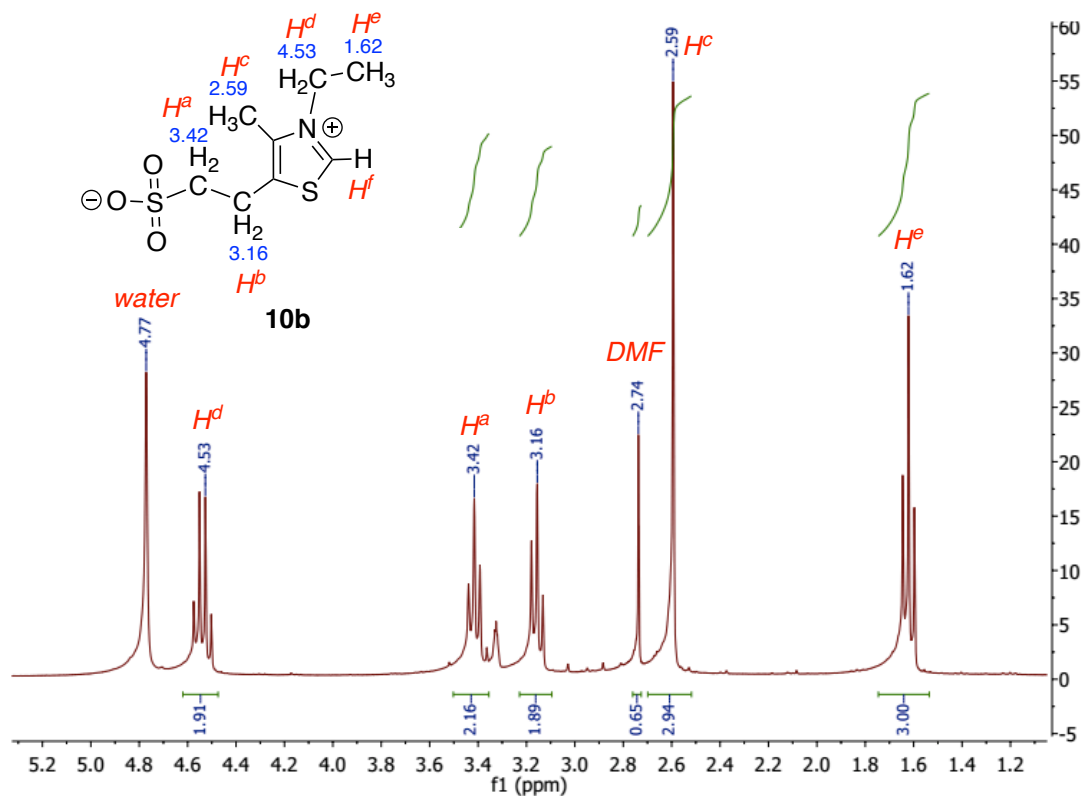


Figure 4.9 ^1H NMR spectrum of Step 3 ethyl-substituted product **10b**

Mass spectrometry was also used to identify charge-handled NHC. The thiazolium zwitterion precatalysts **10a** (**10b**) with a concentration of 0.1 mM was deprotonated by ammonium hydroxide (100 mol%) in a methanol solution, before it was injected into ESI. The charged NHC thiazolyliidene catalyst **10c** (**10d**) was generated *in situ* and was detected

by the mass spectrometer under negative ion mode. The m/z signals corresponding to the catalysts (**10c**, m/z 220; **10d**, m/z 234) were observed and isolated in the spectra (Figure 4.10).

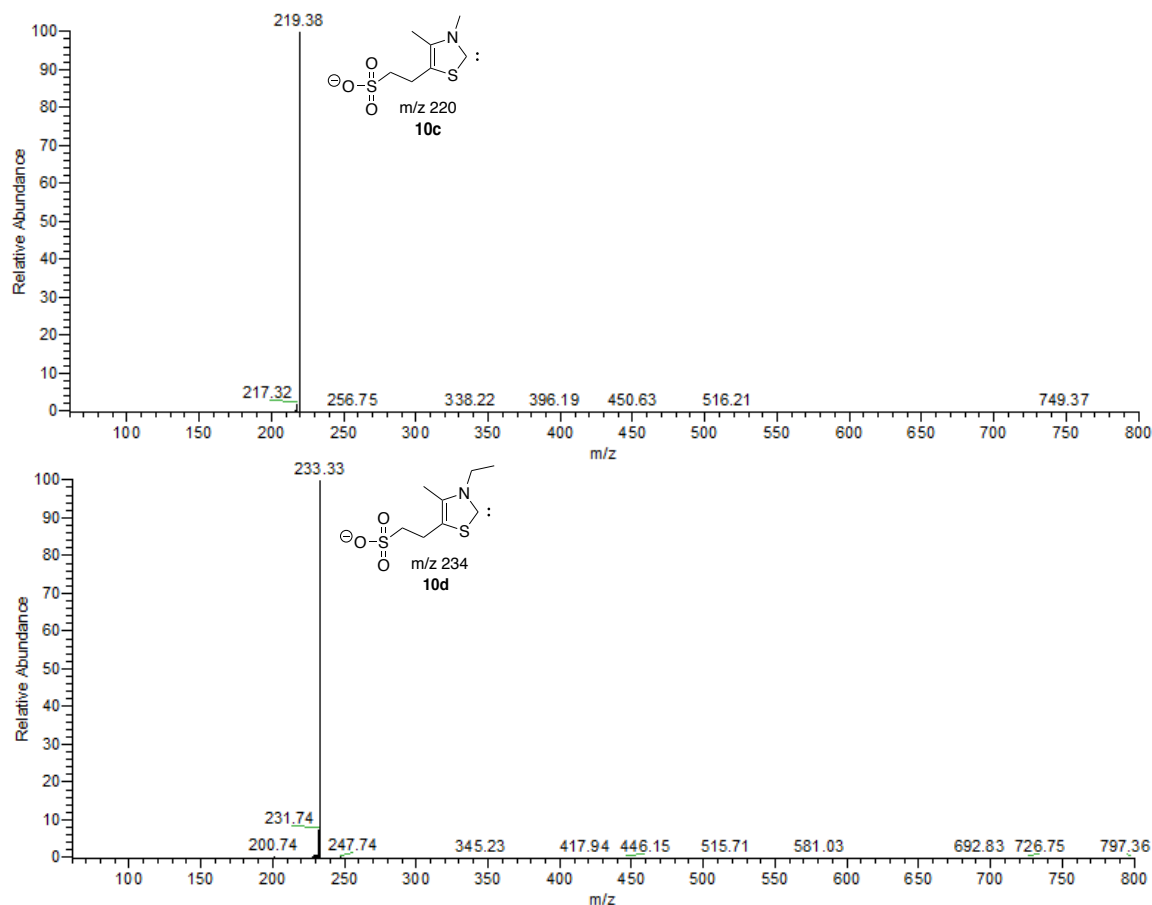


Figure 4.10 MS/MS spectra of **10c** (top) and **10d** (bottom)

Since other possible structures, such as a doubly charged NHC dimer (**10c'**/**10d'**), may have the same mass-to-charge ratio (Figure 4.11), we applied collision-induced dissociation (CID) to support our structural assignment.

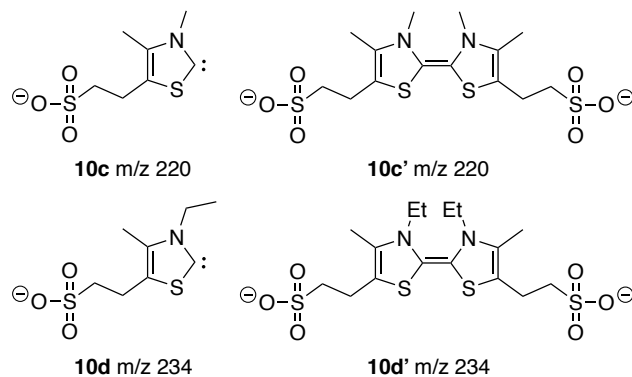


Figure 4.11 Charged-tagged NHC catalysts (**10c** and **10d**) and doubly charged NHC dimers (**10c'** and **10d'**)

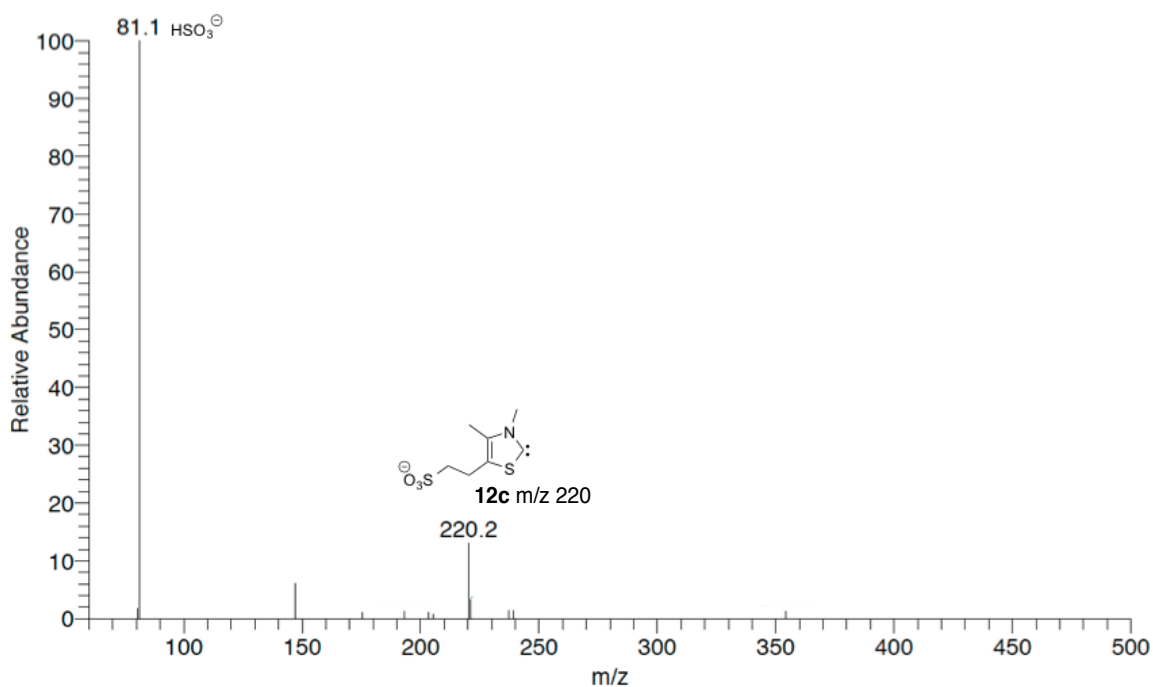


Figure 4.12 Fragmentation of **10c** in positive ion mode

When ion with m/z 220 (**10c**) was isolated and applied with CID energy, only a fragment ion of m/z of 81 was observed, corresponding to HSO_3^+ . If a dimer with m/z 220 were actually formed, a m/z 359 peak should be detected after the loss of HSO_3^+ , which we did not observe. We attribute the m/z 220 peak to catalyst **10c** for addition reasons: when

higher collision energies were applied, the m/z 220 peak decreased and eventually disappeared. A doubly charged NHC dimer (**10c'**), m/z 220, would be expected to dissociate to a daughter ion of m/z 220 (the same mass-to-charge ratio).

Similar CID patterns were observed for **10d**.

4.4 Conclusions

Two novel negatively charge-handled thiazolylidene *N*-heterocyclic carbene (NHC) catalysts have been designed and successfully synthesized. These catalysts were used to study mechanisms of NHC-catalyzed *Umpolung* reactions, including the benzoin condensation and Stetter reaction via mass spectrometry.^{15,16} The sulfonate tag allows intermediates to be tracked during NHC-catalyzed reaction processes.

4.5 References

- (1) Seebach, D. *Angew. Chem. Int. Ed.* **1979**, *18*, 239.
- (2) Richard T. Arnold, Reynold C. Fuson. *J. Am. Chem. Soc.* , **1936**, *58*, 1295.
- (3) L. Baragwanath, C. A. Rose, K. Zeitler, S. J. Connon, *J. Org. Chem.*, **2009**, *74*, 9214.
- (4) S. M. Langdon, M. M. D. Wilde, K. Thai, M. Gravel, *J. Am. Chem. Soc.*, **2014**, *136*, 7359.
- (5) K. Thai, S. M. Langdon, F. Bilodeau, M. Gravel, *Org. Lett.*, **2013**, *15*, 2214.
- (6) Lapworth, A., *J. Chem. Soc. Trans.* **1904**, *85*, 1206.
- (7) Breslow, R., *J. Am. Chem. Soc.* **1958**, *80*, 3719.
- (8) Stetter, H.; Schreckenberger, M., *Angew. Chem. Int. Ed.* **1973**, *12*, 81.
- (9) Berkessel, A.; Elfert, S.; Yatham, V. R.; Neudörfl, J.-M.; Schlörer, N. E.; Teles, J. H., *Angew. Chem. Int. Ed.* **2012**, *51*, 12370.
- (10) Lemal, D. M.; Lovald, R. A.; Kawano, K. I. *J. Am. Chem. Soc.* **1964**, *86*, 2518.
- (11) Castells, J.; López-Calahorra, F.; Geijo, F.; Pérez-Dolz, R.; Bassedas, M. J. *Heterocycl. Chem.* **1986**, *23*, 715.
- (12) Castells, J.; Lopez-Calahorra, F.; Domingo, L., *J. Org. Chem.* **1988**, *53*, 4433.
- (13) Castells, J.; Domingo, L.; López-Calahorra, F.; Martí, J., *Tetrahedron Lett.* **1993**, *34*, 517.
- (14) Picard, J. P.; Calas, R.; Dunogues, J.; Duffaut, N.; Gervai, J.; Lapouyade, P. *J. Org. Chem.* **1979**, *44*, 420.
- (15) Tian, Y.; Lee, J. K. *J. Org. Chem.* **2015** , *80*, 6831.
- (16) Zeng, H.; Wang, K.; Tian, Y.; Niu, Y.; Greene, L.; Hu, Z.; Lee, J. K. *Int. J. Mass Spectrom.* **2014**, *369*, 92.

Chapter 5. Charge-Tagged Triazolylidene Catalysts

5.1 Introduction

The *N*-heterocyclic carbenes (NHCs) are powerful tools in organic chemistry. Because of their distinct electronic and steric properties, NHCs play an important role in transition-metal catalysis as strong two-electron σ -donor ligands. Most NHC ligands on transition-metal-catalysts are imidazolylienes. For example, the second-generation Grubbs catalyst for olefin metathesis uses the imidazolylidene NHC 1,3-bis(2,4,6-trimethylphenyl)-4,5-dihydroimidazol-2-ylidene as a ligand, replacing the first-generation phosphine ligand (Figure 5.1).¹

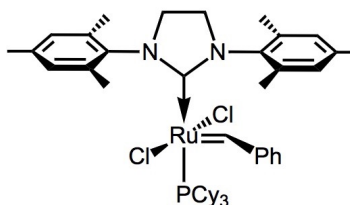


Figure 5.1 Second-generation Grubbs catalyst

As organocatalysts, NHCs are best known for their ability to effect *Umpolung* catalysis. Since Ukai and coworkers discovered the ability of thiazolium salts to catalyze the benzoin condensation in 1943, a wide variety of chiral and achiral thiazolylidene catalysts, generated *in situ* from thiazolium salts, have been developed to catalyze *Umpolung* reactions.^{2,3}

In recent years, NHC catalysts with another framework, the triazolylidene carbenes, have been dominating stable carbene-catalyzed reactions. In 1996, Enders and coworkers

reported the first triazolylidene-catalyzed asymmetric Stetter reaction (Figure 5.2).^{4,5}

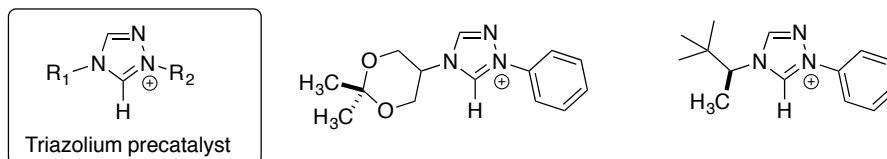


Figure 5.2 Triazolium precatalysts used by Enders

This opened up a new class of catalytic NHC compounds. Since then, much work has been focused on the development of chiral triazolylidene catalysts (Figure 5.3). Two years later, the efforts of Knight and Leeper at designing a chiral bicyclic triazolylidene framework greatly improved the stereoselectivity of triazolylidene catalysts (Figure 5.4).⁶

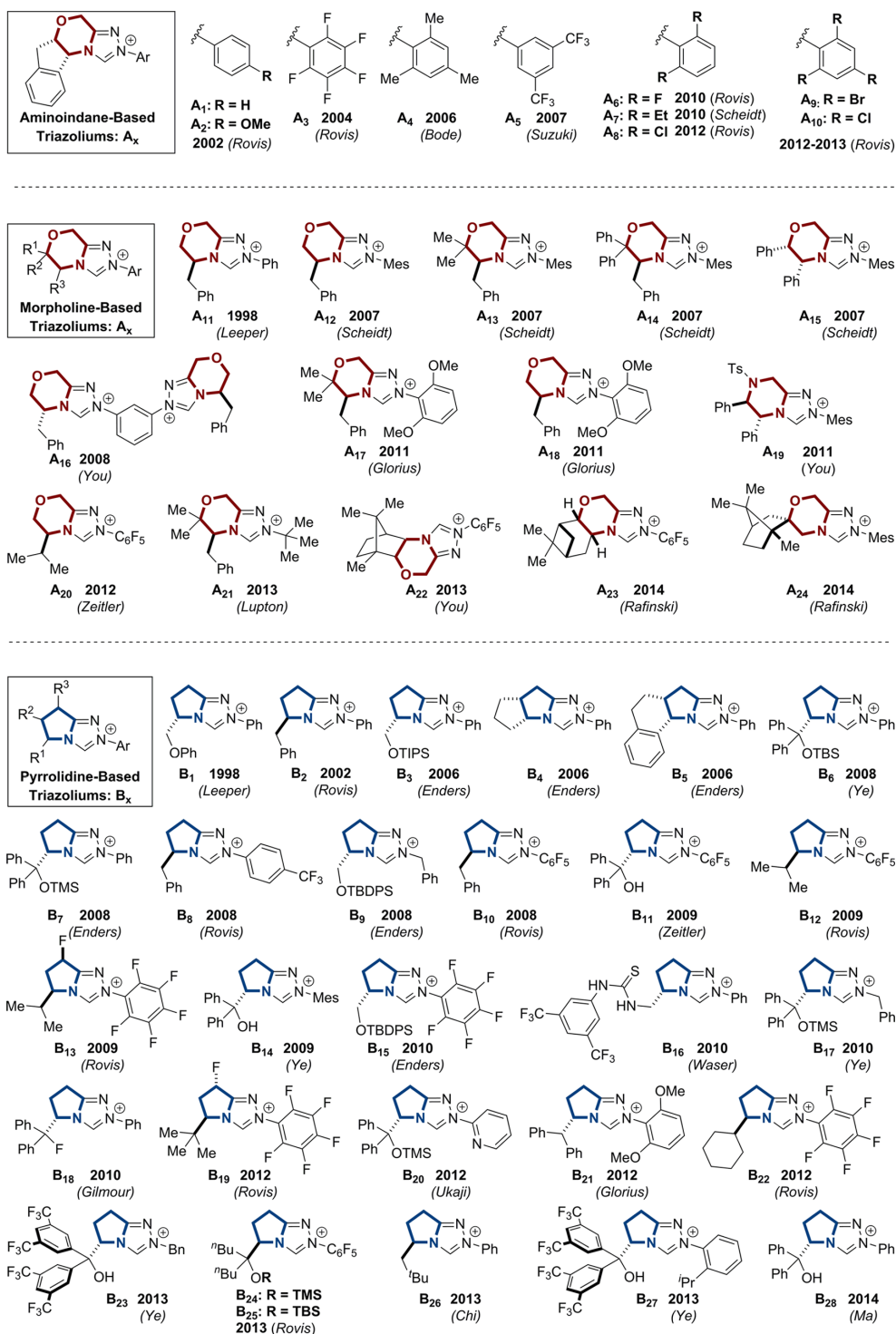


Figure 5.3 Selected triazolium precatalysts⁷ Reprinted (adapted) with permission from (*Chemical Reviews* **2015**, 115 (17), 9307-9387; DOI: 10.1021/acs.chemrev.5b00060).

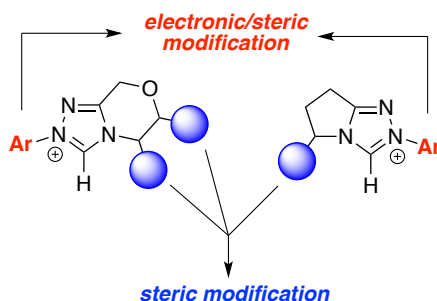


Figure 5.4 Chiral bicyclic triazolium frameworks

Nowadays, carbene-catalyzed chiral and achiral reactions are ubiquitous. Many reaction mechanisms remain unclear though, such as that for the Stetter reaction.⁸ As described in Chapter 4, our group is currently using two charge-tagged thiazolylidene catalysts (**10c** and **10d**) to study *Umpolung* reaction mechanisms in the gas phase. Our research interest covers both the benzoin condensation and Stetter reaction.^{9,10} We electrosprayed these charge-tagged catalysts (**10c** and **10d**) into the mass spectrometer, and then introduced benzaldehyde to ascertain whether the NHC catalysts would add to the aldehyde *in vacuo* to produce a Breslow intermediate. However, no ion signals corresponding to the addition product was found.⁹ Our hypothesis, supported by calculations, is that the formation of the Breslow intermediate in the gas phase requires an intramolecular 1,2-proton transfer. A direct intramolecular 1,2-proton transfer requires a too-high barrier that cannot be overcome in the gas phase. In the solution phase, this proton transfer can be assisted by solvent molecules in a bimolecular reaction. We were able to obtain a sila-Breslow intermediate using an acylsilane in place of the aldehyde reactant as the 1,2-transfer of a silyl group is allowed via the Brook rearrangement.¹¹ The signal peak

of the sila-Breslow intermediate was successfully observed, which supported our hypothesis that the direct 1,2-silyl transfer is more favorable than 1,2-proton transfer in the solvent-free environment. However, the unfavorable intramolecular proton-transfer problem remains unsolved. We sought to develop new strategies to tackle this problem.

Collaborating with the Rovis group, we designed two novel charge-tagged triazolylidene catalysts (**11a-anion** and **11b-anion**), as shown in Figure 5.5.

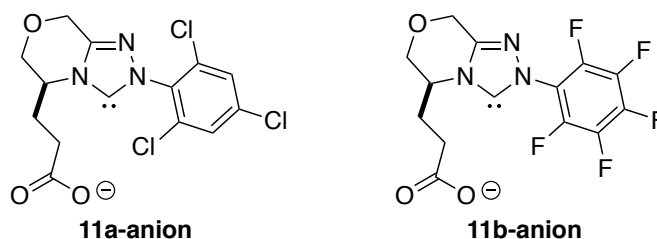


Figure 5.5 Two novel charge-tagged triazolylidene catalysts

Herein, the charge-tagged carboxylate groups would not only be able to make relevant species observable via mass spectrometry, but they can also serve as proton shuttles to effect the 1,2-proton transfer and formation of Breslow intermediate, as shown in Figure 5.6. In addition, these new charged triazolylidene catalysts will enable us to compare the intrinsic catalytic reactivities between thiazolylidenes (as described in Chapter 4) and triazolylidenes.

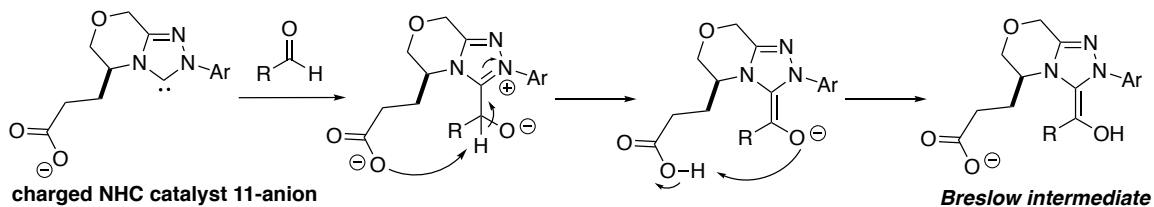
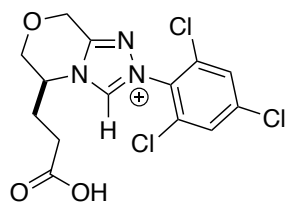
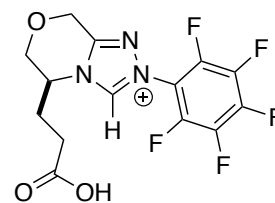


Figure 5.6 Charged tag-mediated formation of Breslow intermediate in the gas phase

A. Protonated 11a and protonated 11b
(selected structures)

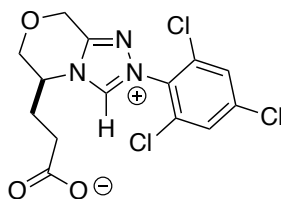


11a-cation

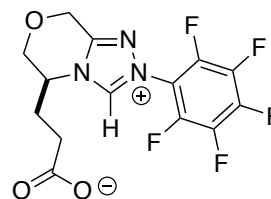


11b-cation

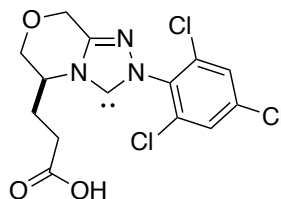
B. Neutral 11a and 11b



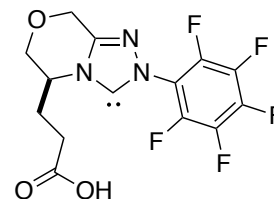
11a-zwitterion



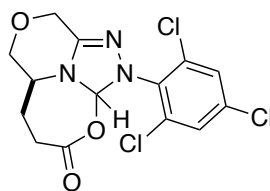
11b-zwitterion



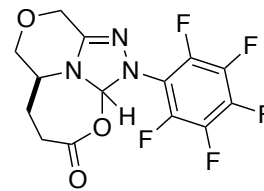
11a-neutral



11b-neutral

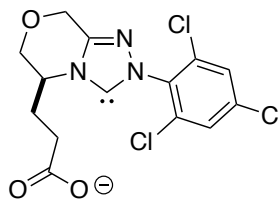


11a-ring

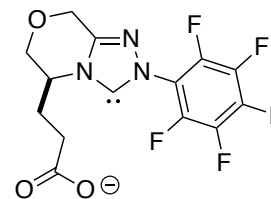


11b-ring

C. Deprotonated 11a and deprotonated 11b
(selected structures)



11a-anion



11b-anion

Figure 5.7 Related species of charge-tagged triazolyldene catalysts

Since the two charge-tagged triazolylidene catalysts are newly developed, fundamental properties of the negatively charged catalysts (**11a-anion** and **11b-anion**) as well as their related species (Figure 5.7) are of significance in understanding their catalytic reactivities in gas-phase *Umpolung* reactions. We named the neutral species as **11a**, for the 2,4,6-trichlorophenyl-substituted neutral species, and **11b**, for the perfluorophenyl-substituted neutral species. There exist three possible uncharged structures for **11a(b)**. They are the **11a(b)-zwitterion**, the **11a(b)-neutral**, and the **11a(b)-ring**, as shown in Figure 5.7.B. Correspondingly, there are multiple possible structures for protonated and deprotonated **11a(b)**. The isomer structures and their relative stabilities will be discussed in section 5.3.1. In Figure 5.7, only selected structures of protonated and deprotonated **11a(b)** are listed; they are the **11a(b)-cation** (Figure 5.7.A) and **11a(b)-anion** (Figure 5.7.C).

Because our gas-phase experimental studies utilize mass spectrometry, and the mass-to-charge ratio does not contain structural information to distinguish isomers, we need to first establish the structures of the charged species in the gas phase. We used calculations to assess the relative stabilities of the different isomers for neutral **11a(b)**, protonated **11a(b)**, and deprotonated **11a(b)**. Acidities of various protonated **11a(b)** cations and proton affinities of deprotonated **11a(b)** anions were also calculated. We measured the gas-phase acidities of protonated **11a** and **11b** experimentally and confirmed that the **11a-cation** and **11b-cation** were generated in the gas phase via electrospray ionization (ESI). They were also calculated to be the most stable structures for protonated **11a** and **11b** cations. The

comparison between calculated and experimental acidities, and the conformation of the gas-phase protonated **11a(b)** structure will be discussed in section 5.3.5. The experimental acidities of the **11a-cation** and **11b-cation** correspond to the proton affinities of the carbene centers (C-2) of **11a-neutral** and **11b-neutral**.

We also propose using these two charge-tagged triazolylidene carbene catalysts in solution-phase catalysis. Our hypothesis was that the presence of the carboxylate group would be able to accelerate the reaction rate of the Stetter reaction in solution. Significant evidence was found by the Rovis group that the rate determining step (RDS) of an intramolecular Stetter reaction was the first proton transfer to the form the Breslow intermediate.¹² The carboxylate group of **11a(b)-anion** catalyst has the potential to play the role of a monoanionic species, which would assist in the rapid formation of the Breslow intermediate via a intramolecular proton-shuttling mechanism, bypassing the symmetry-forbidden direct 1,2-hydrogen shift. This is a similar idea as what is described in Figure 5.6 for gas-phase reactions.

For charged NHC-catalyzed reactions in the solution phase, knowing the structure of the precatalysts is also important for designing the optimal reaction conditions. This is because a base is needed to deprotonate the precatalyst and to generate the negatively-charged NHC catalyst *in situ* for the catalytic process. One cannot know the correct loading of the base without knowing the exact structure of the precatalyst. As shown in Figure 5.7.B, the neutral precatalyst of **11a(b)-anion** can have different structures in the solution

phase. The precatalyst can be a neutral species with either a lactone structure of **11a(b)-ring**, a free carbene structure of **11a(b)-neutral**, or a zwitterion structure of **11a(b)-zwitterion**. It can also be a salt, with the **11a(b)-cation** structure (a triazolium cation with a –COOH group) and a BF_4^- as the counterion. In order to produce the negatively-charged NHC catalyst, one equivalent of base is needed to deprotonate the neutral precatalyst structures, and two equivalents of the base are needed to deprotonate the salt. Solution phase characterizations of **11a(b)** precatalyst in the condensed phase did not provide a solid conclusion of the exact structure. We further used calculations to explore the relative stabilities of neutral **11a(b)** species in the solution phase, in order to better understand the condensed phase experimental findings for precatalyst structure.

5.2 Experimental

5.2.1 LCQ Bracketing Method

Charge-tagged triazolylidene precatalysts were synthesized by the Rovis group. Other reagents were used as purchased.

Gas-phase acidities of protonated **11a(b)** were first measured by the bracketing method using a modified Finnigan LCQ ESI-3D ion trap mass spectrometer, as described in Chapter 1. We chose a series of neutral reference bases with known proton affinities, guided by calculations. The neutral reference bases were leaked into the ion trap with helium buffer gas flow. The precatalysts of the charge-tagged NHCs were dissolved in methanol

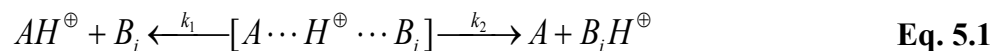
solution with a concentration of 0.1 mM, before they were injected in ESI. A ESI solution flow rate of 20 $\mu\text{L}/\text{min}$ was used. The capillary temperature was 190 $^{\circ}\text{C}$, the spray voltage was 4.5 kV, and the positive ion mode was used to analyze the ions. The protonated **11a(b)** cation was isolated via MS/MS and was allowed to react with neutral reference bases for 0.03 - 10000 ms. The average spectra of up to 10 scans was collected.

Reaction efficiency was used to assess the occurrence or non-occurrence of a proton transfer reaction between the analyte ions and the neutral reference bases. Reaction efficiency was defined as the ratio of the reaction rate constant and the theoretical ion-molecule collisional rate constant obtained from trajectory theory.¹³⁻¹⁵ Reactions that were less than 10% efficient were labeled “-” and reactions with efficiencies higher than 10% were labeled “+” in the bracketing table. All the reactions were performed under pseudo first-order conditions. In order to calculate the reaction rate constant, the pressure of the neutral bases had to be measured. We used a fast control reaction, a proton transfer from a weak base to a neutral reference base (assumed to be 100% efficient), to “back out” the reference base pressure.

5.2.2 Cooks Kinetic Method

The Cooks kinetic method was also used to study the gas-phase acidity of protonated **11a**. A Finnigan LCQ DUO ESI-3D ion trap mass spectrometer was used to conduct Cooks kinetic experiments, as described in Chapter 1. The proton-bound dimer between an analyte and a reference base was dissociated via collision-induced dissociation (CID), and either

the protonated analyte cation or the protonated reference base ion was formed (Eq. 5.1, where “A-H⁺” is the protonated **11a** cation in this case, and “B_i” stands for a series of reference bases). The ratio of these two products yielded the relative proton affinities of the two compounds.



A solution was prepared by mixing the analyte and reference base in a 1:1 ratio in methanol with a concentration of 0.5 mM. The solution was then electrosprayed into the mass spectrometer via ESI with a flow rate of 20 uL/min and a capillary temperature of 190 °C. The spray voltage was 4.5 kV. We saw the protonated **11a** cation (**11a**-H⁺), the protonated reference base, and the proton-bound dimer simultaneously in the mass spectrum. The proton-bound complex ion was isolated under MS-MS and subject to collision-induced energy with an activation time of 30 ms. A total of 40 scans were averaged for resultant spectra.

Data was analyzed using the Cooks “extended” kinetic method.¹⁶⁻²⁰ This method requires acquiring ion abundance ratios at different collision energies. Different collision energies have different T_{eff} (in Kelvin), which is the effective temperature of dissociating proton-bound complexes. This method allows for deconvolution of the enthalpic and entropic contributions. The analysis processes are summarized in Equations 5.2 - 5.4.

$$\ln \frac{k_1}{k_2} = \frac{[AH^{\oplus}]}{[BH^{\oplus}]} \quad \text{Eq. 5.2}$$

$$\ln \frac{k_1}{k_2} = \left[\frac{PA(A)}{RT_{eff}} - \frac{\Delta(\Delta S)}{R} \right] - \frac{PA(B_i)}{RT_{eff}} \quad \text{Eq. 5.3}$$

$$\frac{GB^{app}(A)}{RT_{eff}} = \frac{PA(A)}{RT_{eff}} - \frac{\Delta(\Delta S)}{R} \quad \text{Eq. 5.4}$$

$\Delta(\Delta S)$ is the difference in the ΔS associated with the two dissociation pathways in equation 5.1. A plot of $\ln(k_1/k_2)$, which equals to $\ln([AH^+]/[BiH^+])$, versus the proton affinity of a series of reference bases ($PA(B_i)$), yields the T_{eff} from the slope and the $GB^{app}(A)$ from the y-intercept (Eq. 5.3). Plotting equation 5.4 at different T_{eff} yields the proton affinity of the unknown ($PA(A)$) and $\Delta(\Delta S)$ for the Cooks experiments.

5.2.3 Calculation

Gas-phase calculations were conducted at B3LYP/6-31+G(d) using Gaussian09. Solvation studies were conducted using both the Polarizable Continuum Model (PCM) and the SMD solvation model, where molecules are optimized at B3LYP/6-31+G(d).^{21,22} A dielectric constant of 20.493 for acetone is used to simulate a condensed phase environment. The geometries were fully optimized and frequencies were calculated. All the values were reported as ΔH at 298K. No scaling factor was applied.

5.3 Results and Discussion

5.3.1 Computational Results in the Gas Phase

It was found that density functional theory (DFT) methods generally yielded accurate

values for gas-phase thermochemical properties of triazolium-based compounds (Chapter 3). We utilized DFT method at B3LYP/6-31+G(d) to study the relative stabilities (enthalpy) and isomerism of the **11a**- and **11b**-related species. Acidities of protonated **11a(b)** species and proton affinities of deprotonated **11a(b)** species were also calculated.

5.3.1.1 Relative Stabilities of Neutral **11a(b)** in the Gas Phase

Neutral **11a** has three isomer structures (Figure 5.8). **11a-ring** was calculated to be the most stable isomer, which is 1.1 kcal/mol more favorable than **11a-neutral**, in terms of enthalpy. A third form, an internal zwitterion, **11a-zwitterion**, was calculated to be 27.7 kcal/mol less stable than **11a-ring**.

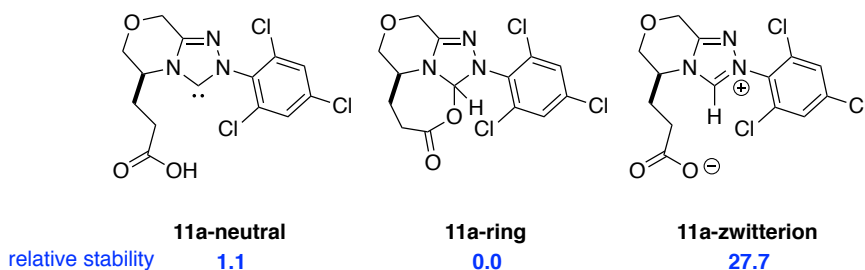


Figure 5.8 Relative stability of isomers of neutral **11a** (kcal/mol). Calculations were conducted at B3LYP/6-31+G(d); reported values are ΔH at 298 K

For neutral **11b** isomers, similar to what was found for neutral **11a**, **11b-ring** was calculated as the most stable structure in the gas phase. It is 2.6 kcal/mol more stable than **11b-neutral**, and 33.1 kcal/mol more stable than **11b-zwitterion** (Figure 5.9).

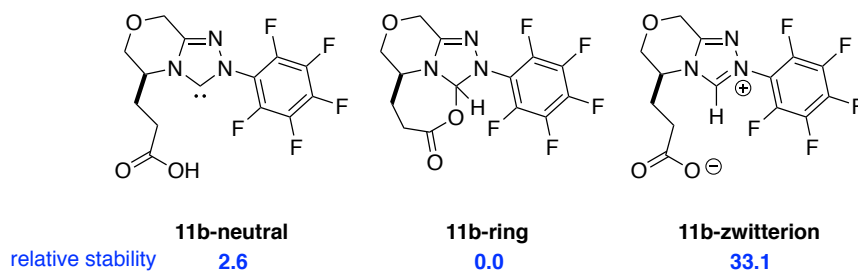


Figure 5.9 Relative stability of isomers of neutral **11b** (kcal/mol). Calculations were conducted at B3LYP/6-31+G(d); reported values are ΔH at 298 K

5.3.1.2 Relative Stabilities of Deprotonated **11a(b)** in the Gas Phase

Deprotonated **11a-zwitterion** and **11a-neutral** shared the same structure: **11a-anion**. On the other hand, the deprotonated **11a-ring** was very unstable and no optimized structure could be found by Gaussian calculation (Figure 5.10). The seven-member lactone ring structure opened during the geometry optimization.

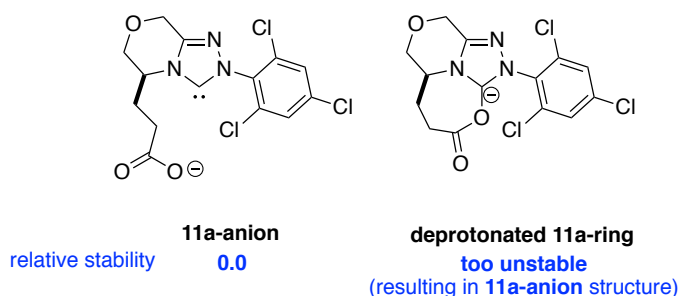


Figure 5.10 Relative stability of isomers of deprotonated **11a** (kcal/mol). Calculations were conducted at B3LYP/6-31+G(d); reported values are ΔH at 298 K

11b-anion was also calculated as the only stable deprotonated **11b** structure. The deprotonated **11b-ring** as shown in Figure 5.11 was very unstable.

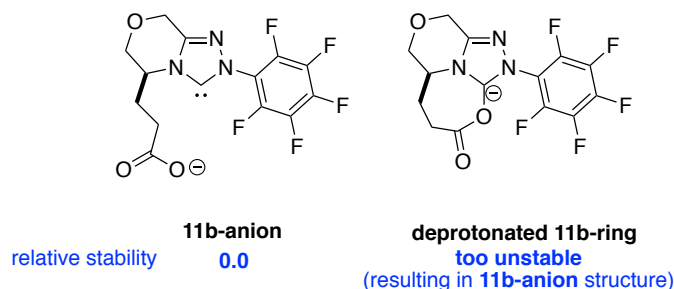


Figure 5.11 Relative stability of isomers of deprotonated **11b** (kcal/mol). Calculations were conducted at B3LYP/6-31+G(d); reported values are ΔH at 298 K

5.3.1.3 Relative Stabilities of Protonated **11a(b)** in the Gas Phase

Protonated **11a** has five stable conformational isomers (Figure 5.12).

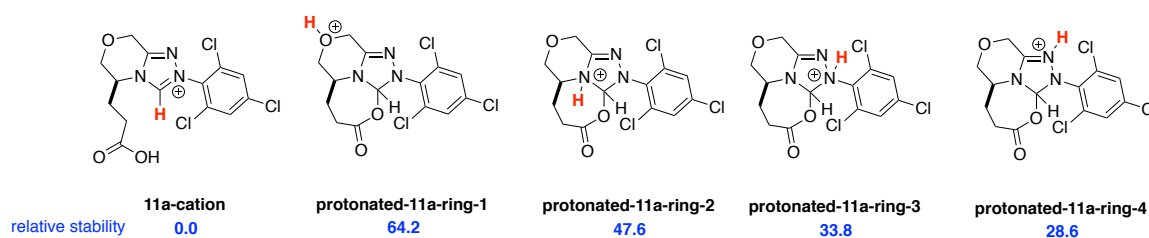


Figure 5.12 Relative stability of isomers of protonated **11a** (kcal/mol). Calculations were conducted at B3LYP/6-31+G(d); reported values are ΔH at 298 K

Protonated **11a-zwitterion** and protonated **11a-neutral** have the same positively-charged cationic structure: **11a-cation**. Protonation on different sites of **11a-ring** provided four isomers with various stabilities, with **protonated-11a-ring-4** being the most stable one. Relative stabilities in the gas phase are summarized in Figure 5.12. **11a-cation** is the most stable structure among all of the isomers. The **protonated-11a-ring-cation-4** was calculated to be 28.6 kcal/mol less stable than **11a-cation**.

Similarly, for protonated **11b**, all five of the possible isomer structures are shown in

Figure 5.13. **11b-cation** is the most stable structure among all the isomers. The **protonated-11b-ring-4** is 26.4 kcal/mol less stable than **11b-cation** but is relatively the most stable of the **protonated-11b-ring**-structured tautomers.

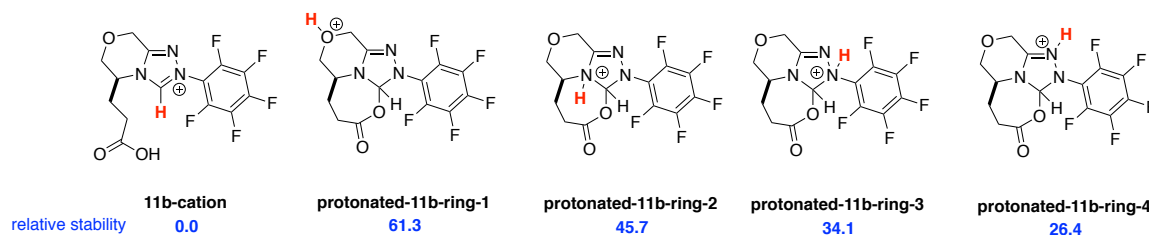


Figure 5.13 Relative stability of isomers of protonated **11b** (kcal/mol). Calculations were conducted at B3LYP/6-31+G(d); reported values are ΔH at 298 K

5.3.1.4 Gas-phase Acidity of Protonated **11a(b)**

Calculated gas-phase acidities (ΔH_{acid}) for different isomers of protonated **11a** and protonated **11b** are listed in Figure 5.14.

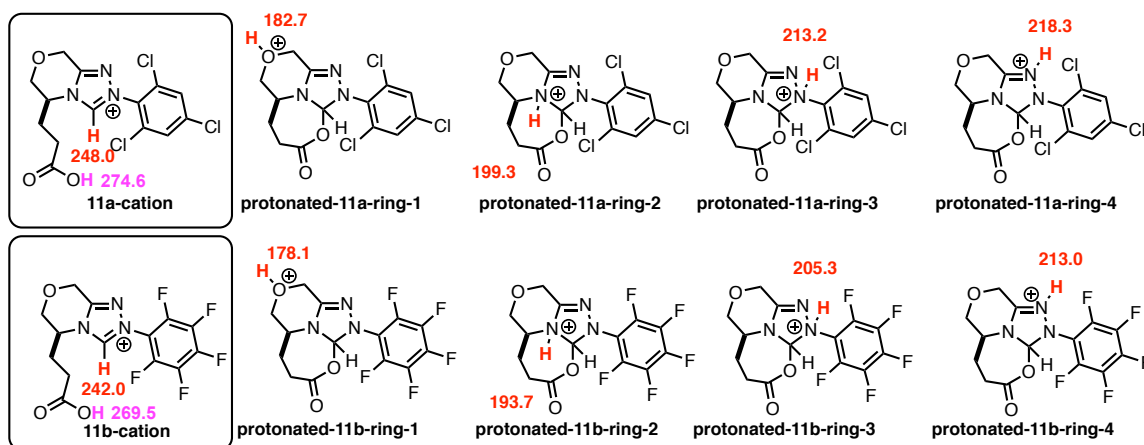


Figure 5.14 Calculated acidities for protonated **11a(b)** cations (kcal/mol). Calculations were conducted at B3LYP/6-31+G(d); reported values are ΔH at 298 K

Since **11a-cation** and **11b-cation** are the most stable structures for protonated **11a** and

11b, they have the highest ΔH_{acid} values (lowest gas-phase acidities) among their isomers. The protonated carbenes are the most acidic sites for both **11a-cation** and **11b-cation**. The carboxylic acid sites are less acidic by around 25 kcal/mol.

We also measured the acidities of protonated **11a** and **11b** experimentally and confirmed the structures of **11a-cation** and **11b-cation** in the gas phase. The experimental results are described in the next section (5.3.2). It is worth noting that the calculated gas-phase acidities of **11a-cation** and **11b-cation** correspond to the calculated proton affinities of the carbene centers (C-2) of **11a-neutral** and **11b-neutral**.

5.3.1.5 Proton Affinity of Deprotonated 11a(b)

11a(b)-anion is the only stable structure of deprotonated **11a(b)** in the gas phase. The proton affinity (PA) of both the carbene site and the carboxylate group of **11a(b)-anion** were calculated, and PA values are listed in Figure 5.15. For both anions, the negatively-charged carboxylate groups were around 30 kcal/mol more basic than the carbene centers.

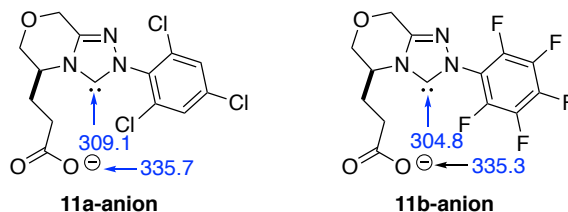


Figure 5.15 Calculated proton affinities of two different sites for **11a-anion** and **11b-anion** (kcal/mol). Calculations were conducted at B3LYP/6-31+G(d); reported values are ΔH at 298 K

5.3.2 Experimental Results in the Gas Phase

5.3.2.1 Bracketing Results

The experimental bracketing results for the acidities of protonated **11a** and **11b** are listed in Table 5.1. The proton transfer reactions between the protonated **11a(b)** and various reference bases with known proton affinities were studied in the gas phase. Electrospray ionization of the **11a(b)** precatalyst successfully yielded the positively-charged protonated **11a(b)** cation in the mass spectra as the major signal peak.

Eight reference bases were used. They were trimethylamine (PA = 234.7 kcal/mol), tributylamine (PA = 238.6 kcal/mol), *N,N,N',N'*-tetramethylenediamine (PA = 242.1 kcal/mol), 1-(Cyclopent-1-en-1-yl)pyrrolidine (PA = 243.6 kcal/mol), *N,N,N',N'*-tetramethyl-1,3-propanediamine (PA = 247.4 kcal/mol), DBN (PA = 248.2 kcal/mol), DBU (PA = 250.5 kcal/mol), and MTBD (PA = 254.0 kcal/mol). The presence of proton transfer from protonated **11a(b)** to a reference base indicates that PA of the given base is higher than that of the conjugate base of protonated **11a(b)** cation. In contrast, absence of proton transfer implies a higher PA of the conjugate base of protonated **11a(b)** cation than the PA of the reference base.

Table 5.1 Summary of results for acidity bracketing of protonated **11a** and **11b**

Reference base ^a	PA (kcal/mol) ^b	Proton transfer to reference base ^c	
		protonated 11a	protonated 11b

TEA	234.7	–	–
TBA	238.6	–	–
TMEDA	242.1	–	–
1-CP	243.6	–	–
TMPDA	247.4	–	Dimer
DBN	248.2	Dimer	+
DBU	250.5	Dimer	+
MTBD	254.0	Dimer	+

^aTEA = trimethylamine; TBA = tributylamine; TMEDA = N,N,N',N'-tetramethylethylenediamine; 1-CP = 1-(cyclopent-1-en-1-yl)pyrrolidine ; TMPDA = N,N,N',N'-tetramethyl-1,3-propanediamine; DBN = 1,5-Diazabicyclo[4.3.0]non-5-ene; DBU = 1,8-diazabicyclo[5.4.0]undec-7-ene; MTBD = 7-Methyl-1,5,7-triazabicyclo[4.4.0]dec-5-ene; ^bReference base PAs typically have an error of ± 2 kcal/mol.

^cThe “+” symbol indicates the occurrence and the “–” symbol indicates the absence of proton transfer.

Protonated **11b** showed no proton transfer with 1-(cyclopent-1-en-1-yl)pyrrolidine (PA = 243.6 kcal/mol) but reacted with DBN (PA = 248.2 kcal/mol). When reacting with N,N,N',N'-tetramethyl-1,3-propanediamine (PA = 247.4 kcal/mol), a proton-bound complex of protonated **11b** and the reference base was observed (noted as “dimer” in Table 5.1), which made it difficult to tell whether a proton transfer had occurred. Therefore, the

experimental acidity of protonated **11b** was bracketed between DBN and 1-(cyclopent-1-en-1-yl)pyrrolidine, as 246 ± 4 kcal/mol. For the bracketing experiments of protonated **11a**, hydrogen-bonded dimers predominantly formed between protonated **11a** and reference bases of DBN, DBU, and MTBD, which made it difficult to find specific cut-off points and draw a solid conclusion about the gas-phase acidity of protonated **11a**. Therefore, Cooks “extended” kinetic method was further used to measure the acidity of protonated **11a** cation (section 5.3.2.2).

5.3.2.2 Cooks Method Results

For our acidity studies of protonated **11a** using Cooks kinetic experiments, we utilized four reference bases and measured the product ion distributions three separate times to ensure reproducibility. The reference bases were DBN (PA = 248.2 kcal/mol), DBU (PA = 250.5 kcal/mol), MTBD (PA = 254.0 kcal/mol), and Imino-tris(dimethylamino)phosphorane (PA = 257.4 kcal/mol). Based on data analysis using Cooks “extended” kinetic method,¹⁵⁻¹⁹ the acidity of protonated **11a** was determined as 254 ± 3 kcal/mol, and the difference in entropy of the two competitive fragmentation channels, $\Delta(\Delta S)$, was found to be 2.3 cal/mol K. It has been noted that the $\Delta(\Delta S)$ value is related to the accuracy of the acidity measurement by the Cooks “extended” method. Ideally, the actual $\Delta(\Delta S)$ value should be less than or equal to 5 cal/mol K; otherwise, the Cooks “extended” kinetic method may underestimate the measured acidity.

5.3.3 Computational Results in the Solution Phase

We used density functional theory (DFT) at B3LYP/6-31+G(d) to calculate the relative stabilities (enthalpy) of neutral **11a(b)** species in solution. Two SCRF (Self-Consistent Reaction Field) solvation methods, the Polarizable Continuum Model (PCM) and the SMD solvation model, were used with a dielectric constant of 20.493 for acetone to simulate a solution-phase environment.

Calculated relative stability results of neutral **11a(b)** are listed in Figure 5.16.

For neutral **11a**, PCM and SMD models yielded slightly different trends. However, both models calculated the **11a-zwitterion** structure to be the most stable species. The triazolium carboxylate zwitterion, **11a-zwitterion**, was calculated by PCM model to be 3.8 kcal/mol more stable than the lactone-structured **11a-ring**, and 5.7 kcal/mol than the carbene carboxylic acid **11a-neutral**. With SMD model, **11a-zwitterion** is calculated to be more stable by 4.5 kcal/mol over **11a-ring**, and 3.9 kcal/mol over **11a-neutral**.

For the calculations of neutral **11b** structures in acetone, **11b-ring** and **11b-zwitterion** were calculated by PCM to have very close stabilities: **11b-zwitterion** is 0.1 kcal/mol less stable than **11b-ring**. **11b-neutral** was calculated to be less stable than **11b-ring** by 3.6 kcal/mol. Using SMD model, we obtained the most stable structure of neutral **11b** as the triazolium carboxylate zwitterion **11b-zwitterion**, which was 1.4 kcal/mol more stable than the lactone-structured **11b-ring** and 2.7 kcal/mol more stable than the **11b-neutral** structure with a free carbene and a carboxylic acid group.

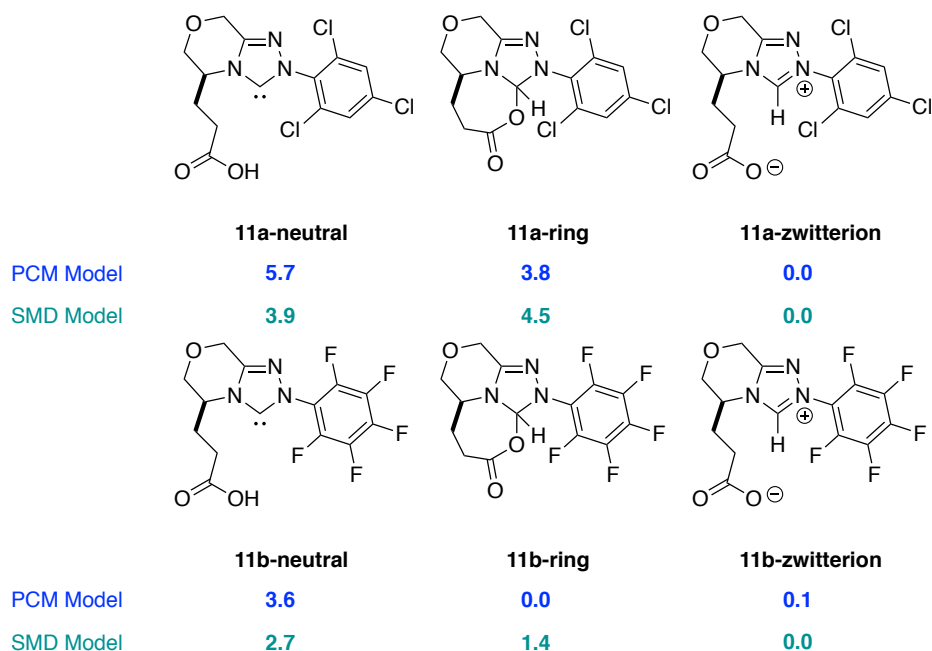


Figure 5.16 Relative stabilities of isomers of neutral **11a** and **11b** in acetone (kcal/mol).

Calculations were conducted at B3LYP/6-31+G(d) using PCM and SMD models;

reported values are ΔH at 298 K

5.3.4 Characterization of **11a(b)** Precatalyst in the Solution Phase

Proton nuclear magnetic resonance spectrum (^1H -NMR) was used to study the structures of **11a** and **11b** in condensed phase. The **11b** precatalyst was also characterized using IR, X-ray crystallography.

Proton nuclear magnetic resonance spectrum (^1H -NMR) using deuterated acetone as the solvent for both **11a** and **11b** precatalyst showed one single peak in the low field (ppm > 10) with a chemical shift at around 10.7 ppm. This was more consistent with the **11a(b)-zwitterion** structure or the **11a(b)-neutral** structure, but not the lactone, because the hydrogen next to the lactone is expected to have a chemical shift in a higher field (between

4 – 7 ppm). The precatalyst could also be protonated in solution (**11a(b)-cation**), with a counterion, as a salt. However, the protons on the carbene site and the carboxylic site of **11a(b)-cation** would yield two peaks in the low field, which were not observed.

Both the **11a(b)-zwitterion** and **11a(b)-neutral** would have a single hydrogen peak in the low field.²³ Lactone (**11a(b)-ring**) would have a single peak as well, but in wrong field area. Thus, we were not able to differentiate the **11a(b)-zwitterion** and **11a(b)-neutral** by using the ¹H-NMR spectrum.

The IR spectrum of **11b** precatalyst had an antisymmetric carboxylate (--COO^-) stretching mode of carbonyl group at 1517 cm^{-1} , which is consistent with a zwitterionic structure (**11b-zwitterion**). A carboxylic acid carbonyl (C=O) stretching mode at 1713 cm^{-1} was also observed, but there is no carboxylic acid O-H stretching mode between 3000 cm^{-1} and 2500 cm^{-1} . This is puzzling; perhaps the lack of an O-H stretching mode discounts **11b-neutral** structure and a salt-containing **11b-cation** (both with a carboxylic acid group), but the 1713 cm^{-1} peak is mysterious. No obvious ester carbonyl (C=O) absorption peak was found between $1750 - 1735\text{ cm}^{-1}$, and as a result, the **11b** precatalyst sample does not appear to be the lactone **11b-ring** structure.

Crystal structure analysis (X-ray diffraction) of **11b** precatalyst demonstrated that, in the crystal structure, both the carbene carbon and carboxylate are protonated, implying a structure of a salt composed of **11b-cation** and BF_4^- anion (Figure 5.17).

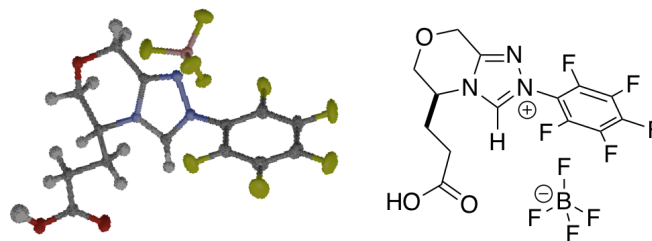


Figure 5.17 Crystal structure of **11b** pre-catalyst

5.3.5 Discussion

Computational results in the gas phase demonstrated that the **11a(b)-neutral** and the **11a(b)-ring** were more favorable than the zwitterion structure, **11a(b)-zwitterion**. This result was not surprising, since separated charges are less stabilized *in vacuo* without the benefit of solvation.

For deprotonated **11a(b)**, the optimized structures of the deprotonated **11a(b)-neutral**, the deprotonated **11a(b)-ring**, and the deprotonated **11a(b)-zwitterion**, all led to the same anion structure, the **11a(b)-anion**. Therefore, we feel confident about the charge-tagged NHC catalyst structure in the gas phase. This negatively-charged species is equipped with a reactive carbene center and a negatively-charged tag, which makes it an observable NHC catalyst in mass spectrometry. We plan to use these anions in the future to study NHC-catalyzed *Umpolung* reaction mechanisms in the gas phase.

The carboxylate group of **11a(b)-anion** was calculated to be around 30 kcal/mol more basic than the carbene site in the gas phase, in terms of enthalpy. It is noteworthy that this trend of basicities on two different sites is opposite to that in the solution phase. It is known that the triazolium salts have a pK_a of 16 – 19 in water, and the pK_a of carboxylic acid is

around 5.⁶ So the conjugate bases of triazoliums, the triazolylidene carbenes, are more basic than the conjugate bases of carboxylic acids, the carboxylates in aqueous solution. The differences between gas phase and aqueous solution are attributable to solvent effects. The charges of triazolium and carboxylate cannot be stabilized by solvation *in vacuo*.

The protonated **11a(b)** had five possible isomers, among which, **11a(b)-cation** was calculated to be the most stable cation structure. Different protonated **11a(b)** species have different calculated gas-phase acidities. We experimentally measured the acidities of protonated **11a(b)** species and compared the experimental data to the calculated acidities of the cation isomers (Table 5.2).

Table 5.2 Calculated (B3LYP/6-31+G(d); 298 K) and experimental acidities for protonated **11a** and protonated **11b**

<i>Protonated 11a(b) species</i>	<i>Calculated acidity</i>	<i>Experimental acidity</i>
11a-cation	<u>248.0</u>	
protonated-11a-ring-1	182.7	
protonated-11a-ring-2	199.3	254 ± 3^a
protonated-11a-ring-3	213.2	
protonated-11a-ring-4	218.3	
11b-cation	<u>242.0</u>	
protonated-11b-ring-1	178.1	
Protonated-11b-ring-2	193.7	246 ± 4^b
protonated-11b-ring-3	205.3	
Protonated-11b-ring-4	213.0	

^aExperimental acidity of protonated **11a**, measured by Cooks kinetic method.

^bExperimental acidity of protonated **11b**, measured by bracketing method.

The gas-phase acidity of protonated **11a** was measured by Cooks kinetic method to be 254 ± 3 kcal/mol, and the acidity value of protonated **11b** was bracketed to be 246 ± 4 kcal/mol. As shown in Table 5.2, these experimental acidity values were more consistent with the calculated acidities of **11a-cation** and **11b-cation**, and less consistent with the

calculated acidities of **protonated-11a(b)-ring** structures. This indicated that the protonated **11a(b)**, generated via ESI, has a structure of **11a(b)-cation**, which was calculated to be the most stable structure in the gas phase among their isomers. Experimental acidities of **11a-cation** and **11b-cation** were 4 - 6 kcal/mol higher than the calculated values. It was also noted that the calculated and measured acidities of **11a-cation** and **11b-cation** are the carbene proton affinities of **11a-neutral** and **11b-neutral** (Figure 5.18).

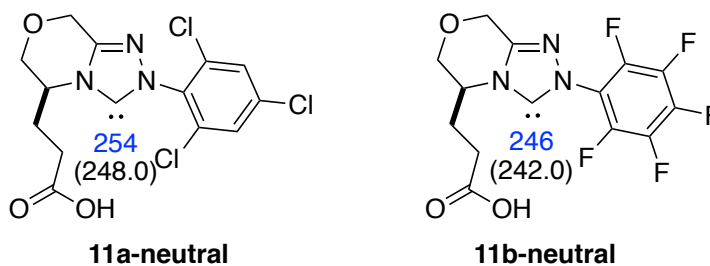


Figure 5.18 Measured (blue) and calculated (black, in parentheses) proton affinities of triazolyldenes of **11a-neutral** and **11b-neutral**, kcal/mol. Calculations were conducted at B3LYP/6-31+G(d); reported values are ΔH at 298 K

In the solution phase, the structure of **11a(b)** precatalyst was studied using both experiments and calculations. IR spectra implies a zwitterion structure as the precatalyst of **11b**. Crystal structure analysis of **11b** precatalyst by X-ray diffraction showed a clear structure of the salt, with the triazolium-carboxylic acid (**11b-cation**) as the cation and BF_4^- as the anion. ^1H NMR spectra of **11a(b)** precursor could not differentiate **11a(b)-zwitterion** from **11a(b)-neutral** in acetone solution. However, calculations using two separate

solvation models suggested that **11a(b)-zwitterion** is more stable than **11a(b)-neutral** in acetone. Therefore, it is highly possible that the **11a(b)** precatalyst in the acetone solution has a triazolium-carboxylate zwitterionic structure.

The calculated relative stabilities of neutral **11a(b)** species in solution differed greatly from those in the gas phase. The zwitterion structure of **11a(b)** was calculated to be the most stable structure in acetone solution but the least stable in the gas phase among the isomers. This is because the separated charges tend to be very “unhappy” in the absence of solvent in the gas phase, but can be well stabilized by solvation in the solution phase.

5.4 Conclusions

We conducted fundamental studies on two newly synthesized charge-tagged triazolylidene catalysts and their relevant species. Relative stabilities of isomers were calculated for protonated, neutral, and deprotonated **11a(b)** structures. Acidities of **11a-cation** and **11b-cation** (the proton affinities of the charge-tagged NHC carbene centers (C-2) of **11a-neutral** and **11b-neutral**) were also successfully calculated and measured. Calculations in solution phase were conducted to understand the structures of precatalysts. NMR and IR, taken together with calculations, support a zwitterion structure in solution (**11a(b)-zwitterion**). In solid state, X-ray studies support the **11a(b)-cation** structure.

5.5 References

- (1) Samojłowicz, C.; Bieniek, M.; Grela, K., *Chem. Rev.* **2009**, *109*, 3708.
- (2) Ukai, T.; Tanaka, R.; Dokawa, T., *J. Pharm. Soc. Jpn.* **1943**, *63*, 296.
- (3) Sheehan, J. C.; Hunneman, D. H., *J. Am. Chem. Soc.* **1966**, *88*, 3666.
- (4) Enders, D.; Breuer, K.; Raabe, G.; Runsink, J.; Teles, J. H.; Melder, J.-P.; Ebel, K.; Brode, S., *Angew. Chem., Int. Ed. Engl.* **1995**, *34*, 1021.
- (5) Enders, D.; Breuer, K.; Runsink, J.; Teles, J. H., *Helvetica Chimica Acta*, **1996**, *79*, 1899.
- (6) Knight, R. L.; Leeper, F. J., *J. Chem. Soc. Perkin Trans.* **1998**, *1*, 1891.
- (7) Flanagan, D. M.; Romanov-Michailidis, F.; White, N. A.; Rovis, T., *Chem. Rev.* **2015**, *115*, 9307.
- (8) Stetter, H.; Schreckenberger, M., *Angew. Chem. Int. Ed.* **1973**, *12*, 81.
- (9) Tian, Y.; Lee, J. K. *J. Org. Chem.* **2015**, *80*, 6831.
- (10) Zeng, H.; Wang, K.; Tian, Y.; Niu, Y.; Greene, L.; Hu, Z.; Lee, J. K. *Int. J. Mass Spectrom.* **2014**, *369*, 92.
- (11) Brook, A. G. *Acc. Chem. Res.* **1974**, *7*, 77.
- (12) Moore, J. L.; Silvestri, A. P.; Read de Alaniz, J.; DiRocco, D. A.; Rovis, T., *Org. Lett.* **2011**, *13*, 1742.
- (13) Chesnavich, W. J.; Su, T.; Bowers, M. T. *J. Chem. Phys.* **1980**, *72*, 2641.
- (14) Su, T.; Chesnavich, W. J. *J. Chem. Phys.* **1982**, *76*, 5183.
- (15) Miller, K. J.; Savchik, J. A. *J. Am. Chem. Soc.* **1979**, *101*, 7206.
- (16) Armentrout, P. B. *J. Am. Chem. Soc. Mass Spectrom.* **2000**, *11*, 371.
- (17) Cheng, X.; Wu, Z.; Fenselau, C. *J. Am. Chem. Soc.* **1993**, *115*, 4844.
- (18) Williams, T. I.; Denault, J. W.; Cooks, R. G. *Int. J. Mass Spectrom.* **2001**, *210/211*, 133.
- (19) Wesdemiotis, C. *J. Mass Spectrom.* **2004**, *39*, 998.
- (20) Sun, X.; Lee, J. K., *J. Org. Chem.* **2007**, *72*, 6548.
- (21) Tomasi, J.; Mennucci, B.; Cammi, R., *Chem. Rev.* **2005**, *105*, 2999.
- (22) Marenich, A. V.; Cramer, C. J.; Truhlar, D. G., *J. Phys. Chem. B* **2009**, *113*, 6378.
- (23) Amyes, T. L.; Diver, S. T.; Richard, J. P.; Rivas, F. M.; Toth, K. *J. Am. Chem. Soc.* **2004**, *126*, 4366.

ELSEVIER LICENSE

TERMS AND CONDITIONS

Mar 20, 2017

This Agreement between YIJIE NIU ("You") and Elsevier ("Elsevier") consists of your license details and the terms and conditions provided by Elsevier and Copyright Clearance Center.

License Number 4073391086916

License date Mar 20, 2017

Licensed Content Publisher Elsevier

Licensed Content Publication International Journal of Mass Spectrometry

Licensed Content Title The benzoin condensation: Charge tagging of the catalyst allows for tracking by mass spectrometry

Licensed Content Author Hao Zeng,Kai Wang,Yuan Tian,Yijie Niu,Landon Greene,Zhichao Hu,Jeehiun K. Lee

Licensed Content Date 15 August 2014

Licensed Content Volume 369

Licensed Content Issue n/a

Licensed Content Pages 6

Start Page 92

End Page 97

Type of Use reuse in a thesis/dissertation

Portion full article

Format both print and electronic

Are you the author of this

Elsevier article?

Yes

Will you be translating? No

Order reference number

Title of your

thesis/dissertation

Gas Phase Kinetic and Thermodynamic Studies of Organic Species

Using Mass Spectrometry

Expected completion date Sep 2017

Estimated size (number of pages)

150

Elsevier VAT number GB 494 6272 12

Requestor Location YIJIE NIU

610 Taylor Road
 PISCATAWAY, NJ 08854
 United States
 Attn: YIJIE NIU
 Publisher Tax ID 980397604
 Total 0.00 USD
[Terms and Conditions](#)

INTRODUCTION

1. The publisher for this copyrighted material is Elsevier. By clicking "accept" in connection with completing this licensing transaction, you agree that the following terms and conditions apply to this transaction (along with the Billing and Payment terms and conditions established by Copyright Clearance Center, Inc. ("CCC"), at the time that you opened your Rightslink account and that are available at any time at <http://myaccount.copyright.com>).

GENERAL TERMS

2. Elsevier hereby grants you permission to reproduce the aforementioned material subject to the terms and conditions indicated.
3. Acknowledgement: If any part of the material to be used (for example, figures) has appeared in our publication with credit or acknowledgement to another source, permission must also be sought from that source. If such permission is not obtained then that material may not be included in your publication/copies. Suitable acknowledgement to the source must be made, either as a footnote or in a reference list at the end of your publication, as follows:
 "Reprinted from Publication title, Vol /edition number, Author(s), Title of article / title of chapter, Pages No., Copyright (Year), with permission from Elsevier [OR APPLICABLE SOCIETY COPYRIGHT OWNER]." Also Lancet special credit - "Reprinted from The Lancet, Vol. number, Author(s), Title of article, Pages No., Copyright (Year), with permission from Elsevier."
4. Reproduction of this material is confined to the purpose and/or media for which permission is hereby given.
5. Altering/Modifying Material: Not Permitted. However figures and illustrations may be

altered/adapted minimally to serve your work. Any other abbreviations, additions, deletions

and/or any other alterations shall be made only with prior written authorization of Elsevier

Ltd. (Please contact Elsevier at permissions@elsevier.com). No modifications can be made

to any Lancet figures/tables and they must be reproduced in full.

6. If the permission fee for the requested use of our material is waived in this instance, please be advised that your future requests for Elsevier materials may attract a fee.

7. Reservation of Rights: Publisher reserves all rights not specifically granted in the combination of (i) the license details provided by you and accepted in the course of this licensing transaction, (ii) these terms and conditions and (iii) CCC's Billing and Payment terms and conditions.

8. License Contingent Upon Payment: While you may exercise the rights licensed immediately upon issuance of the license at the end of the licensing process for the transaction, provided that you have disclosed complete and accurate details of your proposed

use, no license is finally effective unless and until full payment is received from you (either

by publisher or by CCC) as provided in CCC's Billing and Payment terms and conditions. If full payment is not received on a timely basis, then any license preliminarily granted shall be

deemed automatically revoked and shall be void as if never granted. Further, in the event

that you breach any of these terms and conditions or any of CCC's Billing and Payment terms and conditions, the license is automatically revoked and shall be void as if never granted. Use of materials as described in a revoked license, as well as any use of the materials beyond the scope of an unrevoked license, may constitute copyright infringement

and publisher reserves the right to take any and all action to protect its copyright in the materials.

9. Warranties: Publisher makes no representations or warranties with respect to the licensed material.

10. Indemnity: You hereby indemnify and agree to hold harmless publisher and CCC, and their respective officers, directors, employees and agents, from and against any and all claims arising out of your use of the licensed material other than as specifically authorized pursuant to this license.

11. No Transfer of License: This license is personal to you and may not be sublicensed, assigned, or transferred by you to any other person without publisher's written permission.

12. No Amendment Except in Writing: This license may not be amended except in a writing

signed by both parties (or, in the case of publisher, by CCC on publisher's behalf).

13. Objection to Contrary Terms: Publisher hereby objects to any terms contained in any purchase order, acknowledgment, check endorsement or other writing prepared by you, which terms are inconsistent with these terms and conditions or CCC's Billing and Payment

terms and conditions. These terms and conditions, together with CCC's Billing and Payment

terms and conditions (which are incorporated herein), comprise the entire agreement between you and publisher (and CCC) concerning this licensing transaction. In the event of

any conflict between your obligations established by these terms and conditions and those

established by CCC's Billing and Payment terms and conditions, these terms and conditions

shall control.

14. Revocation: Elsevier or Copyright Clearance Center may deny the permissions described

in this License at their sole discretion, for any reason or no reason, with a full refund payable

to you. Notice of such denial will be made using the contact information provided by you.

Failure to receive such notice will not alter or invalidate the denial. In no event will Elsevier

or Copyright Clearance Center be responsible or liable for any costs, expenses or damage

incurred by you as a result of a denial of your permission request, other than a refund of the

amount(s) paid by you to Elsevier and/or Copyright Clearance Center for denied permissions.

LIMITED LICENSE

The following terms and conditions apply only to specific license types:

15. Translation: This permission is granted for non-exclusive world English rights only unless your license was granted for translation rights. If you licensed translation rights you

may only translate this content into the languages you requested. A professional translator must perform all translations and reproduce the content word for word preserving the integrity of the article.

16. Posting licensed content on any Website: The following terms and conditions apply as follows: Licensing material from an Elsevier journal: All content posted to the web site must maintain the copyright information line on the bottom of each image; A hyper-text must be included to the Homepage of the journal from which you are licensing at <http://www.sciencedirect.com/science/journal/xxxxx> or the Elsevier homepage for books at <http://www.elsevier.com>; Central Storage: This license does not include permission for a scanned version of the material to be stored in a central repository such as that provided by Heron/XanEdu.

Licensing material from an Elsevier book: A hyper-text link must be included to the Elsevier homepage at <http://www.elsevier.com> . All content posted to the web site must maintain the copyright information line on the bottom of each image.

Posting licensed content on Electronic reserve: In addition to the above the following clauses are applicable: The web site must be password-protected and made available only to bona fide students registered on a relevant course. This permission is granted for 1 year only.

You may obtain a new license for future website posting.

17. For journal authors: the following clauses are applicable in addition to the above: Preprints:

A preprint is an author's own write-up of research results and analysis, it has not been peerreviewed, nor has it had any other value added to it by a publisher (such as formatting, copyright, technical enhancement etc.).

Authors can share their preprints anywhere at any time. Preprints should not be added to or enhanced in any way in order to appear more like, or to substitute for, the final versions of

articles however authors can update their preprints on arXiv or RePEc with their

Accepted

Author Manuscript (see below).

If accepted for publication, we encourage authors to link from the preprint to their formal

publication via its DOI. Millions of researchers have access to the formal publications on ScienceDirect, and so links will help users to find, access, cite and use the best available version. Please note that Cell Press, The Lancet and some society-owned have different preprint policies. Information on these policies is available on the journal homepage.

Accepted Author Manuscripts: An accepted author manuscript is the manuscript of an article that has been accepted for publication and which typically includes authorincorporated

changes suggested during submission, peer review and editor-author communications.

Authors can share their accepted author manuscript: immediately

via their non-commercial person homepage or blog

by updating a preprint in arXiv or RePEc with the accepted manuscript

via their research institute or institutional repository for internal institutional uses or as part of an invitation-only research collaboration work-group

directly by providing copies to their students or to research collaborators for their personal use

for private scholarly sharing as part of an invitation-only work group on commercial sites with which Elsevier has an agreement

After the embargo period

via non-commercial hosting platforms such as their institutional repository

via commercial sites with which Elsevier has an agreement

In all cases accepted manuscripts should:

link to the formal publication via its DOI

bear a CC-BY-NC-ND license - this is easy to do

if aggregated with other manuscripts, for example in a repository or other site, be shared in alignment with our hosting policy not be added to or enhanced in any way to appear more like, or to substitute for, the published journal article.

Published journal article (JPA): A published journal article (PJA) is the definitive final record of published research that appears or will appear in the journal and embodies all value-adding publishing activities including peer review co-ordination, copy-editing, formatting, (if relevant) pagination and online enrichment.

Policies for sharing publishing journal articles differ for subscription and gold open access

articles:

Subscription Articles: If you are an author, please share a link to your article rather than the full-text. Millions of researchers have access to the formal publications on ScienceDirect, and so links will help your users to find, access, cite, and use the best available version. Theses and dissertations which contain embedded PJAs as part of the formal submission can be posted publicly by the awarding institution with DOI links back to the formal publications on ScienceDirect.

If you are affiliated with a library that subscribes to ScienceDirect you have additional private sharing rights for others' research accessed under that agreement. This includes use

for classroom teaching and internal training at the institution (including use in course packs

and courseware programs), and inclusion of the article for grant funding purposes.

Gold Open Access Articles: May be shared according to the author-selected end-user license and should contain a [CrossMark logo](#), the end user license, and a DOI link to the formal publication on ScienceDirect.

Please refer to Elsevier's [posting policy](#) for further information.

18. For book authors the following clauses are applicable in addition to the above:

Authors are permitted to place a brief summary of their work online only. You are not allowed to download and post the published electronic version of your chapter, nor may you

scan the printed edition to create an electronic version. Posting to a repository: Authors are

permitted to post a summary of their chapter only in their institution's repository.

19. Thesis/Dissertation: If your license is for use in a thesis/dissertation your thesis may be

submitted to your institution in either print or electronic form. Should your thesis be published commercially, please reapply for permission. These requirements include permission for the Library and Archives of Canada to supply single copies, on demand, of the complete thesis and include permission for Proquest/UMI to supply single copies, on demand, of the complete thesis. Should your thesis be published commercially, please reapply for permission. Theses and dissertations which contain embedded PJAs as part of

the formal submission can be posted publicly by the awarding institution with DOI links back to the formal publications on ScienceDirect.

Elsevier Open Access Terms and Conditions

You can publish open access with Elsevier in hundreds of open access journals or in nearly

2000 established subscription journals that support open access publishing. Permitted third

party re-use of these open access articles is defined by the author's choice of Creative Commons user license. See our [open access license policy](#) for more information.

Terms & Conditions applicable to all Open Access articles published with Elsevier:

Any reuse of the article must not represent the author as endorsing the adaptation of the

article nor should the article be modified in such a way as to damage the author's honour or

reputation. If any changes have been made, such changes must be clearly indicated.

The author(s) must be appropriately credited and we ask that you include the end user license and a DOI link to the formal publication on ScienceDirect.

If any part of the material to be used (for example, figures) has appeared in our publication

with credit or acknowledgement to another source it is the responsibility of the user to ensure their reuse complies with the terms and conditions determined by the rights holder.

Additional Terms & Conditions applicable to each Creative Commons user license:

CC BY: The CC-BY license allows users to copy, to create extracts, abstracts and new works from the Article, to alter and revise the Article and to make commercial use of the Article (including reuse and/or resale of the Article by commercial entities), provided the user gives appropriate credit (with a link to the formal publication through the relevant DOI), provides a link to the license, indicates if changes were made and the licensor is not

represented as endorsing the use made of the work. The full details of the license are available at <http://creativecommons.org/licenses/by/4.0>.

CC BY NC SA: The CC BY-NC-SA license allows users to copy, to create extracts, abstracts and new works from the Article, to alter and revise the Article, provided this is not

done for commercial purposes, and that the user gives appropriate credit (with a link to the

formal publication through the relevant DOI), provides a link to the license, indicates if changes were made and the licensor is not represented as endorsing the use made of the

work. Further, any new works must be made available on the same conditions. The full details of the license are available at <http://creativecommons.org/licenses/by-nc-sa/4.0>.

CC BY NC ND: The CC BY-NC-ND license allows users to copy and distribute the Article, provided this is not done for commercial purposes and further does not permit distribution of

the Article if it is changed or edited in any way, and provided the user gives appropriate credit (with a link to the formal publication through the relevant DOI), provides a link to the

license, and that the licensor is not represented as endorsing the use made of the work.

The

full details of the license are available at <http://creativecommons.org/licenses/by-nc-nd/4.0>.

Any commercial reuse of Open Access articles published with a CC BY NC SA or CC BY NC ND license requires permission from Elsevier and will be subject to a fee.

Commercial reuse includes:

Associating advertising with the full text of the Article

Charging fees for document delivery or access

Article aggregation

Systematic distribution via e-mail lists or share buttons

Posting or linking by commercial companies for use by customers of those companies.

20. Other Conditions:

v1.9

Questions? customercare@copyright.com or +18552393415

(toll free in the US) or

+19786462777.



RightsLink®

[Home](#)[Account Info](#)[Help](#)ACS Publications
Most Trusted. Most Cited. Most Read.**Title:**Organocatalytic Reactions
Enabled by N-Heterocyclic
Carbenes**Author:**Darrin M. Flanigan, Fedor
Romanov-Michailidis, Nicholas A.
White, et al

Logged in as:

YIJIE NIU

Account #:

3001128116

[LOGOUT](#)**Publication:** Chemical Reviews**Publisher:** American Chemical Society**Date:** Sep 1, 2015

Copyright © 2015, American Chemical Society

PERMISSION/LICENSE IS GRANTED FOR YOUR ORDER AT NO CHARGE

This type of permission/license, instead of the standard Terms & Conditions, is sent to you because no fee is being charged for your order. Please note the following:

- Permission is granted for your request in both print and electronic formats, and translations.
- If figures and/or tables were requested, they may be adapted or used in part.
- Please print this page for your records and send a copy of it to your publisher/graduate school.
- Appropriate credit for the requested material should be given as follows: "Reprinted (adapted) with permission from (COMPLETE REFERENCE CITATION). Copyright (YEAR) American Chemical Society." Insert appropriate information in place of the capitalized words.
- One-time permission is granted only for the use specified in your request. No additional uses are granted (such as derivative works or other editions). For any other uses, please submit a new request.

If credit is given to another source for the material you requested, permission must be obtained from that source.

[BACK](#)[CLOSE WINDOW](#)